Universidade do Minho
Escola de Engenharia

Luis Filipe Rodrigues Castanheira

Functionality of Ti surfaces: Tribocorrosion of Titanium samples Anodized and Biomodified

July 2011

Functionality of Ti surfaces: Tribocorrosion of Titanium samples Anodized and Biomodified
Luis Filipe Rodrigues Castanheira
UMinho | 2011

Universidade do Minho
Escola de Engenharia

Luis Filipe Rodrigues Castanheira

Functionality of Ti surfaces: Tribocorrosion of Titanium samples Anodized and Biomodified

Master Degree in Biomedical Engineering
Area of Biomaterials, Biomechanics and Rehabilitation

Supervisor:
Professor Luís Augusto Rocha
Co-supervisors:
Prof. Pierre Ponthiaux
Prof. François Wenger

July 2011

University of Minho, 2011

Preface

"All truths are easy to understand once they are discovered; the point is to discover them."

Galileo Galilei

Acknowledgements

I would like to thank my supervisor in Portugal, Professor Luis Rocha from the University of Minho, to accept me as his student for my master thesis. The project in which I was involved was very interesting and challenging.

A special word of recognition and gratitude to Professor Pierre Ponthiaux and Professor François Wenger, that accepted me for a whole academic year at the *Laboratoire de Génie des Procédés et Matériaux* of École Centrale Paris to perform my master thesis. The continuous discussion of ideas, the total support and the availability to aid me in any situation was very reassuring, as well for the moments of rest where the conversations were about anything but work. It will always be a special year of my life.

Also I would like to thank to Professor Mariana Henriques from the University of Minho, for the availability and the words of encouragement during my work, as well to Professor Didier Lutomski and Professor Jean-Pierre Celis, for their great support and suggestions for the development of the work.

I wish to thank to Mathilde Charters, Jamila El Bekri and Nathalie Ruscassier for the help on all the equipments that I had to work with, as well for some moments of distraction. As well, I would like to thank to Alexandra and Fernando from CT2M for providing the samples for the work.

Finally, to all the colleagues that I met at École Centrale Paris I wish the best of luck for them and for their projects, especially to Claudiu Ionescu, Florentina Sorcaru and Eugenie.

Functionality of Ti surfaces: Tribocorrosion of Titanium samples anodized and biomodified

Abstract

Dental implants have become increasingly common for the management of tooth loss. Meanwhile, several implants still fail as a permanent solution despite the intense research on this subject. Failures on these implants are usually related to the loosening of the implant, causing inflammations, infections, decrease in bone density and release of toxic agents to the human body. On the bases of these problems are phenomena like corrosion and wear of the material composing the dental implant.

In this way, it becomes necessary to better understand the mechanisms of corrosion and wear behind dental implants. The present work will increase the knowledge on the tribocorrosion mechanisms of titanium as well it will study the influence of a new surface treatment by anodization. Experimental tests will resemble the conditions presented on the oral cavity and will subject Etched and Anodized titanium samples, as well biomodified titanium samples, to tribocorrosion evaluations. The effects of the normal load and velocity of rotation on the process of tribocorrosion will be addressed and the effect of the biological material (osteoblastic cells MG63) on the degradation and corrosion behavior will be compared with the non cultivated samples. In addition, prior to cellular culture, some samples will be subjected to tribocorrosion tests to determine if the changes of the superficial properties present more affinity for osteoblast growth.

Funcionalidade de superfícies de Ti: Tribocorrosão de amostras de Titânio anodizadas e biomodificadas

Resumo

Os implantes dentários tornaram-se cada vez mais comuns no tratamento da perda de dentes. No entanto, diversos implantes continuam a falhar como uma solução permanente independentemente da intensa investigação existente na área. As falhas nestes implantes são, normalmente, relacionadas com a perda de fixação do implante que conduz a inflamações, infecções, diminuição da densidade óssea e libertação de agentes tóxicos para o organismo. Na base destes problemas estão fenómenos como corrosão e desgaste do material que compõem o implante dentário.

Deste modo, torna-se necessário compreender melhor os mecanismos de corrosão e desgaste por detrás dos implantes dentários. O presente trabalho vai permitir aumentar o conhecimento dos mecanismos de tribocorrosão do titânio, assim como estudar a influência de um novo tratamento de superfície realizado por anodização. Os testes experimentais vão simular as condições na cavidade oral e irão submeter amostras de titânio Etched e Anodizadas, assim como amostras Biomodificadas, a avaliação de tribocorrosão. O efeito da força normal e velocidade de rotação no processo de tribocorrosão serão abordados e o efeito da presença de material biológico (células osteoblásticas MG63) na degradação e na corrosão do material será comparado com as amostras não sujeitas a cultura. Além disso, antes da cultura celular, algumas amostras serão sujeitas a testes de tribocorrosão de modo a determinar se a alteração da superfície apresenta maior afinidade para o crescimento de osteoblastos.

Objective and Structure of the thesis

The objective of this master thesis was the study of the tribocorrosion behavior of functionalized titanium samples, by evaluating a new surface treatment for future implementation in dental implants. Several titanium samples were studied to acknowledge the advantages of the superficial treatment applied on the tribocorrosion properties of the material as well starting tribocorrosion tests with the presence of biological tissue (osteoblast cells) on the surface of the material. Additionally, the effect of changes in normal load and velocity were considered.

The first chapter of this dissertation consists of an overview of the application of titanium as biomaterial, more specially the Ti as dental implant material. The biocompatibility, the mechanical properties, the corrosion and wear resistance of the material are addressed. As well, the mechanisms of tribocorrosion are defined and presented, including the most important parameters as normal load, velocity and type of electrolyte. Chapters 2 presents the experimental protocol used to perform the study and Chapter 3 presents the results and discussion of the performed tests, where the influence of the normal load, velocity of sliding and presence of cell layer.

On chapter 4 is presented the general conclusions of the master thesis and future work is suggested on Chapter 5.

Chapter 6 consists in a group of preliminary results that were obtained during this work but aren’t integrated on the main objective of the thesis. This is a first attempt to test new experimental conditions, and to provide bases for future students working on the subject.

Table of Contents

List of Figures

List of Tables

List of Abbreviations

A_0: sample area (cm^2)

A_{act}: area of active material in the wear track (cm^2)

A_{tr}: wear track area (cm^2)

B: constant (mV)

CPE_p: constant phase element associated with passive film

CPE_{pb}: constant phase element associated with barrier film

CPE_{pp}: constant phase element associated with porous structure

d: density of material ($g.cm^{-3}$)

e: average wear track width (cm)

E_{corr}: corrosion potential (V vs. ref)

EDS: Energy Dispersive X-Ray Spectroscopy

EIS: Electrochemical Impedance Spectroscopy

E_{oc}: open-circuit potential (V vs. ref)

E_r: reduced elastic modulus

F: Faraday constant (96,485 $C.mol^{-1}$)

H: Hardness

HF: Hydrofluoric Acid

HNO_3: Nitric Acid

i_{act}: corrosion current density of active material ($mA.cm^{-2}$)

i_{corr}: corrosion current density before sliding ($mA.cm^{-2}$)

L: wear track length (cm)

M: molecular weight ($g.mol^{-1}$)

N: number of cycles

n: number of electrons

NHE: Natural Hydrogen Electrode

OCP: Open-Circuit Potential

Ra: Average Rugosity (µm)

R_{act}: polarization resistance of active area in the wear track (Ω)

r_{act}: specific polarization resistance of active material ($\Omega.cm^2$)

R_p: polarization resistance of passive film (Ω)

r_p: specific polarization resistance before sliding ($\Omega.cm^2$)

R_{pass}: polarization resistance of passive area (Ω)

R_{pb}: polarization resistance of barrier film (Ω)

R_{pp}: polarization resistance of porous structure (Ω)

R_{ps}: polarization resistance measured during sliding (Ω)

R_s: Resistance of the electrolyte (Ω)

Rz: Single Roughness Depth (µm)

S: average cross-sectional area of wear track (cm^2)

Sa: Average Rugosity (µm)

SEM: Scanning Electron Microscope

Sz: Single Roughness Depth (µm)

t_{lat}: latency time (s)

T_r: rotation period (s)

V_{tr}: volume of the wear track (cm^3)

W_{act}^{c}: specific material loss due to the corrosion of active material ($cm^3.cm^{-2}.cycle^{-1}$)

W_{act}^{m}: specific material loss due to the mechanical wear of active material ($cm^3.cm^{-2}.cycle^{-1}$)

W_{tr}: material loss on the wear track (cm^3)

XRD: X-Ray Diffraction

Chapter 1 - Introduction

1.1. Dental Implants

Dental implants have become increasingly common for the management of tooth loss, congenital defects and trauma or even just to improve esthetic appearance [(1)]. A dental implant is not a single block of a material that will anchor a tooth. On Figure 1 it is possible to see a common dental implant and its scheme, evidencing its several parts. An endosseous part called the "Implant Body" is the screw that contacts with the bone and allows the fixation of the implant to the jaw. After, to connect the ceramic tooth to the screw there are some mechanical linkages: the "Abutment", which links the implant body to the rest of the parts, the "Abutment screw", to fixate the abutment to the implant body, the "Cylinder", which will be in contact with the mucosa and preventing the mucosa to grow over the implant body, and at last the "Ceramic Tooth" that will replace the lost tooth [(2)(3)].

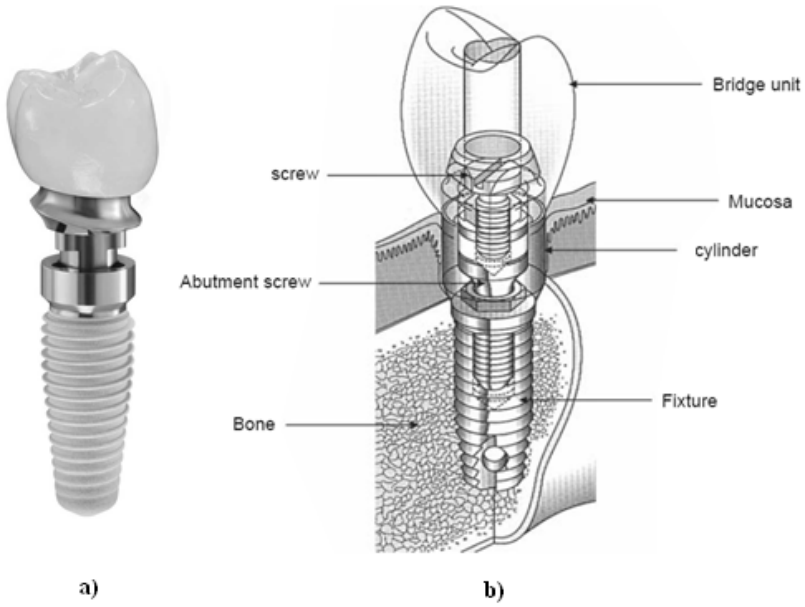

Figure 1 - a) Dental Implant b) Scheme of dental implant [(4)(3)].

Meanwhile, several implants still fail as a permanent solution despite the intense research on this subject. A dental implant is subjected to a surrounding environment that is characterized by a group of biomechanical and biochemical conditions, which are specific from patient to patient. In this way it is very difficult to predict how the device will perform [(5)(6)].

Failures on these implants are usually related to the loosening of the implant, causing inflammations, infections, decrease in bone density and release of toxic agents to the human body. On the bases of this problem are mechanical and chemical phenomena, like wear and corrosion of the material composing the dental implant. In these situations, the coincident impact of wear and corrosion in the presence of biological fluid sets the basis of a tribocorrosion system, which will create a synergetic effect and increase the degradation of the material of the implant [(7)], and eventually leading to the failure of the treatment.

1.2. Biomaterials

Biomaterials use increased in the late 1800s after the introduction of aseptic surgical technique by Dr. Joseph Lister in the 1860s [8]. Biomaterials science is the study of the physical and biological properties of materials (metallic, ceramic, polymeric and composites) with a special attention to the interaction between the material and the biological environment. This field of knowledge has evolved through time with the emergence of medical devices like fixation plates, total hip replacement, dental implants, cornea replacements, blood vessels replacements and so on. Nowadays it still requires more research and developments, in order to deepen the knowledge on the complex biological response that the materials stimulate after implantation, develop new surfaces to induce specific reactions of the cells and proteins to enhance the biological compatibility of the material, to create new materials that increase cellular adhesion, proliferation and differentiation [9].

1.2.1. Definition of Biomaterial

The definition of a biomaterial is usually referred to a "*non viable material used in a medical device, intended to interact with biological systems*" as Williams defined in 1987. However, the definition has evolved through time in order to make it more complete and the following is also considered, "*any substance (other than drugs) or combination of substances, synthetic or natural in origin, which can be used for any period of time, as a whole or as a part of a system which treats, augments, or replaces any tissue, organ, or function of the body*" [6] [8] [10].

1.2.2. Properties of Biomaterials

Like in all engineering projects, a medical device has a list of particularities that should be followed in order to the medical device perform its desired function. In this way, the properties of the materials used in medical devices, *biomaterials*, will depend on the function of the medical device. For instance, the biomaterial for an orthopedic prosthetic (knee or hip, the most common) has to present better mechanical properties, as elastic modulus and fatigue resistance, to withstand the loadings induced by daily life activities like walking or climbing stairs, than the biomaterial for an artificial blood vessel, that has to have also certain mechanical properties, but more importantly, has to have a lower thrombogenicity (tendency to form blood clots) in order to maintain the blood flux. Mechanical properties and thrombogenicity are specific properties that will belong to a certain device, but a property common to all biomaterials is *biocompatibility*.

The biocompatibility definition has also evolved [10][11] , but a complete and straightforward manner of defining it, is as "*the acceptance of an artificial implant by the surrounding tissues and by the body as a whole, by not irritating the surrounding structures, not provoking an abnormal inflammatory response, not inciting allergic or immunologic reactions, and not causing cancer*" [9]. This is the most important property of a biomaterial and that determines it acceptance by the human

body. The biocompatibility of a material is defined by a thorough evaluation of in-vitro tests, which follow strictly protocols based on international standards that control all the variables like number of cells per test, cell growth, type of cells, in order to allow the reproduction of the results at different laboratories [(10)(12)]. Currently the *International Organization for Standardization* (ISO) has the ISO 10993 composed by 20 parts, that allows the evaluation of the biological behaviour of materials and medical devices, but also the *American Society for Testing Materials* (ASTM) developed standards to evaluate medical devices like the F748 or F1027 [(13)]. If such behaviour, like the toxicologist potential or the incompatibility with the organism of certain material, is not evaluated at the early stages of the project of a medical device, it will be lost a considerable amount of time and funding on the project.

1.3. Osseointegration

In the 1950s Professor Per-Ingvar Brånemark, a Swedish orthopedic surgeon, was doing research on the growth of bone tissue, by implanting titanium chambers on the femurs of rabbits, to then remove them and study the newly formed bone. Brånemark was surprised when, in removing the chambers, verified that they had developed a bond with the bone. The potential of this discovery was recognized and after further experiments, Brånemark confirmed that with certain conditions, it was possible to combine titanium with living bone. The phenomenon was designed as *osseointegration*, which is "*a direct structural and functional connection between ordered living bone and the surface of a load-carrying implant*" [(2)].

In the field of dental implants, osseointegration is an essential process that the implant has to surpass, since its success relies on the fixation and stability provided by such a phenomenon. Through the study of osseointegration, a number of prerequisites have been identified as precursors of this phenomenon. Biocompatibility, chemistry and roughness of the surface, alignment of the implant, design of the implant, surgical technique, bone quality and loading conditions after surgery are thought to be required to obtain a proper connection between bone and implant [(14)(15)]. On Figure 2, it is possible to see all the stages during the process of osseointegration.

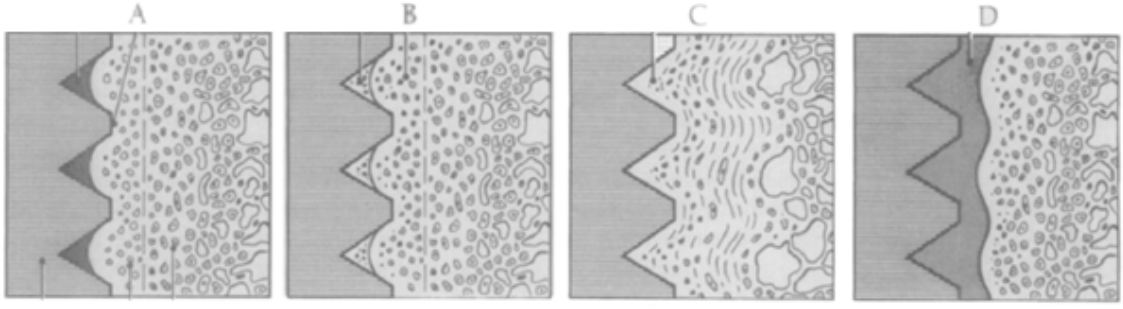

Figure 2 - Scheme of osseointegration stages **[(16)]**.

Right after surgery (A), due to the lesion made on the bone jaw, a series of oncollagenous proteins and growth factors are activated in order to start bone regeneration. Following the surgery the implant is not completely in contact with the adjacent tissues, and the threads of the implant are the

only components that guarantee the immobilization during the first healing period. During the first weeks (4th to 6th week) after surgery (B), there's the formation of woven bone (a primitive type of bone) and the revascularization and remineralization of damage bone. Afterwards there is the adaptation of the bone mass to the loading conditions (C). This is the last stage of osseointegration and starts around the 3th month until the rest of the implant life. It is characterized by a remodeling and a functional adaptation of the bone structure to the masticatory loads. In certain patients, the osseointegration is not successful (D) and a nonmineralized connective tissue layer forms at the interface bone-implant. This can be due to infections, early loading, bad bone quality and so on [14] [16].

The factors that are related to influence the osseointegration of the implant are divided as systemic or local. Table 1 demonstrates these factors and refers their effects.

Table 1 – Factors influencing osseointegration [2].

Factors influencing Osseointegration		
Local Factors	**Material**	CP Titanium is the basis material for osseointegration but also zirconium and hydroxyapatite bound with bone tissue.
	Surface Morphology	CP Ti oxide film allows and conducts bone formation. Also surface coatings with hydroxyapatite or calcium phosphates may functionalize materials surface.
	Heat	During implantation the drilling may increase the temperature up to 50 °C and the tissues may start to become necrotic. Favors formation of fibrous capsule.
	Initial Stability	The ability of the implant to be early constrained by the bone tissue increases the rate of a successful osseointegration. Screw shaped implants are more stable due to their contour.
	Early Loading	High initial loads may induce the formation of fibrous capsule and loosening of the implant.
	Late Loading	As bone is a strain-sensitive material, a certain range of loads allows bone growth. Loads should be applied gradually and excessive loads may break the osseointegrated interface.
Systemic Factors	**Contamination**	The sterilization of the environment as of the instruments is crucial to decrease the rate of infection during implantation.
	Bone Quality	It depends on bone density, anatomy, volume and thickness of cortical and cancellous bone. Is very difficult to evaluate precisely.

1.4. Human organism environment

The environment at which biomaterials are exposed consists in a aqueous solution with several ionic species (cations and anions), organic molecules (proteins and cells) and dissolved oxygen, with a buffered pH of 7.4 (after surgery the pH may present lower values as 5 on the surrounding tissues, but increases gradually after weeks) and a medium temperature of 37°C, being an excellent electrolyte to promote corrosion mechanisms and hydrolysis reactions. Also, the hydrodynamic conditions around the surface of the biomaterial influences mass transfer and, consequently, corrosion. In this way, the human body is considered a highly corrosive environment for metallic biomaterials, which can induce corrosion and material degradation. On Table 2 and Table 3 are presented the properties of the physiological environment and their effects on material degradation and the ionic composition of the

blood plasma, respectively [10] [14] [17] [18]. Also, the fact that the concentration of oxygen in body fluids is one fourth of that in air, this will interfere with some electrochemical reactions that control the amount of release of metal ions to the organism [19].

Table 2 - Properties of the physiological environment and their effects on material degradation [17].

Properties		Effects
Ionic Concentration		Encourage electrochemical reactions that can contribute to corrosion processes.
Proteins	**Positive Effect**	Protein adsorption protects material restricting the dissolution of metallic ions. Decrease of the friction coefficient.
	Negative Effect	Formation of biofilms and ionic complexes metal-protein that are removed and eliminated. For the equilibrium maintenance new complexes are continually formed and the corrosion tendency of the material increases.
O_2 Concentration		Influences the stability of the passive film and adding the protein adsorption, may arise obstructions to the diffusion of oxygen in certain areas, causing corrosion processes and weakening of the passive film.
pH		pH shifts may indicate corrosion processes resulting from infections and from the action of the immune system.
Temperature		May accelerate electrochemical reactions and change corrosion processes.

Table 3 – Ionic composition of the blood plasma [17].

Ions	Concentration (mmol/l)
Na^+	142.0
K^+	5.0
Mg^{2+}	1.5
Ca^{2+}	2.5
Cl^-	103.0
HCO_3^{2-}	27.0
HPO_4^-	1.0
SO_4^{2-}	0.5

1.5. Titanium

Titanium and titanium alloys are widely used in several industrial areas. After the second half of the twentieth century the modern industry was able to design applications in titanium, being this material applied in military and civil applications, as airplanes and engines, but also on biomedical

devices and components, especially as hard tissue replacements because of their desirable properties, such as relatively low modulus, good fatigue strength, formability, machinability, corrosion resistance and biocompatibility [20].

1.5.1. Titanium Properties

The properties of titanium and its alloys will depend on their basic structure and how is the material manipulated during the mechanical and thermal treatment during manufacture. Titanium is a nonmagnetic material and has good heat-transfer properties, lower than that of steel and aluminum. The melting point is around 1660 °C (3000 °F) and for its commercial alloys around 538 °C (1000 °F). Its basic structure at room temperature is hexagonal close-packed arrangement (HCP α-titanium) and when heated, the atomic structure undergoes a transformation to a body-centered cubic arrangement (BCC β-titanium) at 882 °C [21][22]. The atomic unit cells of the hexagonal close-packed and the body-centered cubic are present on Figure 3.

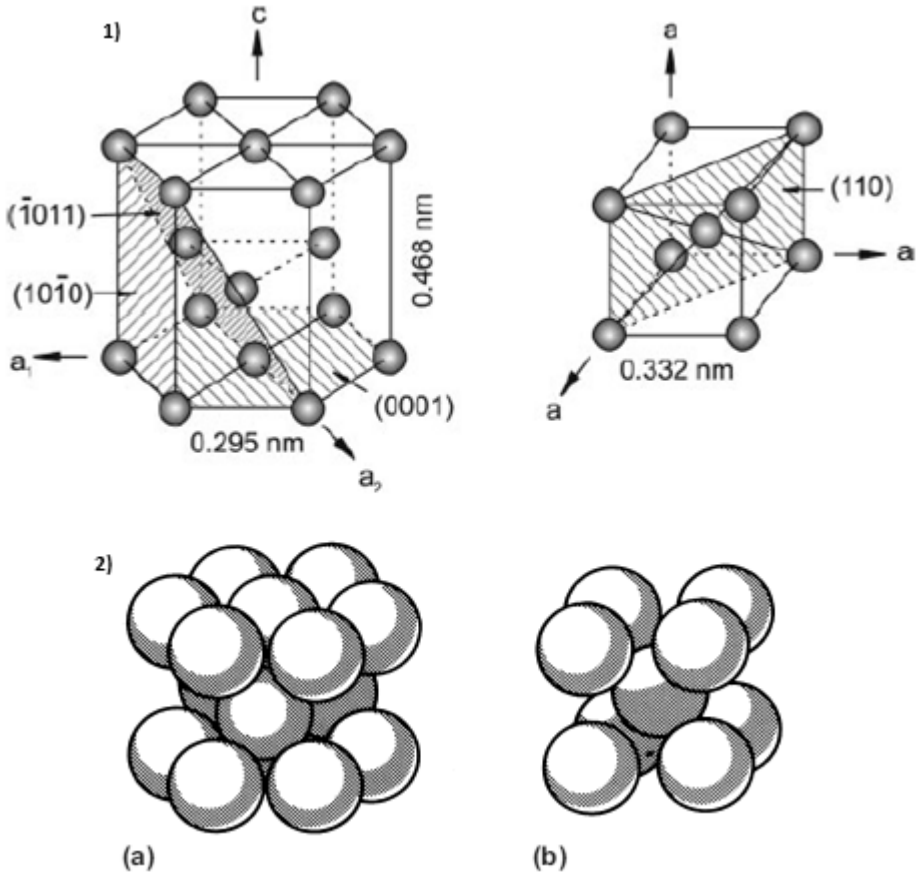

Figure 3 – 1) Crystal structure of HCP α-titanium and BCC β-titanium 2) Scheme of the crystal structure a) HCP b) BCC [20][21].

The presence of this two different crystal structures and their behaviour under heat (β-transus temperature) set the basis for the appreciated properties that this material presents. Also, this modification on the morphology of the crystalline unit can be controlled and modified by the addition

of alloying elements in order to present the BCC arrangement at lower temperatures. The alloying elements will also determine most of the physical properties and the chemical properties of the alloys. In this way, the alloying elements for titanium can be classified as neutral, α-stabilizers and β-stabilizers. Neutral elements will have a minor effect on the β-transus temperature, α-stabilizers will allow the presence of α-phase at higher temperatures and β-stabilizers will shift the β-phase to lower temperatures. The classification of the titanium alloys are related to these elements, being classified as α-alloys, near α-alloys, α+β alloys, near β-alloys and β-alloys. Table 4 shows the effects of alloying elements on structure and on some properties of the alloys [13] [20] [21][22].

Table 4 - Effects of alloying elements on titanium [23].

Type/material property	α and near α	α+β	β and near β
α-Stabilizing elements	Al, Sn, Ga, Zr, C, O, N		
β-Stabilizing elements			V, Mo, Nb, Ta, Cr
Typical materials	Commercially pure Ti Ti-5Al-2.5Sn Ti-5Al-6Sn-2Zr-1Mo Ti-6Al-2Sn-4Zr-2Mo Ti-8Al-1Mo-1V	Ti-5Al-2.5Fe Ti-5Al-2Mo-2Fe Ti-5Al-3Mo-4Zr Ti-5Al-2.5Fe Ti-6Al-7Nb Ti-6Al-4V Ti-6Al-6V-2Sn Ti-6Al-2Sn-4Zr-6Mo	Ti-3Al-8V-6Cr-4Mo-4Zr Ti-4.5Al-3V-2Mo-2Fe Ti-5Al-2Sn-2Zr-4Mo-4Cr Ti-6Al-6Fe-3Al Ti-10V-2Fe-3Al Ti-13V-11Cr-3Al Ti-15V-3Cr-3Al-3Sn Ti-35V-15Cr Ti-8Mo-8V-2Fe-3Sn Ti-11.5Mo-6Zr-4.5Sn Ti-30Mo, Ti-40Mo Ti-13Nb-13Zr Ti-25Pd-5Cr Ti-20Cr-0.2Sn Ti-30Ta
β-Transus temperature	Higher ←		→ Lower
Specific density	Lower →		→ Higher
Room temperature strength	→		→
Room temperature toughness	→		→
Modulus of elasticity	←		←
Machinability	←		←
Age hardenability	→		→
Heat resistance	←		←
Weldability	←		←
High-temperature strength	←		←
Heat-treatability	→		→
Plastic formability	→		→
Strain-rate sensitivity	→		→
Superplastic formability	→		→
Creep resistance	←		←

According to the needs of the society, the most requested materials based on titanium are commercially pure titanium (CP titanium) and Ti-6Al-4V [10]. CP titanium is considered an α-alloy,

and these alloys are mainly used in the chemical and processing engineering industry, revealing excellent corrosion resistance. By the evaluation of Table 5 it is possible to see that the main difference between the different grades of CP titanium is their content in oxygen. This element is an interstitial alloying element and when combined with small concentrations of other elements (e.g. like iron) it spreads the scopus of utilization of this material. Also, the mechanical properties vary, where grades of higher purity reveal a decrease in strength (Table 6) and have lower transformation temperatures. The grade 2 CP titanium is the most used and has tensile strengths in the order of 390 and 540 MPa [23], and it's the material approached in this master thesis [20] [21].

Table 5 – Chemical compositions of Titanium and its Alloys [9].

Element	Grade 1	Grade 2	Grade 3	Grade 4	Ti6Al4V[a]
Nitrogen	0.03	0.03	0.05	0.05	0.05
Carbon	0.10	0.10	0.10	0.10	0.08
Hydrogen	0.015	0.015	0.015	0.015	0.0125
Iron	0.20	0.30	0.30	0.50	0.25
Oxygen	0.18	0.25	0.35	0.40	0.13
Titanium			Balance		

Table 6 – Mechanical properties of Ti and its Alloys [9].

Properties	Grade 1	Grade 2	Grade 3	Grade 4	Ti6Al4V	Ti13Nb13Zr
Tensile strength (MPa)	240	345	450	550	860	1030
Yield strength (0.2% offset) (MPa)	170	275	380	485	795	900
Elongation (%)	24	20	18	15	10	15
Reduction of area (%)	30	30	30	25	25	45

1.5.2. Titanium Oxide Film

Titanium isn't a material that is selected to be used in several different industries just because of the set of mechanical properties that it reveals. Another property that makes titanium such a requested material is the stability that it shows under corrosion conditions, revealing higher resistance than stainless steels in marine and industrial environments [21][22].

The excellent corrosion resistance of titanium and its alloys is a result of the formation, on the surface of the material, of a stable oxide film of 2 to 7 nm in thickness that is especially adherent and protective. This oxide film forms spontaneously once the material is in contact to air or humidity, due to the great affinity that titanium has to react with oxygen [5] [24]. In addition, if the oxide film is damaged by mechanical action, it has the capability of self-healing (repassivation) in the presence of mediums rich in oxygen (air, water, humidity) [20]. By the other hand, titanium may suffer from crevice corrosion, due to the faster consummation of oxygen in the crevices that will weaken the repassivation

ability if the film is damaged. The physical properties of the oxide film as nature, composition and thickness will depend on the environmental conditions at which the material is exposed. Usually, the passive film is composed by anatase (TiO_2), a tetragonal form of titanium dioxide [(24)] and the most common and stable thermodynamically film. Other crystal structures of TiO_2 are rutile and brookite [(23)]. Along with these properties, the oxide film reveals great chemical resistance in several environments (sulfur, organic compounds and oxidizing acids) and only certain substances like hydrochloric acid, sulfuric acid and phosphoric acid are able to induce corrosion when present in high concentrations and at high temperatures. Fluoride compounds like sodium fluoride (NaF) and hydrofluoric acid (HF) are also responsible for the activation of the surface and corrosion phenomena on titanium [(21)(22)]. The latter is pertinent to the thematic of the present master thesis since several products for oral hygiene (tooth pastes, mouth rinses) contain fluor in their composition and may interfere with the stability of the dental implant [(25)].

The Pourbaix diagram (Figure 4) of titanium shows the range where the passive film TiO2 of titanium is stable.

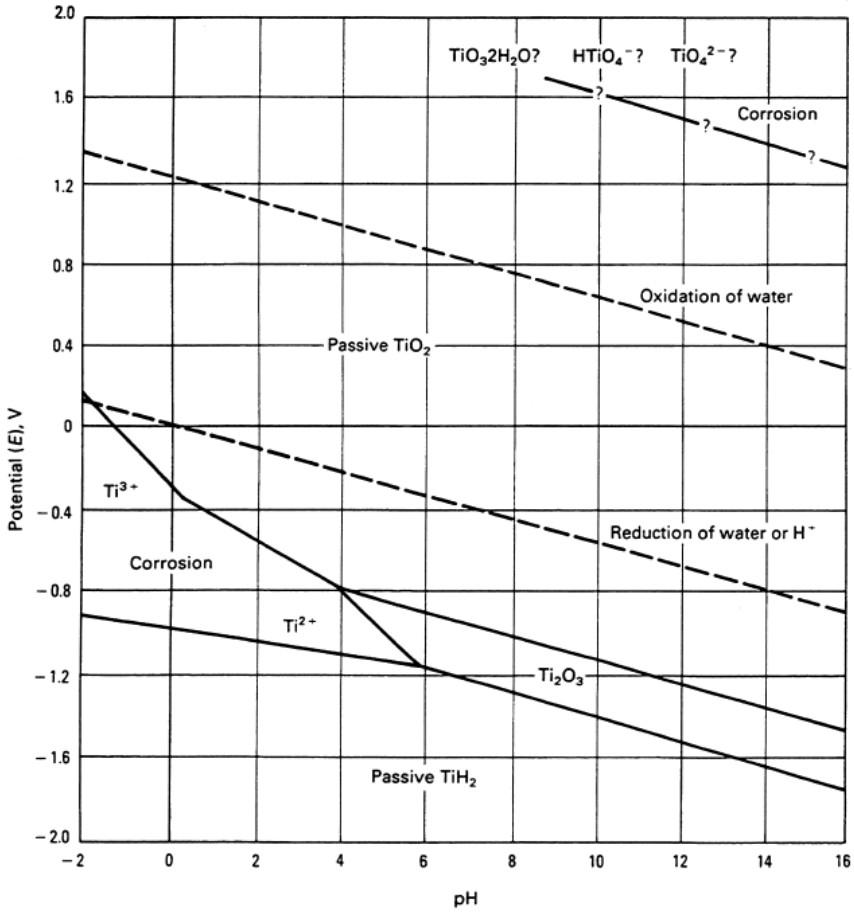

Figure 4 - Pourbaix diagram for Titanium [(21)].

It is possible to acknowledge that the film (TiO_2) is stable over a wide range of pH and at both cathodic and anodic potentials. The passivity zone ends at very low potentials under acidic pH.

When a medical device made of titanium is implanted on the human body, the material will have contact with extracellular body fluids as blood and plasma (aqueous solutions). Due to the nature of the biological fluids, titanium will suffer from a continuous process of partial dissolution and reprecipitation (Figure 5), where the composition and properties of the passive film will change accordingly to the time of exposure and the surrounding environment [26].

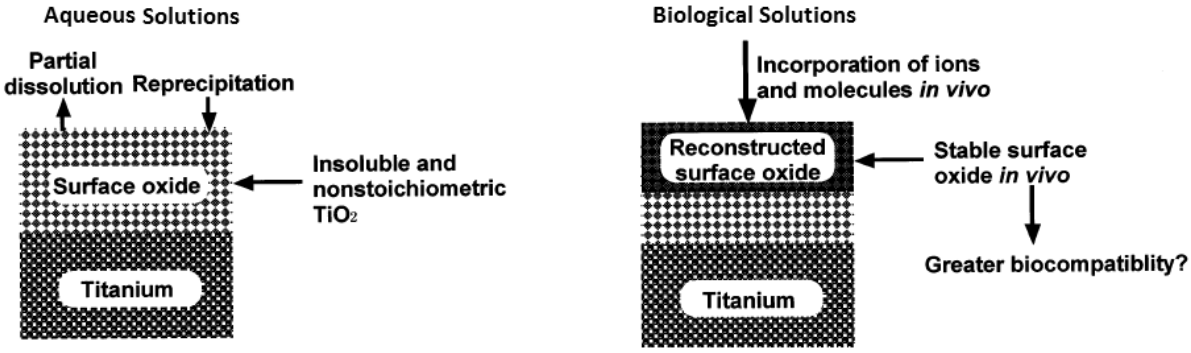

Figure 5 – Schematic of surface oxide film on Titanium [26].

As the scheme of Figure 5 presents, on biological solutions the passive film will incorporate different components (proteins, cells) and especially calcium, phosphorus and sulfur ions [19]. The phosphorus ions will be adsorbed to the surface of the material and after the calcium ions will form complexes with the phosphorus and as the ratio Ca/P increases, this may lead to the precipitation of calcium phosphate. This set the basis for the process known as osseointegration.

Several studies have been made in order to understand the principles behind the passive film of Titanium. Jouanny et al [27] evaluated the structural and mechanical properties of TiO_2 deposited by radiofrequency sputtering on silicon and Ti-6Al-4V substrates. With radiofrequency sputtering it is possible to control variables as substrate to target distance, the total pressure, the oxygen partial pressure and the bias voltage, in order to see the influence of each one on the passive film. It was observed that the crystal phase of the film relies mostly on the total pressure and oxygen fraction applied during sputtering. The films are composed by columns and the rutile phase is present at low pressure, with discontinuous columns and a wavy topography while the anatase phase is present at higher pressure with columns that extend over the whole thickness of the film. The presence of different phases at different pressures is supported by the Ti-O phase diagram that presents the phase boundary regions as function of oxygen and pressure (P_{O2}/P_T and P_T). Concerning the mechanical properties, rutile phase shows a higher hardness against the anatase phase (15 GPa vs 69 GPa, respectively). On the other hand, the evaluation of the passive film of titanium on saline solutions or simulated biological solutions will provide another insight to what happens inside the human body. The electrochemical behaviour of the passive film of CP Titanium, Ti-6Al-4V and Ti-13.4Al-29Nb was assessed as function of immersion time on Hank's solution [28]. Hank's solution is usually used in several works since it is very similar (in ionic composition) with the biological medium. The

potentiodynamic polarization tests revealed stable passive behaviour and similar passive current densities for all alloys, and with the increase of immersion time, the free corrosion potential increased to more noble values. Also, the values of polarization resistance (R_p) of the films, obtained by electrochemical impedance spectroscopy tests (EIS), increased with higher immersion times for CP Titanium and Ti-13.4Al-29Nb, revealing an improvement on the corrosion resistance. However, the Ti-6Al-4V alloy, due to the dissolution of vanadium that will generate vacancies on the oxide film, had a decrease of R_p. By this way, the influence of the alloying elements on the corrosion resistance of Titanium must also be considered. Huang et al [29] characterized the titanium oxide film of Ti Grade 2 grown in saline solution at different sweep rates. The morphology of the anodic films was consistent with an inner compact layer and an outer porous layer. The mainly component of the passive films was TiO_2 but films produced at higher sweep rates presented also hydroxides and lower oxides. This is an indication that the composition of the passive film will depend on the velocity of formation. Also, through the electrochemical point of view, was found a linear increase of the current density and a decrease of the R_p values, both with higher values of sweep rates. Such results state that the protection ability provided by the passive film to Titanium will depend on the conditions of growth of the passive film like, for instance, the velocity of formation of the film. Fonseca et al [30] made another approach to study the corrosion of titanium, by simulating a potential inflammatory response of the human body. Titanium samples were tested in PBS solution where was added hydrogen peroxide (H_2O_2, chemical species produced by white blood cells during immune response) and at pH 5.2 due to the injury made on the biological system. The corrosion resistance of titanium decreased in solutions with H_2O_2 in a relation of 300 times against the control (PBS). This could be result to the adsorption of anionic species to the passive film in the interface oxide/electrolyte, which will increase the oxidation of titanium. When PBS is inserted on the solution, the corrosion resistance increases again, behavior possibly related to the removal of the adsorbed anionic species. The SEM micrographs showed that the surface of titanium is severely attacked by the H_2O_2 through the creation of a porous structure and some pitting attack.

The passivating nature of titanium provides it with a special quality that makes it an ideal material for biomedical applications, especially for implantable devices. However, there are yet several aspects concerning the reactivity of the passive film of titanium and its composition/morphology that are unclear and research must continue to provide a better understanding.

1.6. Surface modification of biomaterials

Several materials in our actual society hold a collection of properties that makes them suitable for a number of applications. In the selection of a material for an application, the properties of the material will be thoroughly evaluated in order to assure that the application will perform its function

properly, when exposed to its operating conditions and during the expected time frame for which the application was designed. The evaluation will gather information on properties such as mechanical, thermal, optical, magnetic and so on, properties of the bulk material. However, besides all this properties, a biomaterial after implantation will react with the human body, not through the properties of the bulk, but through the interaction between the surface of the biomaterial and the biological tissues and fluids. The biomaterial surface holds a huge responsibility in order to prevent the rejection of the material.

In this way, surface modification of biomaterials like titanium, will offer the possibility to provide or enhance specific surface properties like biocompatibility, bioactivity, corrosion and wear resistance, which are different from those in the bulk. Surface modification techniques are divided into mechanical, chemical and physical methods in agreement with the principles of the technique. On this master thesis it will be studied a surface modification technique designed as "Anodic Oxidation".

1.6.1. Anodic Oxidation

Anodic oxidation is an electrochemical technique that allows the improvement of the properties of the passive film of the base metal. As a result, the passive film will reveal an increase of its thickness and if intended, the addition of chemical species to it. As a result of the modification of the properties of the passive film, the corrosion resistance and wear resistance of the surface of the material will be enhanced [(31)].

The setup to make anodic oxidation is simple and doesn't require specific equipment. Figure 6 presents a plan of an anodic oxidation system and the required equipment.

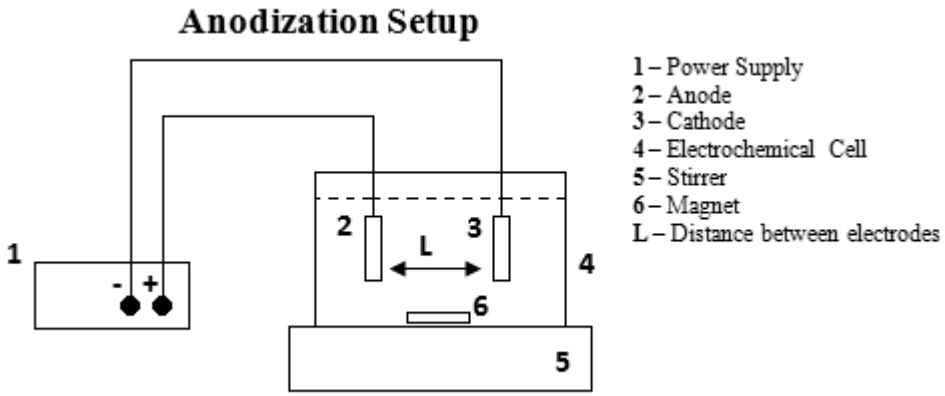

Figure 6 - Scheme of anodic oxidation setup.

The name anodic oxidation or anodization is due to the fact that a DC potential is applied to the anode, which will be the selected material. The electric field created by the potential will cause several interactions between the electrodes and the solution. It will originate the release of ionic species from the cathode (ex. hydrogen) and the diffusion of ionic species to the surface of the anode

(ex. oxygen) as well; species from the solution may be incorporated into the anode. The main parameters of this technique are the potential applied to the anode, the composition of the solution, pH and the temperature [15][32].

The fact that this technique is simple and will improve the qualities of the passive film, makes it an excellent option to be applied in the field of the biomedical devices. In the case of titanium, during anodization the expected reactions are the oxidation of titanium ($Ti \leftrightarrow Ti^{2+} + 2e^-$) and the reaction with oxygen to produce titanium dioxide ($Ti^{2+} + 2O^{2-} \leftrightarrow TiO_2 + 2e^-$) and to allow the growth of the Anodized passive film. The resulted Anodized films are normally micro or nano porous and thick (more than 1000 nm). The porosity will provide rugosity for the cells to attach and develop biological tissue at the surface and the thickening of the film will provide protection against dissolution and corrosion of titanium [15][32][33].

The anodic oxidation of titanium has been studied by some researchers. Won Seol et al [34] observed how the voltage applied during anodization modified the Anodized film. The electrolyte used on the anodization process was a mixture of glycerophosphate (GP) and calcium acetate (CA), in order to attempt to incorporate calcium phosphate (CaP) on the Anodized film, improving the bioactivity of the surface. The substrate material was titanium grade 2. Four voltages were applied (220 V, 260 V, 300 V and 340 V) and with the increasing of the voltage, concerning the morphology and composition, it was possibly to see by SEM that on the surface starts to appear a porous structure, the Anodized film, and the pore diameter increased and the overall porosity decreased. The X-Ray Diffraction (XRD) results revealed that the anatase phase was present in all samples but the rutile phase was only present on the Anodized film produced at 340 V. This might be related to the fact that with higher voltages, the film will be thicker and the crystalline structure changes, being sensitive to referred parameter of the technique. The incorporation of CaP was confirmed by EDS and the Ca/P ratio increased with the applied voltage. The electrochemical behavior of the Anodized samples was studied by potentiodynamic polarization tests. The corrosion resistance of titanium was modified, showing an improvement with the anodization process. The Anodized samples revealed lower passive current densities and more noble corrosion potentials comparing to non Anodized samples. A relation between the corrosion potential and the voltage could be stated (higher anodization voltage provides more noble corrosion potentials) but the same could not be addressed to the passive current density. Krupa et al [35] produced oxide layers enriched with CaP on titanium grade 2 and evaluated the corrosion resistance in similar body fluid (SBF) at 37ºC and pH 7.4, to simulate biological conditions on the human body. The samples were Anodized in solutions with different calcium acetate concentrations (0.2M and 0.4M of CA) and exposed to SBF 13h and 1000h before EIS and potentiodynamic tests, in order to guarantee the stabilization of the potential and the evaluation of long term exposition. Once again, it was possible the incorporation of CaP on the Anodized film through the treatment, the ratio Ca/P was higher for the samples Anodized in solution with higher concentration of CA and the thickness of the passive film increased during anodization. The EIS data were fitted with equivalent

circuits, considering a single barrier (R_b) film for the control group (CP Ti2) while the Anodized film was structured with an outer porous layer (R_p) and an inner compact layer (R_b). The corrosion resistance of the oxidized samples increased (at 13h) but with longer exposure times decreased, accordingly with the values of R_b. However, when one compares these values with the R_p, it is in evidence that the latter reveals an increase with longer exposure times (more evident in the 0.4M CA samples), providing protection against corrosion processes. The composition of the Anodized film may play some effect and the reactions occurring at the oxide/solution interface, allows the formation of precipitates in the pores that will decrease the infiltration of solution to deeper layers of the material and protecting it from dissolution processes. In general, when compared to the control group (CP Ti2), the Anodized samples reveal superior behavior. The potentiodynamic tests at both exposure times confirmed the better corrosion behavior of the Anodized samples, presenting lower passive current densities than CP Ti2, with the sample Anodized with a higher concentration of CA revealing lower values at 1000h of exposure. Further reading can be found [36] [37] [38].

Through the mentioned works it is possible to perceive the importance that each variable of the anodization process may have on the final result. In order to obtain an enhanced corrosion resistance and also to provide bioactivity to titanium, it is necessary to find the specific conditions that will result in the expected outcome.

1.7. Tribocorrosion

1.7.1. Tribocorrosion definition

Tribocorrosion is defined as the conjunct action of electrochemical phenomena and mechanical wear on the surface of a material subjected to a tribological contact, in the presence of a corrosive medium. It encompasses all the aspects related to Tribology (friction, wear, and lubrication) from the contact between the surfaces in relative motion, as all the aspects concerning Corrosion due to the action of the corrosive medium. The materials that are exposed to this type of degradation suffer an irreversible transformation that results from the physico-chemical and mechanical surface interactions occurring at the contact [7] [39].

Several industrial processes present tribocorrosion phenomena like food processing, nuclear reactors, transportation, mining, chemical pumps and cutting tools, as also on the biomedical devices, more specifically on orthopedic implants (knee and hip) and dental implants, being the latter the subject of study of this master thesis [39][40].

1.7.2. Synergism between wear and corrosion

The merger between wear and corrosion has revealed a high level of complexity when one attempts to understand all the phenomena occurring at these systems. Friction will affect the way as the surface of the metal reacts and corrosion will transform the composition and mechanical properties

of the surface, so it is not possible to extrapolate data from just tribological tests or corrosion tests to evaluate the tribocorrosion behaviour of a material [41][42]. This is a characteristic property of tribocorrosion, the *synergism* that exists between wear and corrosion.

When there is a mechanical contact between a passivating metal and a counter-body (Figure 7), a depassivation process of the surface will occur causing a consequent exposure of bare material. This material, in contact with a solution will initiate corrosion processes. Though, if the material has the ability to repassivate in the solution at which it is exposed, the material will be re-protected by the re-growth of the passive film. One should also consider that the previous destruction of the protective passive film by friction, possibly may induce the production of particles (oxide debris), that will be present on the interface acting as a material flux [7][41].

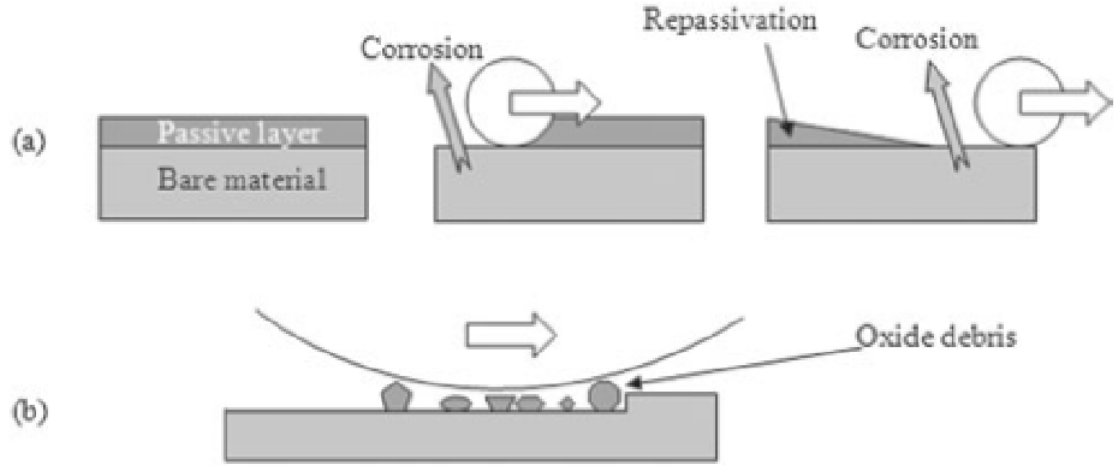

Figure 7 - Schematic representation of (a) corrosion accelerated by friction and (b) abrasion accelerated by corrosion products on passivating metals [7].

This material flux has been reported [42] and is relevant to help understanding the phenomena occurring at tribocorrosion systems. The oxide debris may form “third body effects” on the contact interface, which consequently will affect the tribological conditions and in turn the corrosion behaviour. For example, the particles are produced by classical wear mechanisms as adhesion, abrasion or fatigue and after some sliding cycles, eventually the particles will detach of the surface and will be exposed to the simultaneous effect of the solution and of the tribological contact. From this moment, these particles may undergo a number of transformations that will affect the tribocorrosion phenomena. On one hand, active surface from the bare material will be exposed and will react immediately with the environment, starting corrosion processes, on the other, the particle may be chemically dissolved as ions to the solution, among other phenomena that can occur. The Figure 8 represents all the paths that these oxide debris/particles may follow, being this image no more than a magnification of the contact present on Figure 7 b).

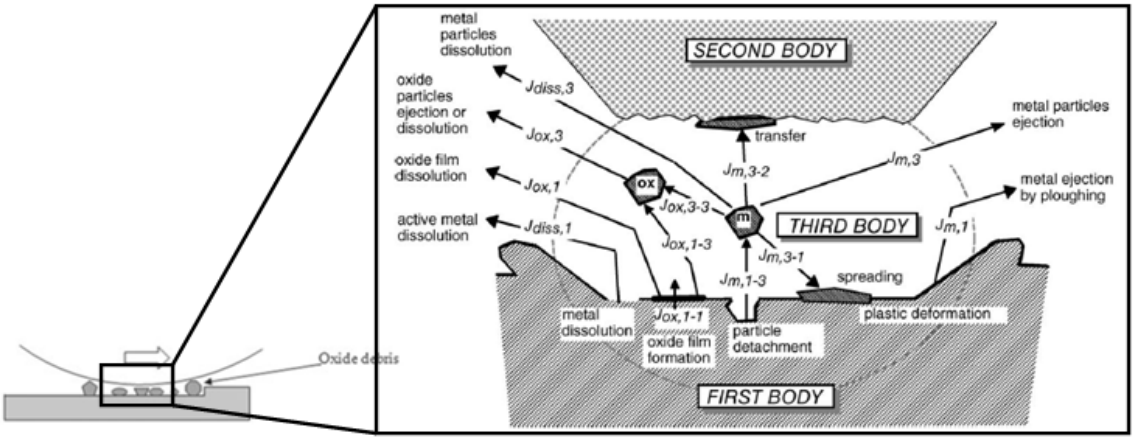

Figure 8 - Fluxes of wear particles on a tribocorrosion system [7][42].

The synergism present in tribocorrosion, was first introduced by Watson et al [43], and can be expressed through the relationship between mechanical and chemical degradation by the following equation:

(1)

where *T* is the total degradation, *W* the degradation due to wear in absence of corrosion, *C* the degradation due to corrosion in the absence of wear and *S* the synergy contribution. It's possible to divide *S* into its two components: the contribution of wear to corrosion and the contribution of corrosion to wear. Some authors [44] may define the synergistic effects with different nomenclatures as so the *ASTMG standard 119-04* "*Guide for Determining Synergism Between Wear and Corrosion*", which defines "*synergy*" as the effect of corrosion on the wear while the effect of wear on corrosion is defined as "*additive*". This standard provides the possibility to evaluate the wear rate attributed to the synergism, on metallic materials, but recently, a new protocol [7] has been developed that allows the monitoring and evaluation of the chemical-mechanical degradation of passivating metallic materials in electrically conductive liquid environments, under periodic mechanical solicitation. Thereby, the passivating nature of some metals is now acknowledged by this new protocol and it aims to complete the *ASTM* standard. This new approach will provide more detailed insight into the phenomena occurring at the sliding contact of a material immersed in a corrosive environment. On the chapter 2 the procedure provided by the protocol is exposed and applied to the present master thesis.

1.7.3. Evaluation of tribocorrosion phenomena

Tribocorrosion focus on the study of the phenomena occurring at the interface of tribological systems exposed to corrosive solutions. In this way, tribocorrosion will depend on the properties of the solution, of the material, on the mechanical and electrochemical properties of the contact and also, if the tribocorrosion system is associated to a living system or a biomedical device, of the biological environment that will contribute with a whole new set of variables (Table 7) [39][40].

Table 7 - Variables affecting tribocorrosion [39][40] [41].

Variables of Tribocorrosion				
Solution	**Material**	**Electrochemical**	**Mechanical**	**Biological**
Viscosity	Hardness	Applied Potentials	Normal Force	Protein
Temperature	Microstructure	Repassivation Kinetics	Sliding Velocity	Cells
pH	Surface Roughness	Film Growth	Contacting Bodies	Biological Fluids
Condutivity	Properties od Passive Film	Rate of Dissolution	Frequency	Biofilms
Dissolved Oxygen	Wear debris		Alignement	

To evaluate the tribocorrosion behavior of certain material, one should have attention to all this variables and attempt to simulate the conditions to which the material will be exposed. The experimental apparatus to evaluate the tribocorrosion performance of a material has to have means to collect information on the mechanical and corrosion responses of the system defined. Basically, to a tribometer, which will record the mechanical parameters, will be associated an electrochemical cell with a reference electrode, a counter electrode and a working electrode (material to be studied), being all this components connected to a potentiostat, in order to evaluate the electrochemical phenomena. In Figure 9 is exemplified such experimental apparatus.

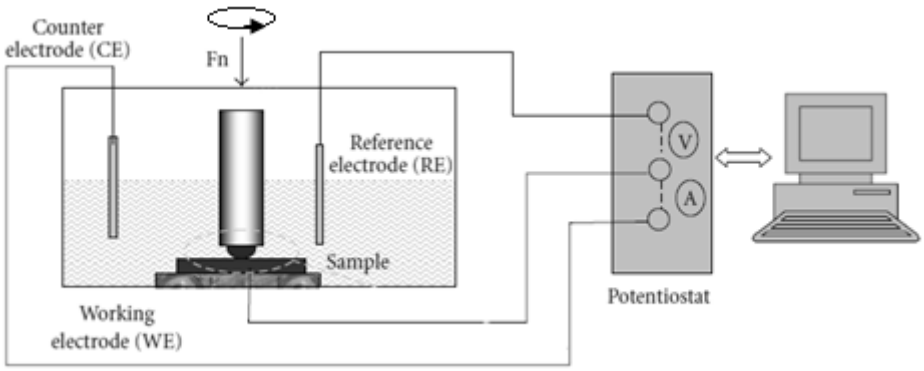

Figure 9 - Experimental apparatus for tribocorrosion tests [39].

The most common experimental arrangements to apply sliding under a tribocorrosion test are unidirectional sliding tests, reciprocating sliding tests and fretting tests (small amplitude oscillation), performed with a counter-body that can be a cylindrical pin or a sphere (Figure 10). The different morphology of the counter-body provides advantages in relation to each other. A flat pin surface has the advantage that the nominal contact area is well defined, a spherical contact is free of alignment problems, but the nominal contact area is less well defined (it is calculated from Hertzian contact mechanics) and it may vary during the experiment due to the evolution of the wear track [41].

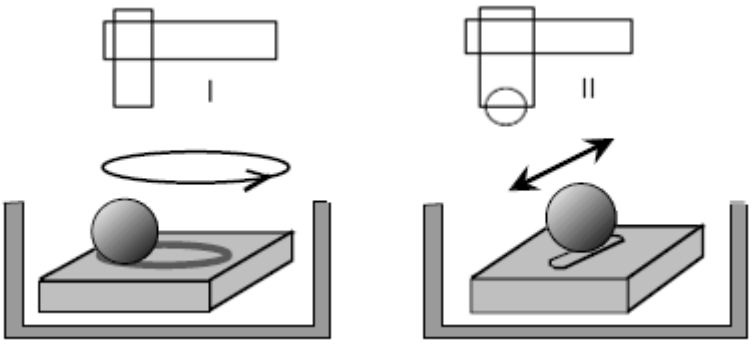

Figure 10 - (I) Cylinder (II) Sphere. (a) Unidirectional Sliding (b) Reciprocating Sliding [41].

1.7.4. Tribocorrosion – Research overview

The fact that tribocorrosion encompasses such a complexity has increased the interest on research, to improve the knowledge on this area. The variables that affect tribocorrosion have been studied by Diomidis et al [45][46] through the application of the protocol that extends the *ASTMG standard 119-04* to passivating metals. The effect of different contact areas on the open circuit potential was demonstrated, where the samples with a superior active area showed more cathodic potentials. This reveals that one should not discard the relevance of the galvanic coupling between active-passive areas on the electrochemical behaviour of the material. Also, the use of continuous sliding tests enabled the evaluation of the behaviour of the passive film under friction while with intermittent sliding tests, the self-healing properties of the film were investigated. Thus, it was possible to observe that with a superior latency time, the corrosive component of the active wear track is the most influential factor on the amount of wear at which the material is subjected.

As well, some industrial areas are interested on the effects of tribocorrosion. For instance, on nuclear power plants, tribocorrosion systems are present on pressurized water reactors (PWRs) [47]. On these reactors exists a control rod drive mechanism (CRDM), made of Stellite grade 6, responsible for the control of the neutron flux in the core of the PWRs. The CRDM can be withdraw, hold or insert full-length according to the needs of the reactor, and operates in an environment characterized by temperatures on the range of 200 and 250°C, in a coolant solution composed by hydrogen, boric acid and lithium hydroxide at 155 bar. Before using this material, laboratory tests have been made to evaluate wear and corrosion, but in the late 1990s, it was found that the wear rates of CRDM on the power plants were around four times higher than predicted. The cycles of passivation and depassivation of the oxide film of Stellite grade 6, due to the movement of the rod, weren't considered and the lifetime of these components were affected. The characterization of the function of the CRDM and its operating environment describes a tribocorrosion system and demonstrates the synergy between wear and corrosion, and explains why the wear rate was higher on the plants than on the laboratory tests. Another industry where tribocorrosion is present is the medical devices industry. Several studies have been made in order to understand the corrosion and tribocorrosion mechanisms

behind the failure of dental implants. The influence of pH and corrosion inhibitors in artificial saliva on the tribocorrosion behaviour of titanium has revealed interesting results, where the addition of citric acid or anodic inhibitor to artificial saliva resulted in a minor enhancement of the tribocorrosion behaviour of titanium under fretting. These components may affect the reactions on the contact area, leading to the formation of a tribolayer which together with the passive film of titanium, protects the material from the corrosion processes and decreased the removal of material [48]. On the other hand, the effect of biofilms formed on dental implants revealed both advantages and disadvantages. The formation of these structures around the implant lowers the pH (presence of microorganisms), leading to the decrease of titanium resistance to corrosion. On the other hand, this "coat" around the implant acts as a lubricant, lowering the friction coefficient [49]. The passive film of TiO_2 has also been evaluated. It is known that the film is thermodynamically stable in the pH range between 2 and 12, but the effect of some chemical species like H_2O_2 (produced on inflammatory responses) can modify the structure of the passive film and decrease the corrosion resistance [30] [50]. Other important factor related to tribocorrosion mechanisms on the human body is related to the biological tissues and fluids. The composition of the oral fluids can differ from person to person, depending on the eating habits of each one. In addition, mouth-rinses and toothpastes, used to prevent caries, are rich in fluoride ions. Though, these ions influence the corrosion resistance of titanium and it has been reported [25] that titanium in contact with fluoride ions reveals a lower corrosion resistance, leading to the dissolution of titanium to the human body. But when was added albumin (a saliva protein), it prevented the corrosion of the material and there was an inferior dissolution of titanium, revealing that this protein aids preventing the corrosion of the implant. So, in this case, the adsorption of a biological element into the implant surface helped against the corrosion of the implant. Other works studied also how the proteins affect the tribocorrosion mechanisms [51][52][53].

In general, tribocorrosion is a multidisciplinary area that presents many challenges and that has still significant progresses to reach. On the biomedical area there are several issues related to this phenomena that need to be overcome, in order to produce better implants to improve the life quality of patients.

Chapter 2 - Materials and Methods

2.1. Materials

Commercially pure titanium grade 2 (Goodfellow Cambridge Limited, England) samples were cut from the same original plate in square form of 20 x 20 x 2 mm. On these samples were applied two different treatments in order to create the Etched group (control) and the Anodized group of samples.

For the Etched group, the samples were cleaned in an ultrasonic bath with acetone for 3 min and after they were Etched in Kroll's reagent (2 ml HF and 10 ml HNO3 in 88 ml H2O) during 10 min. Following the etching with Kroll's reagent the samples were cleaned for 15 min in warmed water (60°C) in ultrasonic bath and left to dry in dry air.

For the Anodized group, following the etching the samples were subjected to anodization. The anodization process was performed in an agitated solution of 0.7 mol/l calcium acetate + 0.04 mol/l β-glycerophosphate, during 1 minute at 300V DC (GPR-30H10D), at room temperature. The anode was a titanium sample and the cathode was a platinum leaf, approximately 8 cm apart. After anodization the samples were cleaned during 10 min in propanol and after 5 min in distilled water, both in ultrasonic bath.

2.2. Materials Characterization

Before characterization the samples were prepared as follows: cleaning in warmed water (60°C) in an ultrasonic bath and dried with pressurized air, and stored for 24h in a desiccator. The storage during 24h in a desiccator allowed the formation of a stable surface film on the Etched test samples and the evaporation of water from the Anodized samples.

The morphology of both group of samples was observed by scanning electron microscopy (SEM) JEOL JSM – T220A SCANNING MICROSCOPE coupled with an Energy Dispersive Spectrometer (EDS) INCA model 5785 from Oxford Systems.

The evaluation of the roughness of both group of samples was done with a Microtopograph (station Micromesure STIL, model CHR150-N, France) with an optic sensor from ZEISS with a range of measurement between 0 and 80 µm and with an Interferometer (New-View 6300, Zygo Corp., Middlefield, CT) with a vertical resolution of 0,1 nm, using a 5× Michelson interferometric objective with a working distance of 9,3 mm and a lateral resolution of 2,72 µm. The methodology applied on the Microtopographer (Figure 11) consisted on 2D evaluation, by taking four profiles from the center of the sample, with a length of 1 mm (step of evaluation of 1 µm and cadency frequency of 300 Hz) and in 3D evaluation, considering the evaluation of 4 squares of 1000 µm x 1000 µm (step of evaluation of 1 µm and cadency frequency of 300 Hz) that were displaced from the center of the sample by ± 4000 µm in X and ± 2000 µm in Y, in order to compare the values.

Figure 11 - Profile and Square evaluation of samples.

For the 2D evaluation, the profiles were treated with a micro-rugosity filter with a cut-off of 0,8 mm separating the roughness from the waviness and the selected height parameters were the Average Roughness, that is the arithmetic average of the absolute values of the roughness profile (Ra) and Single Roughness Depth, that is the vertical distance between the highest peak and the deepest valley (Rz). For the 3D evaluation, the profiles were treated based on the adaptation of the 2D parameters to 3D evaluation, as stated on the recent norm ISO 25178, and the height parameters selected were Sa and Sz, that are analogous to Ra and Rz. For the Microtopograph 6 samples of each were used and for the Interferometer 2 samples of each were used. The value for each parameter is the average of all measurements. The methodology applied on the Interferometer was similar to the one of the Microtopographer, by scanning 4 areas on the surface of the samples like Figure 11 shows. After it were extracted 4 profiles from each surface and performed 2D evaluation. The results were treated with the same micro-rugosity filter mentioned for the Microtopographer results. For the Anodized samples, in order to obtain the interference fringes on the Interferometer, it was necessary to coat the samples with gold. Such procedure has been used to evaluate titanium oxides by White Light Interferometry [(54)] in order to avoid phase shift errors and wrong measurements of real topography.

2.3. Electrochemical Evaluation without sliding

For the electrochemical evaluation without sliding, before the tests the samples were prepared as described on the materials characterization. On the day of the test, the sample was placed on the sample holder and isolated with an insulating silicone, in order to have just the sample surface (working electrode) exposed to the solution. The silicon was left to dry for 1 hour.

The electrochemical tests performed to study the state of the material on the selected electrolyte were the Open Circuit Potential (OCP) and Electrochemical Impedance Spectroscopy (EIS). The OCP test was measured right after the immersion of the material on artificial saliva for approximately 18 hours and the EIS measurement was performed after 5 hours of immersion. A three electrode system was used, with a platinized titanium gauze as counter-electrode, a reference electrode of Silver/Silver Chloride (Ag/AgCl) with a potential of + 0.019 V vs. Natural Hydrogen Electrode (NHE) and the sample as working electrode. The electrochemical measurements were done with a potentiostat Solartron ELECTROCHEMICAL INTERFACE SI1287 and a Solartron Schlumberger 1250 FREQUENCY RESPONSE ANALYSER connected to a computer with *Corrware* and *ZPlot*

software. EIS data were obtained by applying a sinusoidal signal of ±10 mV over the E_{oc} of the sample recorded. The electrode response was analyzed in the range of 10 kHz to 10^{-3} Hz.

The impedance spectra that resulted from the EIS measurements were interpreted by using equivalent circuits in the software *ZView*. For the Etched samples the fitting was obtained with the circuit in Figure 12A (Randles circuit) and for the Anodized samples the fitting was obtained with the circuit in Figure 12B. The latter considers the existence of a thicker layer and represents the porous structure of the Anodized passive film. In the circuits the elements represents: R_s, solution resistance, R_p, resistance of passive film, CPE_p, constant phase element associated with passive film, R_{pp}, resistance of porous structure, CPE_{pp}, constant phase element associated with porous structure, R_{pb}, resistance of barrier film, CPE_{pb}, constant phase element associated with barrier film.

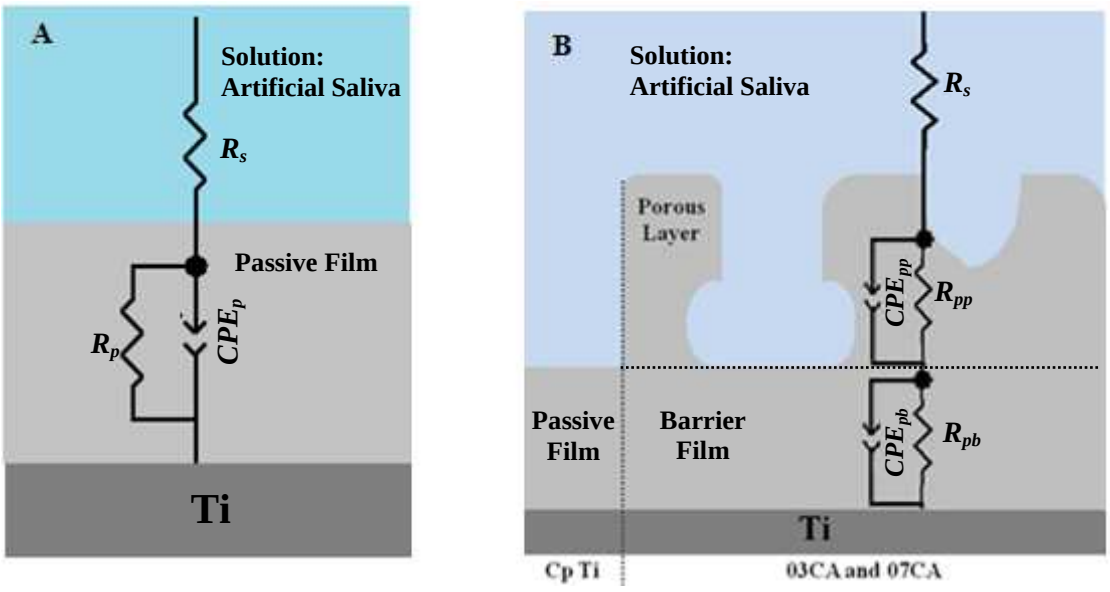

Figure 12 - Equivalent circuits: A) Etched Samples B) Anodized Samples.

With the software *ZView* it was performed the fitting and obtained the values of R_s and R_p for the Etched samples. In this way the specific polarization resistance (r_p) was calculated as $r_p = R_p . A_o$ (2) with A_o the total area of the sample that is exposed to the electrolyte. The corrosion current density (i) is given by $i = \frac{B}{r_p}$ (3) with B a constant that for many metallic materials has a value between 13 mV and 35 mV and in the present work an intermediate value of 24 mV was used. For the Anodized samples the fitting provided the R_{pp} and R_{pb} and the specific polarization resistance of the porous and barrier layer were calculated replacing R_p on equation (2) with the polarization resistance of the porous layer and of the barrier layer and the corrosion current density by replacing r_p by the specific polarization resistance of barrier film (r_{pb}) on equation (3).

2.4. Tribocorrosion Testing

The tribocorrosion characterization of the samples is based on the study of the influence of the normal load, of the velocity of sliding and on the presence of a biological layer on the surface of the material.

2.4.1. Samples Preparation for tribocorrosion testing

For the tribocorrosion characterization, before the tests the non-biomodified samples were prepared in an analogous method to the material characterization. On the day of the test, the sample was placed on the sample holder and isolated with an insulating silicone, in order to have just the sample surface (working electrode) exposed to the solution. The silicon was left to dry for 1 hour. Finally the sample was placed on the tribometer, the horizontality was verified and the test was started.

The biomodified samples had different preparation. Both sets of biomodified samples were prepared at *Université Paris 13 Nord* by *Helena Felgueiras* and first the samples were sterilized accordingly to the following protocol:

- 4 hours in NaCl 1.5M solution,
- 4 hours in NaCl 0.15M solution,
- 12 hours in PBS (Gibco),
- 15 min in U.V. light sterilization (each side of the samples),
- 24h in Dulbeco's Modified Eagle Medium (DMEM) at 37°C + Fungizone (Gibco) + Penicillin Streptomycin (Gibco),
- 12 hours in DMEM.

After, the osteoblastic cells were cultivated on the samples. It was used a primary cell line of osteoblasts MG63 and 1 million cells were placed on the well. The cells were left on the incubator during 5 days and maintained at 37°C and 5% CO_2. The composition of the culture medium is given in Table 8.

Table 8 - Chemical Composition of Culture Medium.

DMEM	FBS	Ps	Fz
88%	10%	1%	1%

On the day of the tribocorrosion test, the biomodified samples were moved to École Centrale Paris. Between the transport and the preparation of the sample (isolation of sample holder) to start the test, in average were passed 1h30m. The samples were identified as BioEtched samples and BioAnodized samples.

2.4.2 Tribocorrosion conditions

Sliding tests combined with in-situ electrochemical measurements grant the possibility to evaluate the tribocorrosion behavior of the material. Unidirectional sliding tests were done with a unidirectional pin-on-disc tribometer (Multispecimen-tester, FALEX-TETRA) stationed on a stabilizer table (Vibration Isolation System with StabilizerTM Technology, BenchTopTM, Newport) in order to avoid interferences to the test. Before the sliding tests the counter-body was degreased with ethanol in ultrasonic bath for 5 min. The counter-body was an alumina ball (Al_2O_3 yield strength = 15.4 GPa) of 10 mm diameter and the normal load applied was 0.4 N and 0.8 N (204 MPa and 258 MPa, respectively), in order to understand the corrosion and wear processes on titanium and on the surface treatment as well. The mentioned normal forces were selected to generate a maximum Hertzian contact pressure smaller than the yield strength of C.P. Ti grade 2 (275 MPa) to avoid plastic deformation. The radius of the sliding was defined as 4 mm and the tests were carried with two distinct velocities, 100 rpm (1,67 Hz) and 2 rpm (0,032 Hz), and the number of contact events was 7200. Simultaneously, electrochemical measurements that consisted of open-circuit potential (E_{oc}) and electrochemical impedance spectroscopy (EIS) were done before and during sliding. After sliding an open-circuit potential was performed. A three electrode system was used, with a platinized titanium gauze as counter-electrode, a reference electrode of Silver/Silver Chloride (Ag/AgCl) with a potential of + 0.019 V vs Natural Hydrogen Electrode (NHE) and the sample as working electrode. The electrochemical measurements were done with a potentiostat Solartron ELECTROCHEMICAL INTERFACE SI1287 and a Solartron Schlumberger 1250 FREQUENCY RESPONSE ANALYSER connected to a computer with *Corrware* and *ZPlot software*. EIS data were obtained by applying a sinusoidal signal of ±10 mV over the E_{oc} of the sample recorded before or during sliding tests. The electrode response was analyzed in the range of 10 kHz to 10^{-3} Hz before sliding and from 10 kHz to 10^{-2} Hz during sliding. The tribocorrosion behavior of the non-biomodified and biomodified samples was evaluated in Fusayama artificial saliva solution at room temperature buffered to a pH of 5.5. The buffer solutions were NaOH and KCl. The chemical composition of the Fusayama artificial saliva is given in Table 10. In Figure 13 it is presented a scheme of the tribocorrosion setup and in Figure 14 a picture of the tribocorrosion setup. Table 9 shows the identification of the samples.

Table 9 - Samples identification and test conditions.

Type of Sample	*Non Biomodified*				*Biomodified*	
	L = 0,4 N		*L = 0,8 N*		*L = 0,4 N*	*L = 0,8 N*
	100 rpm	*2 rpm*	*100 rpm*	*2 rpm*	*100 rpm*	
Ecthed	E10		E16		BE2	BE5
	E12	E19	E17	E21	BE3	BE6
	E15		E18		BE4	BE7
Anodized	A32		A30		BA1	BA4
	A37	A425	A51	A426	BA2	BA5
	A63		A65		BA3	BA6

Table 10 - Chemical Composition of the Fusayama artificial saliva (g/L).

NaCl	KCl	$CaCl_2.2H_2O$	$Na_2S.9H_2O$	$NaH_2PO_4.2H_2O$	Urea
0,4	0,4	0,795	0,005	0,69	1

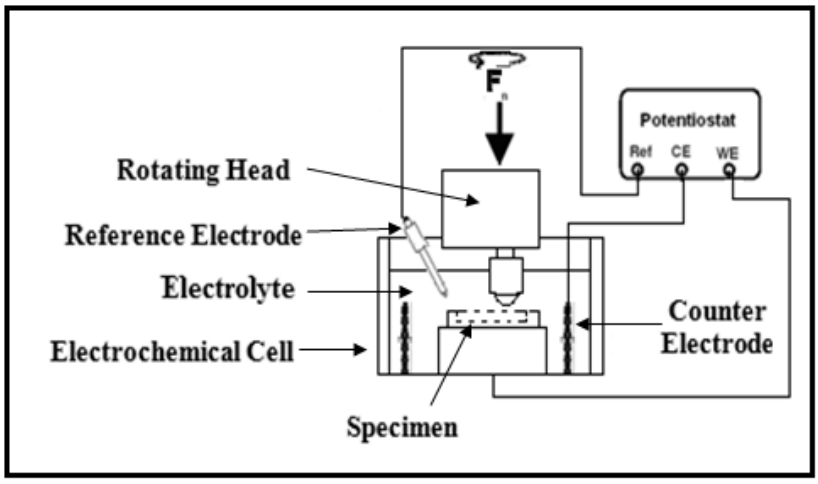

Figure 13 - Tribocorrosion setup scheme.

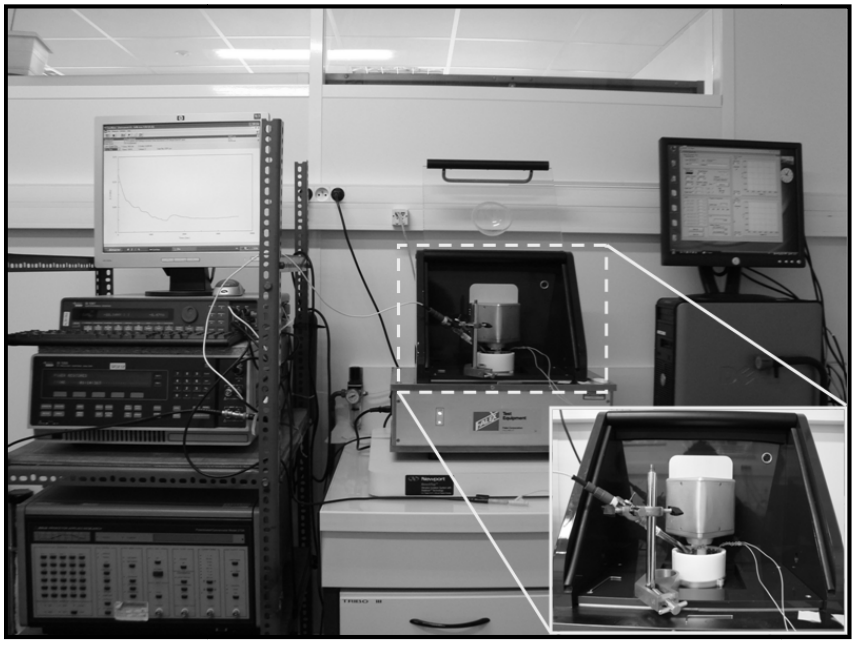

Figure 14 - Tribocorrosion setup in École Centrale Paris.

After the tribocorrosion tests, the morphology of the wear track was evaluated by SEM and Microtopography. In order to obtain the wear track volume, square evaluation (Figure 15) was also performed on 4 places of the wear track (0°/ 90°/180°/270°) and the dimension of the squares were of 2000 µm x 500 µm (step of evaluation of 1 µm and cadency frequency of 300 Hz).

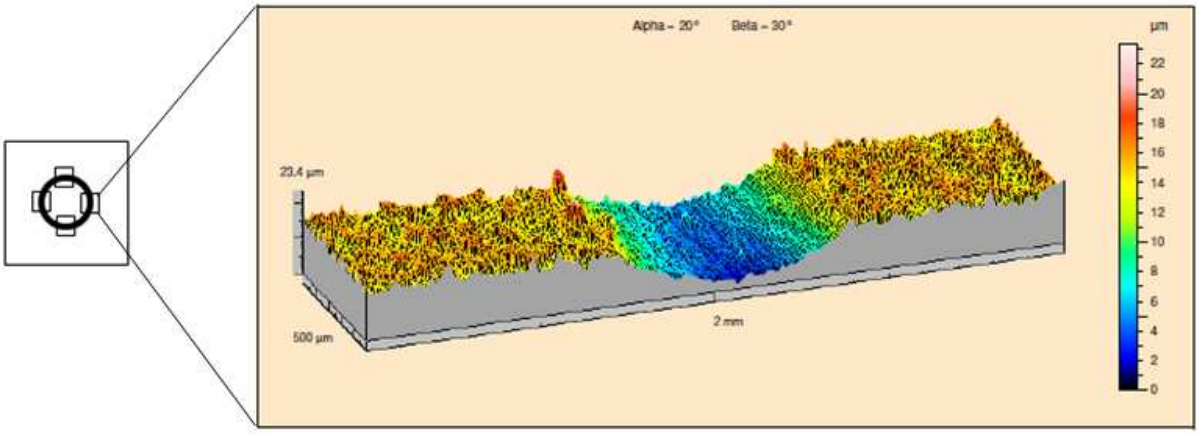

Figure 15 - Evaluation of the wear track with 2D microtopography.

2.4.3. Electrochemical Impedance Spectroscopy analyzes under sliding

The EIS measurements during friction were treated accordingly to the protocol *"A methodology for the assessment of the tribocorrosion of passivating metallic materials"* [(55)], with the same circuits presented previously (Figure 12) and allow the collection of the values of the polarization resistance of the active area in the wear track, R_{act}, the specific polarization resistance of the active material, r_{act}, and the corrosion current density of the active material, i_{act}, for the Etched samples. In order to calculate this variables, at first is necessary to distinguish the total area of the sample that is exposed to the electrolyte, A_o, and the area of the sliding track, A_{tr}, both represented schematically in Figure 16.

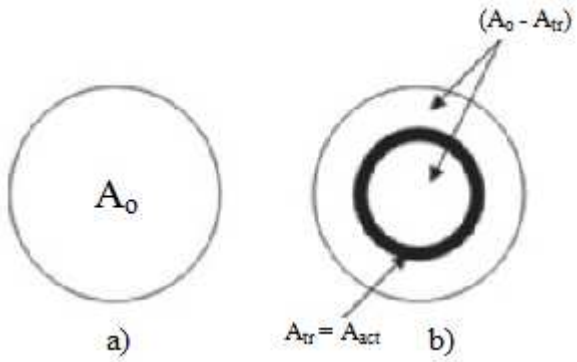

Figure 16 - a) Total area exposed to electrolyte b) Area of the sliding track [(55)].

A_{tr} will be obtained through microtopography, collecting the values of the average track width, e, and with the length of the sliding track, L: $A_{tr} = eL$. In a continuous sliding test A_{tr} is considered to be equal to the active area of the sliding track, A_{act} . The latter will be characterized by a polarization resistance R_{act} and the area outside the wear track (A_o-A_{tr}) is considered to be in a passive state characterized by a polarization resistance R_{pass}. In this way the polarization resistance under sliding is:

$$\frac{1}{R_{ps}} = \frac{1}{R_{act}} + \frac{1}{R_{pass}} \quad (4)$$

with R_{pass} given as:

$$R_{pass} = \frac{r_p}{(A_0 - A_{act})} \quad (5)$$

with r_p the specific polarization resistance of the passive material before sliding. At this point it is possible to calculate r_{act} as $r_{act} = R_{act}.A_{act}$ (6) and i_{act} as $i_{act} = \frac{B}{r_{act}}$ (7).

2.5. Wear Quantification

In order to evaluate the contribution of all the phenomena in a tribocorrosion mechanism to the material loss, in the present master thesis is applied the protocol previously referred [55]. With the microtopographic evaluation of the wear track it is possible to obtain the average area of the cross-section of the wear track, *S*, to calculate the wear track volume $V_{tr} = SL$ and the corresponding mass loss, $W_{tr} = SLd$. Afterwards, the overall material loss that results from the synergism between wear and corrosion may be expressed through the relationship between mechanical and chemical degradation:

$$W_{tr} = W_{act}^{c} + W_{act}^{m} \quad (8)$$

with W_{tr} the material loss in the sliding track, W_{act}^{c} the material loss due to corrosion of active material in the sliding track and W_{act}^{m} the material loss due to mechanical wear of active material in the sliding track.

The test configuration in a continuous unidirectional sliding mode results in the formation of a permanent reactive sliding track. From this, it is possible to calculate W_{act}^{c} from the Faraday's law as:

$$W_{act}^{c} = \left(\frac{C}{F.d}\right).i_{act}.A_{act}.N.t_{lat} \quad (9)$$

with d the density of the material, F the Faraday constant (*96.485C*), i_{act} the corrosion current density of the active material, A_{act} the active area of the sliding track , N the number of cycles and t_{lat} the latency time that is the time between two contact successive events at a given point in the sliding track. In a continuous unidirectional sliding test t_{lat} is equal to the rotation period, T_r. In equation (9), since in the present work it has been evaluated a pure metal and not an alloy, C is given by $C = \frac{M}{n}$ (10), with M the molecular weight of titanium and n the number of electrons involved in the oxidation process of titanium ($n = 4$).

The material loss due to mechanical wear of the active material, W_{act}^{m}, will be obtained as:

$$W_{act}^{m} = W_{tr} - W_{act}^{c} \quad (11)$$

2.6. Characterization techniques

2.6.1. In-situ techniques

The following techniques are classified as in-situ techniques, since they allow the monitoring of the electrochemical reactions and the evaluation of the state of the surface of the material in real time, during the mechanical solicitation induced on the material. This is very important to provide the possibility of determining the amount of metal transformed in oxide or dissolved, in a tribocorrosion system.

2.6.1.1. Open Circuit Potential (OCP)

The open circuit potential is a technique that allows the monitoring of the surface state of a material in contact with an electrolyte. Thus, it will be possible to evaluate the electrochemical reactions occurring at the surface of the material and distinguish the tendency of the material to corrode. This technique relies on the recording of the potential difference between the surface of the material and a reference electrode. The potential difference measured between the material and the reference electrode is the Corrosion Potential (E_{corr}) of the material in the tested electrolyte. In that case, the material will be in equilibrium with the electrolyte and the velocity of oxidation will be equal to the velocity of reduction. There are different reference electrodes available, and each one has a set of properties that makes them suitable for measurements at different conditions, like at high temperatures [(56)(57)].

In a tribocorrosion system, the surface of the material will be subjected to mechanical solicitations and the knowledge of which electrochemical reactions are occurring (oxidation or reduction), are of extreme importance to determine the degradation rate of the material. Passive metals are known to exhibit noble potentials due to the formation of the passive film that protects the bare surface against corrosion. But, if the film is disrupted by mechanical action, the bare material is exposed and oxidation of the metal starts shifting the potential to less noble values. OCP technique permits the visualization of the shift and of the potential recorded during friction, which will be a galvanic coupling between the worn material and the unworn material. Ponthiaux et al [(58)] identified four parameters affecting the corrosion potential during friction: (1) the intrinsic corrosion potentials of the worn and unworn surfaces, (2) the ratio between worn and unworn areas, (3) the relative position of worn and unworn areas and (4) the mechanisms and kinetics of the involved reactions. However, a precise description of the local surface conditions inside and outside the wear track is not yet possible with OCP measurements and one of the drawbacks of OCP is that it doesn't provide information on the kinetics of the reactions of passivation. New approaches have been studied [(59)] but also other electrochemical techniques may be explored to contribute with new information for the study of a tribocorrosion system.

2.6.1.2. Electrochemical Impedance Spectroscopy (EIS)

The electrochemical impedance evaluation is a method that allows the investigation of the corrosion mechanisms and their capacitance and charge-transfer kinetics, completing the information provided by the evaluation of the potential [57][60]. This technique requires that the electrochemical system is in a quasi-steady state condition, meaning that the potential of the material to be evaluated should not present significant fluctuations ($\Delta E_{oc} < 1mv.min^{-1}$) [55]. The measurement of the impedance is made through the imposition of a small amplitude sinusoidal signal (± 10 mV) that will generate only a small perturbation on the open circuit potential of the tested material, while the frequency of the sinusoidal signal will change in a defined range of frequencies. The resulted response of the system to the perturbation is measured with a potentiostat and a frequency response analyzer.

By this way, it will be possible to obtain the polarization resistance of the passive film. The information from the impedance measurements may be displayed with Nyquist plot and with Bode plot. In the Nyquist plot, the imaginary component (*Z"*) of the impedance is plotted against the real component (*Z'*), resulting in a semicircle centered on the real axis (Figure 17). The distance between the imaginary axis and the first point gives the resistance of the solution (R_s) and the point where the semicircle crosses the real axis gives the polarization resistance (R_p) of the material.

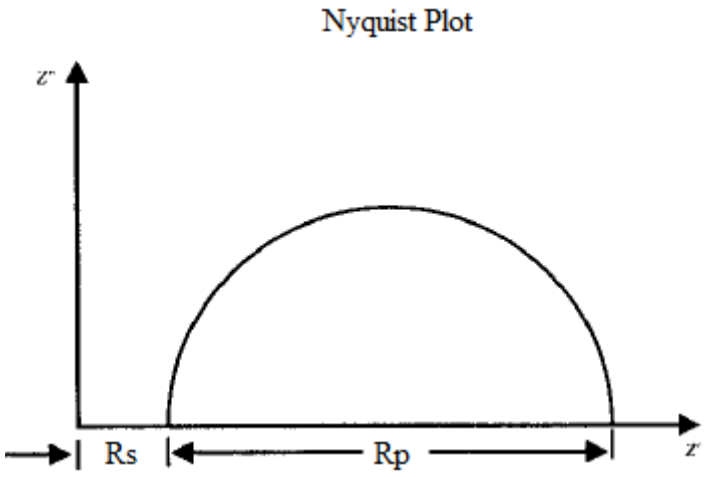

Figure 17 - Nyquist plot [56].

Through the evaluation of the R_p values is possible to characterize if the surface is in a passive state ($Rp \geq 100\,000\ \Omega.cm^2$) or in an active state ($Rp \leq 1000\ \Omega.cm^2$) [55]. In addition, with the polarization resistance of the material is possible to obtain the corrosion current of the material [58]. Due to the fact that the evaluation at very low frequencies may take several hours and the plot may not cross the real axis, extrapolating methods in software's (*ZView*) are used to calculate the system parameters. The extrapolating is obtained through equivalent circuits like the ones previously presented (Chapter 2) that will use electrical components to simulate the resistive and the capacitive behaviour of the passive film.

The Bode plot illustrates the magnitude of the impedance |Z| in log scale versus the frequency on a log scale and the phase angle against the log frequency (Figure 18).

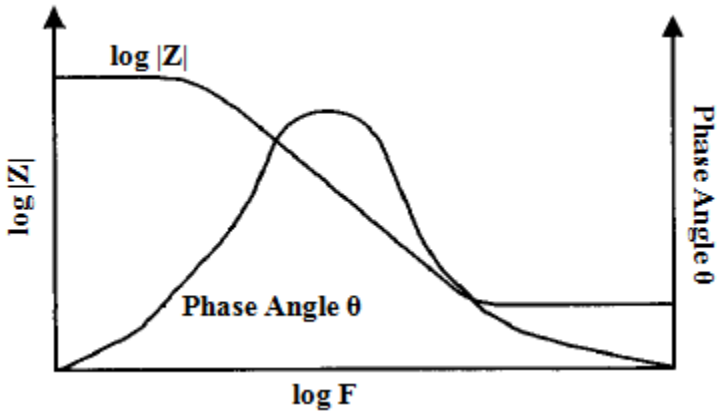

Figure 18 - Bode plot [56].

This plot turns the evaluation of the total impedance of the system easier than the Nyquist plot and the phase angle may provide some information on the state of the surface of the material [60][56][61].

Both electrochemical techniques allowed the assessment of the electrochemical behavior of the samples studied on this master thesis, before, during and after friction, with the information of OCP being completed with data collected from EIS.

2.6.2. Ex-situ techniques

The ex-situ techniques are those that allow, after the tribocorrosion experiment, the evaluation of the state of the surface of the tested material and the characterization of the mechanisms that affected the surface of the material. It's a group of techniques used to identify and follow the evidences left by the tribocorrosion process.

2.6.2.1. Scanning Electron Microscopy (SEM)

SEM technique is one of the scientifical techniques that is transversal to several areas of research. Since its commercial availability in 1965, it has been subjected to several design modifications to decrease the size of the equipments, to improve their ability in imaging resolution and to make the equipment more user-friendly.

The principal characteristics that make SEM such a required technique are its large depth of field and its resolution [62]. The depth of field allows a focalized visualization of a certain area of the sample and its three dimensional structure while the resolution is related to the ability to distinguish closely spaced features at high magnifications. The operating principle of SEM is based on the use of an electron beam to scan the surface of the sample. In order to create the electron beam, a filament of tungsten is heated by the passage of an electrical current and releases electrons. The electrons are

guided by a series of magnets, which are the lenses of the electron microscope, which will focus the beam to the sample and scan the surface. The interactions of the electron beam with the surface of the sample will incite the ejections of backscattered and secondary electrons from the sample, which will be captured by detectors that converts them into an image. The only requirement for the samples to be visualized on SEM is that they must be electrically conductive [(63)(64)].

SEM is mainly used to characterize the morphological aspects of the sample, to observe the crystal structure and also to evaluate the chemical composition of the sample. The latter is performed by the coupling of Energy-Dispersive Spectroscopy equipment that will provide the chemical composition of the sample within a maximum depth from the surface of the sample, depending on the equipment. In addition it is possible to perform spatial evaluation of the distribution of the elements (elemental maps), to see if exists preferential zones with a specific chemical composition [(65)].

All this properties makes SEM an indispensable tool to the thorough evaluation of materials and degradation processes of materials. The SEM equipment of École Centrale Paris is represented in Figure 19. On the present work, SEM was a helpful tool to characterize the morphology and the chemistry of the surface of the samples before the tribocorrosion tests and after, enabled the evaluation of the morphology of the wear track in order to identify the wear mechanism and to see if some chemical species were adsorbed or transferred to the material.

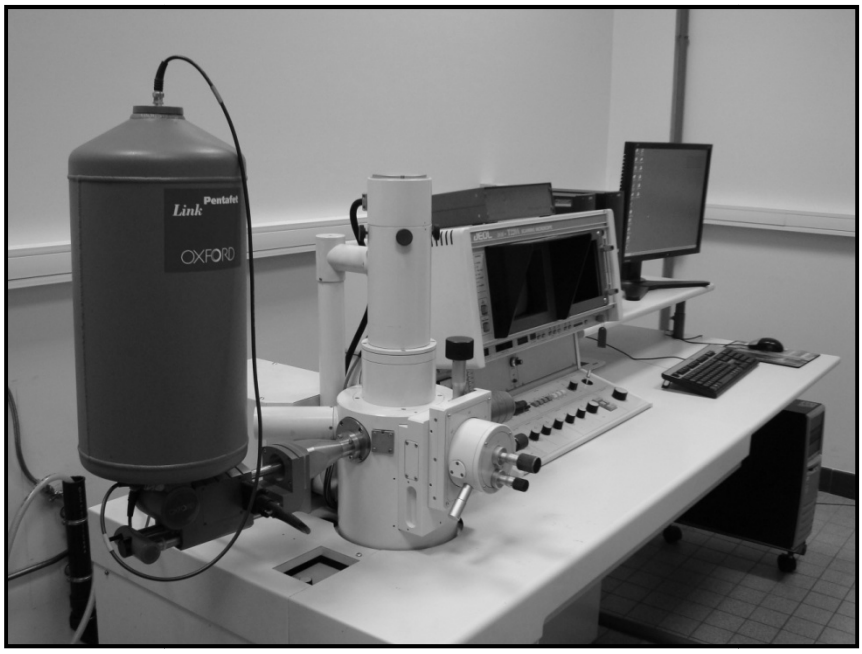

Figure 19 - JEOL JSM – T220A SCANNING MICROSCOPE coupled with an EDS INCA model 5785 from Oxford Systems.

2.6.2.2. Microtopography

Surface topography is a very important characteristic of a material, since the contact between any components is made by the surface. The imperfections found in one surface influence the

chemical reactions and the roughness will dictate the mechanical behaviour of the contact and the resulting wear [66]. The surface of a material can be characterized by several parameters, but the most important and common parameter to characterize the topography of a material is the average rugosity (Ra). The average rugosity of a material (Ra) is the arithmetic average of the absolute values of the roughness profile ordinates [67].

Microtopography technique is very useful to evaluate the surface rugosity of a material and also to evaluate the wear track. The measurements of microtopography are made by contact methods and non-contact methods [68]. In contact methods, there is a stylus tip that is in direct contact with the surface of the material and is connected to a displacement sensor that will provide the surface topography of the material evaluated. These techniques are being replaced due to the fact that the direct contact with the surface will damage the surface of the material and modify the properties of the surface, turning the sample non useable after the measurements. Non-direct contacts like AFM or Confocal Chromatic Technology are preferred to obtain the topography of the materials [69] [70]. The latter is specific for the equipment available at the laboratory of École Centrale Paris (station Micromesure STIL, model CHR150-N, France) and was on this technique that the topographic measurements were based. The equipment is composed by a displacement table in the X and Y axes, which moves the sample in those directions. When performing a measurement, the sample is under an optical sensor that sends to the surface of the sample a beam of white light and analyzes the reflected beam, with the help of a confocal microscopy device that has incorporated a chromatic lens. On the surface, the reflected beam will be composed by a certain wavelength that is focused at the surface. The chromatic lens permits the interpretation of the surface rugosity by the evaluation of the specific wave length that was reflected by the sample, and then determines the specific position in the measuring field. As the sample is in a displacement table, it is possible to define in which axis or axes the sample will be analyzed, the step of the measurement and the frequency at which the points will be measured. Another possibility of this technique is that permits not only the evaluation of profiles (2D evaluation) but also the evaluation of a certain area of surface (3D evaluation), where the sample will be displaced in both axes and the sensor will measure a series of profiles parallels among them. With the information from a 3D measurement it is possible to create 3D models of the area analyzed in order to obtain a better visualization of the surface [69]. In Figure 20 is possible to distinguish the 2D evaluation and the 3D evaluation of a sample and in

Figure 21 is the microtopographer of École Centrale Paris.

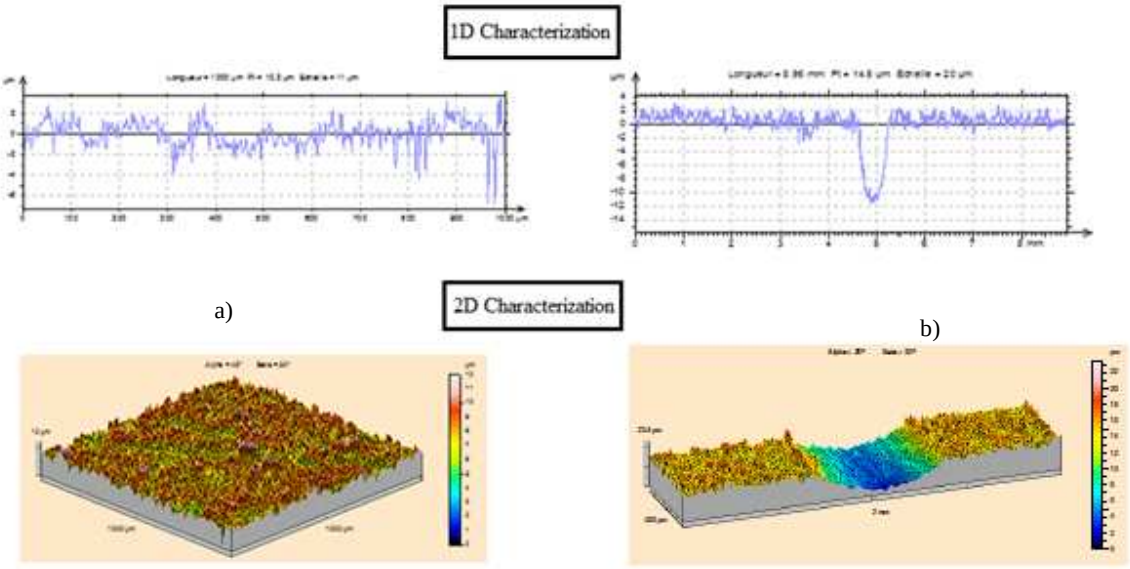

Figure 20 - 2D and 3D Characterization of material: a) before friction and b) after friction.

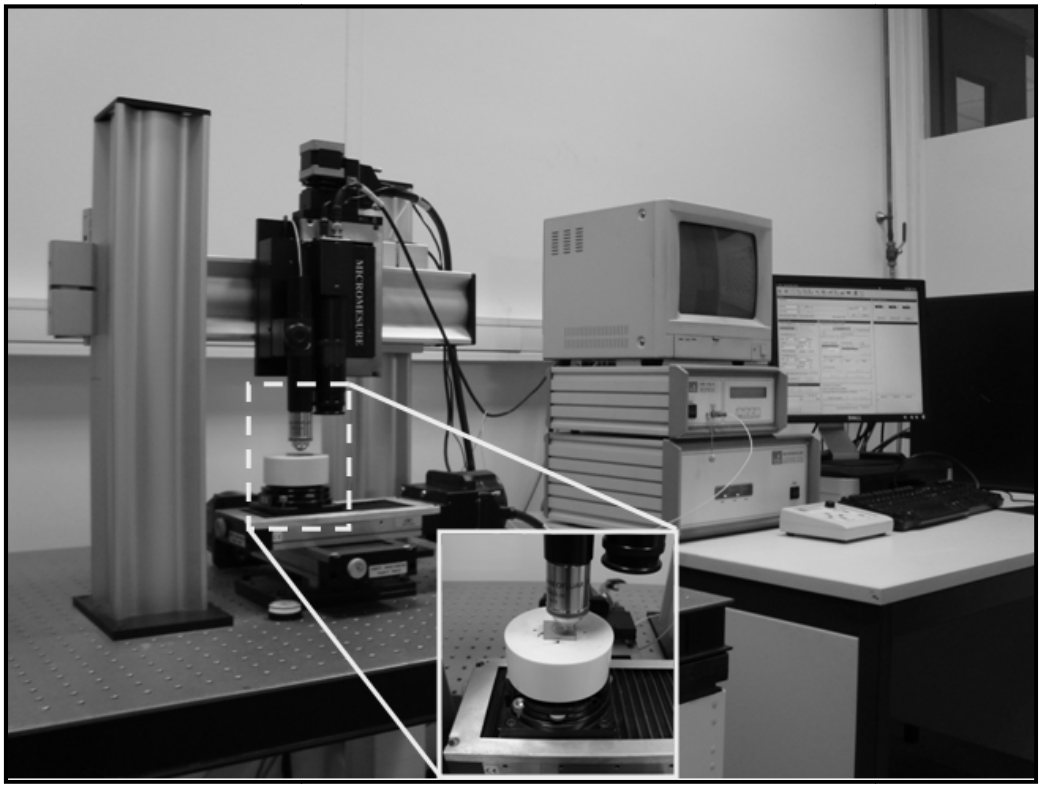

Figure 21 - Microtopographer of École Centrale Paris.

With the microtopographer it was possible to perform the surface evaluation of the samples and the characterization of the wear track volume that resulted from the tribocorrosion tests.

2.6.2.3. Interferometry

The Interferometer is an equipment that allows the measurement and the evaluation of the surface topography as well. It's based on white light Interferometry, so it's a non-contact method as the microtopography.

The scanning interferometry of white light is used to characterize and measure the surface of samples providing a structural analysis of the surface without touching it (non-contact method). The light beam emitted by the microscope is divided in two parts, within the interferometer, one comes to reflect on the monitored surface and the other in an area of high-quality reference surface, internal to the objective. The two beams are then recombined and directed to a camera based on semi-conductors (CCD). The interference between the two light waves creates an interferogram consisting of black and white stripes, called fringes, whose shape represents the surface structure of the analyzed surface. The measured sample is scanned vertically by moving the objective with a piezoelectric transducer. When scanning through the lens, the video system records the variation of intensity of each pixel of the camera. These intensities are converted to a scale of heights by the software MetroPro. In addition, images of the examined surface are displayed on the screen (window in real time). The measurements are performed in three dimensions: the vertical measurements, perpendicular to the surface, are performed by interferometry, the cross-cutting (transversal) measures, in the plane of the surface, are carried out by calculating the pixel size depending on the field of view of the used objective. These techniques allow the analysis and quantification of the surface topography of samples. On Figure 22 it's represented the interferometer available at École Centrale Paris.

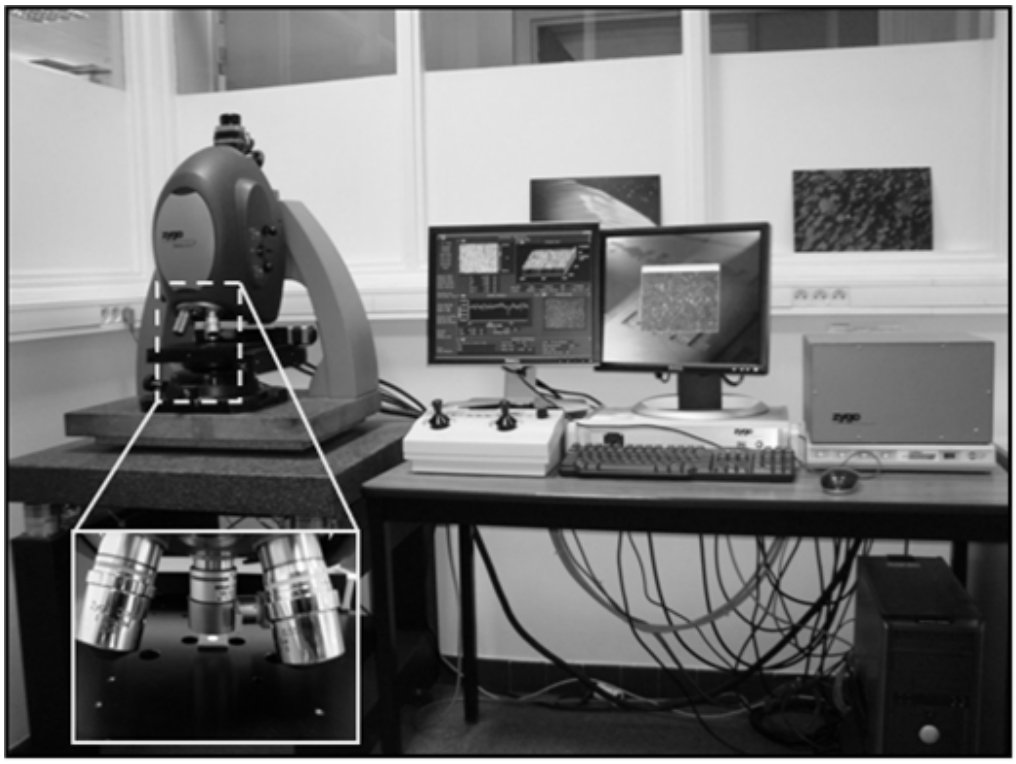

Figure 22 - Interferometer of École Centrale Paris.

Chapter 3 - Results and Discussion

In this chapter the results obtained for the evaluation of Etched titanium and Anodized titanium are presented and discussed. First is presented the material characterization by Scanning Electron Microscopy (SEM) to visualize the morphology and chemical composition of the material and the topographic characterization of the material by Confocal Chromatic Microscopy and by White Light Interferometry.

After, by Open Circuit Measurements (OCP) and Electrochemical Impedance Spectroscopy (EIS) is evaluated the electrochemical behaviour of the material without sliding.

Furthermore, the tribocorrosion behaviour was assessed by coupling electrochemical equipment to a tribometer, to study the passive properties of titanium and the properties of the Anodized film under friction by OCP and EIS under continuous unidirectional friction. The effect of normal load, velocity and the presence of a cell layer on the surface of the material will be presented and discussed.

Finally, tribological evaluation is performed through characterization of the wear mechanisms by SEM pictures and also through the calculation of the amount of wear that resulted from the tests, in order to verify the influence of the electrochemical wear and the influence of the mechanical wear.

3.1. Material Characterization

The characterization of the studied materials is of extreme importance to understand how the properties of the material may influence the tribocorrosion behaviour, from the tribological contact to the electrochemical interaction with the electrolyte. To obtain information on the materials, SEM evaluation was performed to assess the morphology of the surface of the samples and after with Microtopography and Interferometry the topographical properties of the surface were studied.

3.1.1 Morphology and Chemical Evaluation

The morphology of the Etched and Anodized samples was observed by SEM. In Figure 23 are presented micrographs of both types of samples.

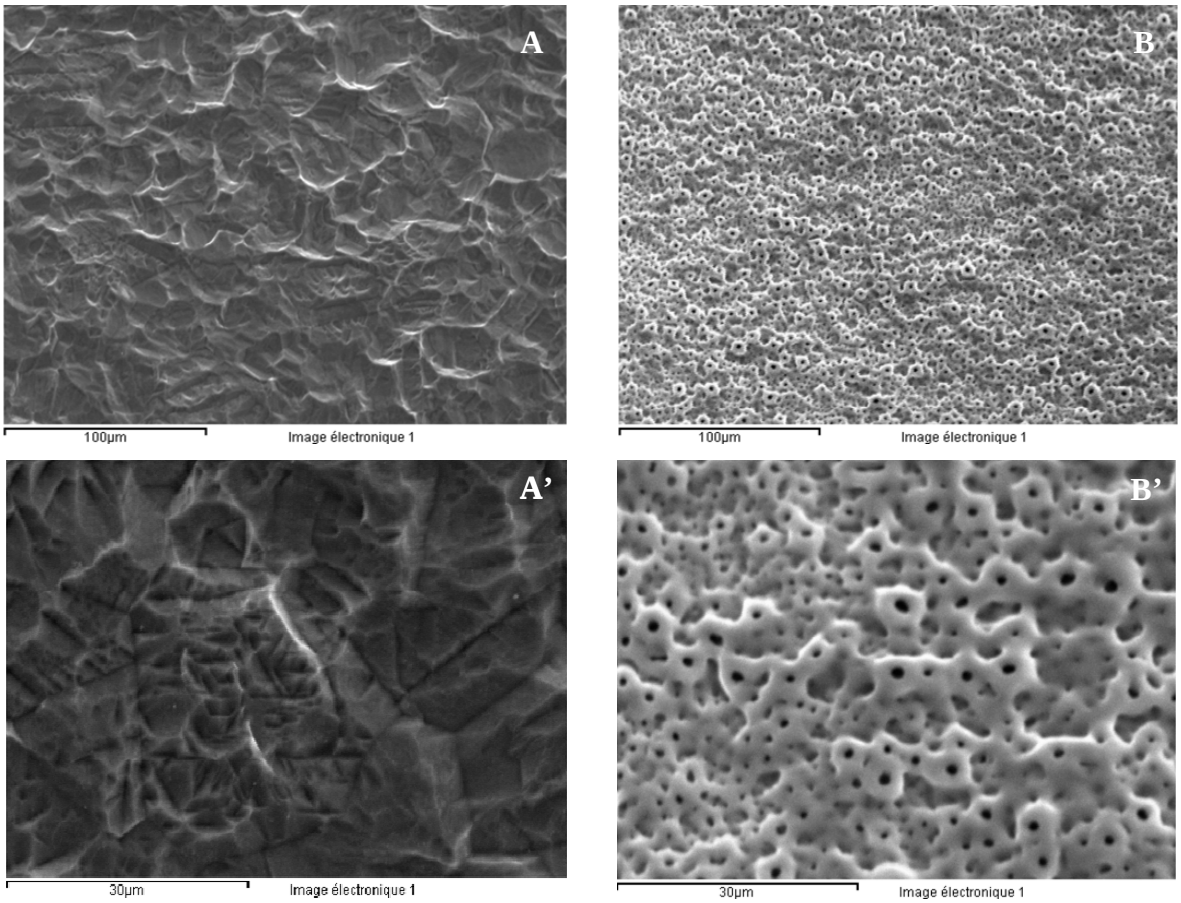

Figure 23 – Surface morphology: A) Etched samples (500x) A') Etched Samples (1000x) B) Anodized samples (500x) B') Anodized Sample (2000x).

The Etched samples were submitted to a chemical treatment, an etching process in Kroll's reagent, in order to clean the surface and to eliminate any substance that was adhere to it. This process allows a normalization of the surface of the samples. They were not mechanically polished, and the morphology observed in Figure 23 A) and A') is characterized by a wavy and rough surface, that results from the action of the Kroll's reagent (acidic solution). The samples that were subjected to the anodization process show a very distinct morphology. At first, the resulted surface is characterized by

a porous Anodized film, where the pores have a different range of diameters. The porosity results from the gas evolution and the current discharges (sparkling) during the anodization process, due to the high voltage applied (300V DC)[71][72]. By Figure 23 B) is possible to distinguish a certain waviness of the porous Anodized film. Such characteristic is related to the fact that the Anodized film grows over the surface of the Etched titanium sample (which already presents waviness), and in turn will show an effect of the base surface that it's beneath. Then, at higher magnifications (Figure 23 B')) is possible to distinguish two kinds of pores on the Anodized film: ones located at the top, with bigger diameters and more perceptible (that may be even fused with each others) while others have smaller diameters and seem to be below the firsts. In order to better characterize the Anodized film, on a previous work a transversal cut has been made on an Anodized sample. Figure 24 allows a better visualization of the complex morphology of the Anodized film created over titanium.

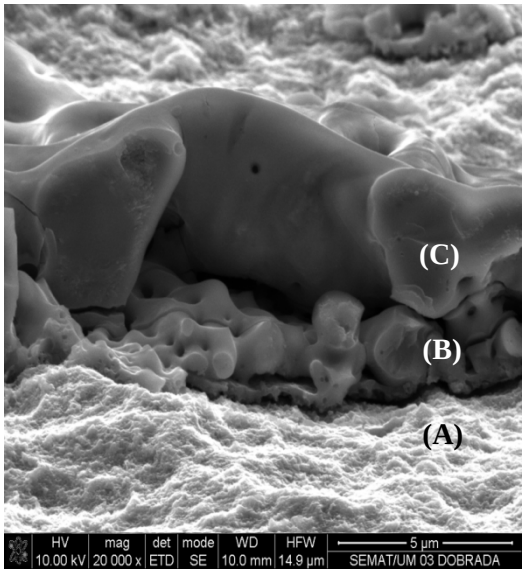

Figure 24 - Transversal cut of Anodized film.

It is possible to identify three distinct zones on Figure 24. In the first zone (A) is showed the surface of the base material, titanium with a compact passive film over the surface. On top of it, there is an intermediary zone (B) of approximately 3 µm, where is possible to identify several small pores interconnected among them. Finally, on top of zone (B), there is a thicker structure (≈ 5µm) characterized by bigger pores that can be also interconnected. In general, the anodization process provides a micropattern porous structure to the surface of titanium and a protective surface with a thickness of ≈ 8µm and considering the final purpose of the studied material, a dental implant, the porosity created by the anodization process will enhance the frictional forces between the implant and the surrounding tissues (bone), possibly increasing the fixation of the implant screw after implantation, decreasing the rate of failure by loosening and failed osseointegration.

The latter discussion presents the base morphologies of the samples before the tribocorrosion experiences.

The chemical evaluation on the surfaces was done by Energy Dispersion X-Ray Spectroscopy (EDS) and the resulted spectra are in Figure 25.

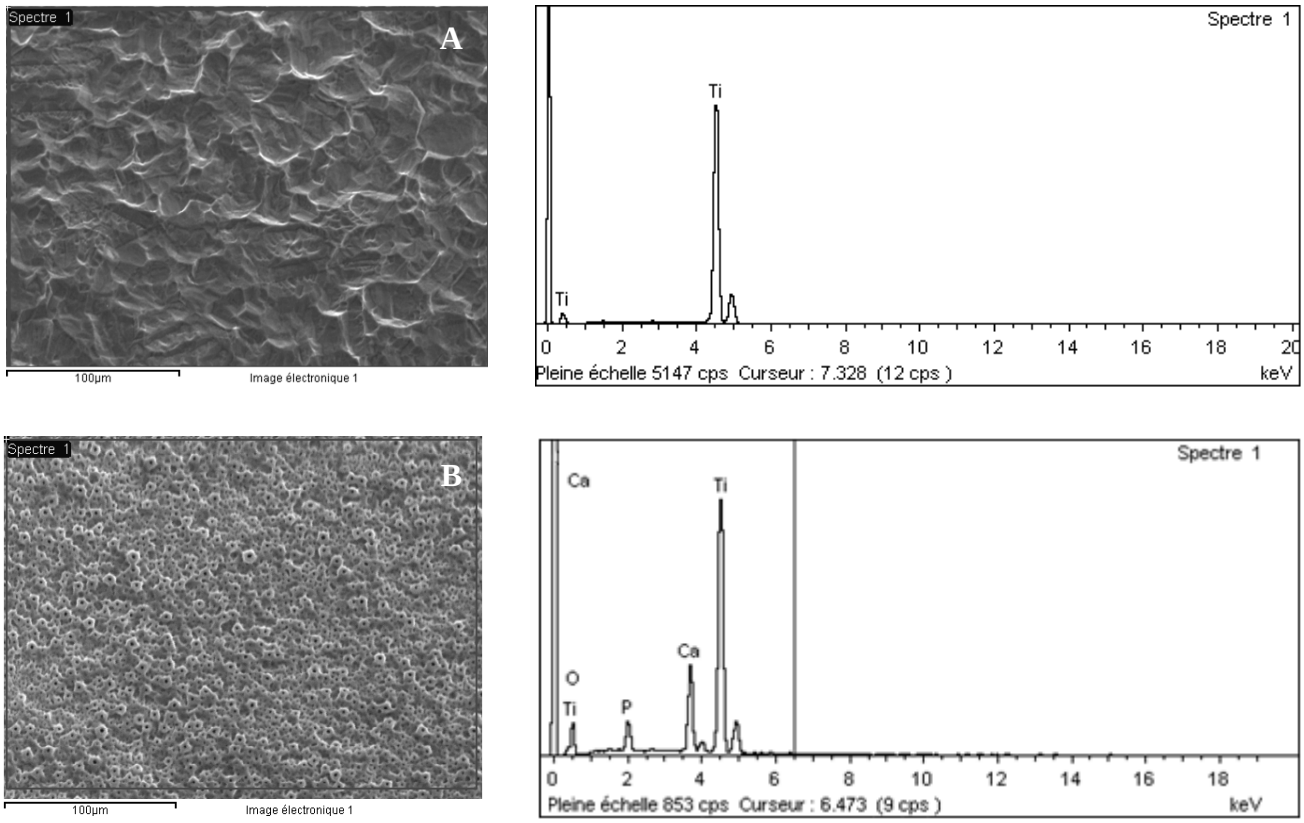

Figure 25 - EDS analysis: A) Etched sample B) Anodized sample.

On the Etched samples the only peaks that were identified were the ones that corresponded to titanium, with 100% mass of titanium. On the Anodized samples, it is possible to distinguish more elements aside titanium. The peaks of calcium, phosphorous and oxygen are along with the peaks of titanium. The presence of these elements is justified with the anodization process. During the treatment, the ions contained in the electrolyte can migrate to the oxide layer due to the discharge phenomenon of the anodic oxidation process [73]. To achieve such result the anodization solution is composed by calcium acetate and β-glycerophosphate, which will provide the calcium and the phosphate ions to the Anodized film. The mass percentage of the elements were 53,28 % for oxygen, 3,09 % for phosphorous, 7,39 % for calcium and 36,24 % for titanium and from other EDS evaluations, the values do not vary much from sample to sample. One of the objectives of the anodization process, beyond improving the corrosion resistance of titanium by the thickening of the passive film, is to permit the incorporation of calcium phosphate in order to improve the osseointegration properties of the surface of the material, turning it bioactive. Thus, it is possible to confirm the incorporation of Calcium Phosphate on the surface of titanium.

The crystal structure of the anodic oxide layer studied in this work was examined by X-Ray Diffractometer (XRD) in the Center for Mechanical and Materials Technologies (CT2M) of University of Minho in previous studies. The results showed that the anodic films revealed both anatase and rutile phase. The presence of the rutile phase on the anodic film is benefic, from the point of view of the application, due to the fact that this phase reveals better mechanical properties than the anatase phase, in terms of reduced elastic modulus (Er) and hardness (H) [(27)], so could increase the mechanical performance of the dental implant.

However, it is worthwhile to mention a variation on the morphology of the surface of the Etched samples that was noticed on the beginning of the work. In Figure 26 it is possible to visualize two types of morphologies for Etched samples. For the case of A) and A'), those are the *standard* surfaces used on the work, while on B) and B') it is noticed a different morphology. Through the micrographs and especially from B') is noticed a structure that seems to result from the formation of cracks and by the detachment of particles of the material from the surface. While the *standard* surfaces are obtained with an ultrasonically cleaning of the Etched samples with heated water (≈ 60°C) and dried with pressurized air, the sample on B was ultrasonically cleaned in ethanol and left to dry at open air. This cleaning with ethanol was suggested by *the COST 533 Inter lab TriboGuidelines protocol "Tribocorrosion testing for the characterization of Ti biomedical alloys in artificial saliva"* that served as base for the protocol followed on this master thesis, and such cleaning process was adopted during the first set of tests of Etched samples with 0,4 N at 100 rpm. One important aspect of this difference on the surface is the fact that the electrochemical behaviour of the material may be different, and in a tribocorrosion study is desired to have always the same base surface. On the other hand, the cleaning process does not influence the EDS result of the material, not revealing any adsorption of different chemical species (Figure 27).

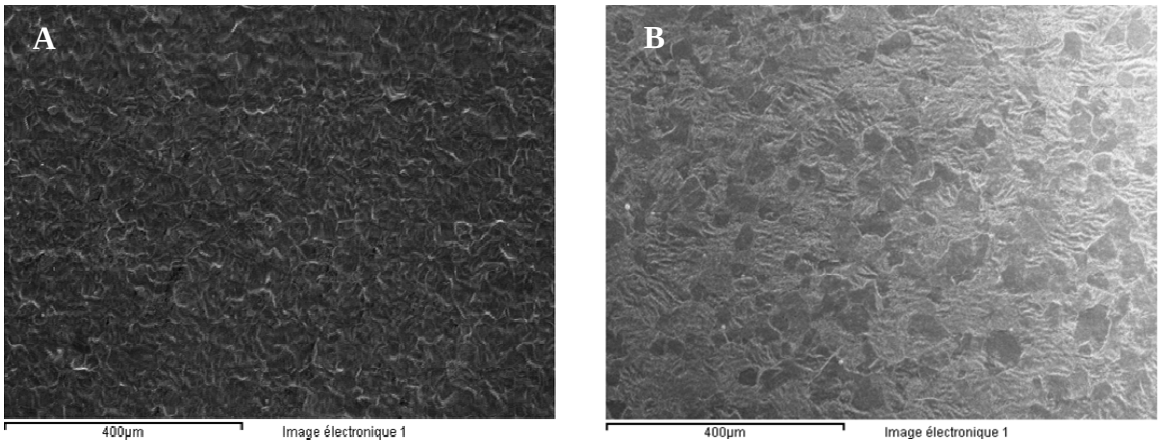

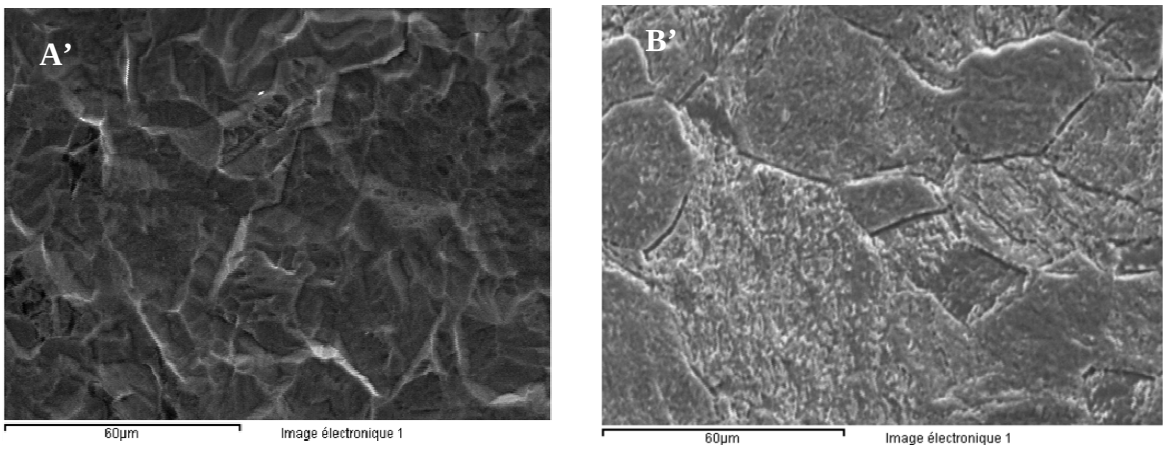

Figure 26 - Surface morphology: A) Etched sample water cleaning (150x) A') Etched Sample water cleaning (1000x) B) Etched Sample ethanol cleaning (150x) B') Etched Sample ethanol cleaning (2000x).

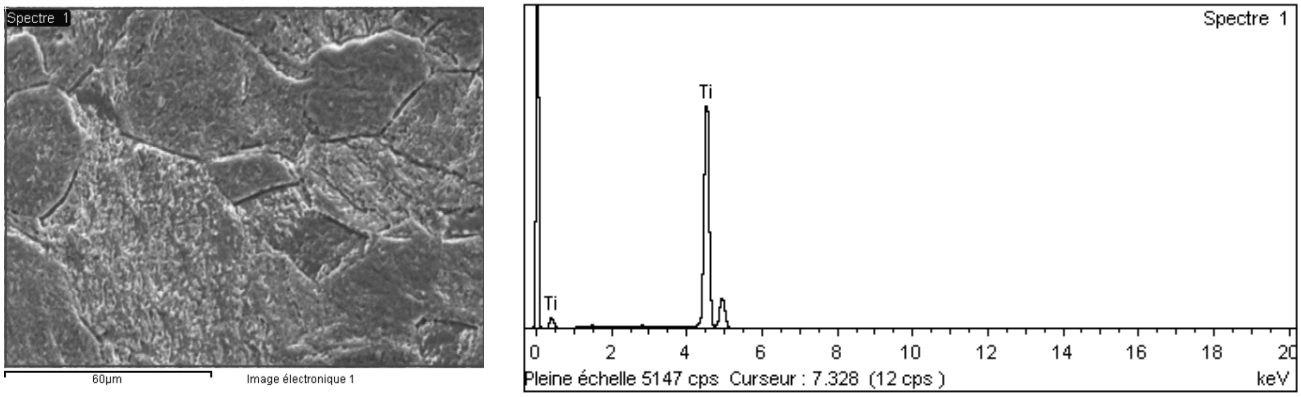

Figure 27 – EDS analysis of Etched Sample cleaned with ethanol.

After, when the difference was referred in a follow-up presentation of the work, and as this different morphology could influence the electrochemical behaviour of the material, the cleaning was established to be with ultrasonically bath with heated water (≈ 60°C) and dried with pressurized air.

3.1.2 Topographical Evaluation

Although SEM evaluation gives the opportunity to observe how is the morphology of the surface of the tested materials, it isn't possible to quantify certain morphological aspects regarding the topography, as the surface roughness, crucial for implant materials as titanium. First is discussed the results obtained by Microtopographer (Confocal Chromatic Microscopy) and Interferometer (White Light Interferometry) to evaluate the topography of the samples and then is presented a classification code for the studied materials, since there is a lack of standardization in the mode to classify the materials that are presented in scientific publications, leading to a misunderstanding of the nature of the material.

3.1.2.1. Measurements with Microtopographer (Confocal Chromatic Microscopy) and Interferometer (White Light Interferometry)

To evaluate the surface topography of the Etched and Anodized samples were employed two different evaluation modes and two different techniques: 2D evaluation (profilometry) and 3D evaluation (surface evaluation) and the Microtopographer (Confocal Chromatic Microscopy) and the Interferometer (White Light Interferometry). By doing so it is possible to compare the evaluation modes and to confirm the data obtained. 2D evaluation or profilometry is the standard method to evaluate topographical properties of surfaces, due to the extended use on the development and study of components for mechanical engineering. However, it will provide a local description of the topography, since the profile is done with a certain length in a certain zone. In this way, it will not be possible to have an idea of the evolution of the parameters over the surface of the material that is being evaluated. With 3D evaluation or surface evaluation, the fact that it will be scanned a whole area, a more reliable statistical analysis (due to the large amount of data) and a more realistic evolution of the topographical properties over the surface of the material will be performed. The mean value ± SD of the different profile and surface parameters studied are presented on Table 11 and on Figure 28 and Figure 29 are presented the 3D models of the surfaces evaluated on each sample by Microtopographer and Interferometer, respectively. The average rugosity (Ra or Sa) and single roughness depth (Rz or Sz) of the studied samples were selected due to the fact that are the common parameters presented in other publications related to Anodized titanium. The filtering of the data is given in Chapter 2.

Table 11 - Topographic properties measured by Microtopographer and Interferometer.

Techniques	Samples	2D Evaluation		3D Evaluation	
		Ra (µm)	Rz (µm)	Sa (µm)	Sz (µm)
Microtopographer	Etched	0,88 (± 0,08)	7,62 (± 1,16)	1,08 (± 0,01)	12,97 (± 0,30)
	Anodized	0,83 (±0,08)	6,30 (± 0,66)	1,03 (± 0,05)	10,85 (± 1,20)
Interferometer	Etched	0,98 (± 0,04)	6,01 (± 0,41)	0,98 (± 0,01)	10,71 (± 0,42)
	Anodized	1,00 (± 0,02)	6,63 (± 0,32)	1,02 (± 0,03)	10,52 (± 0,74)

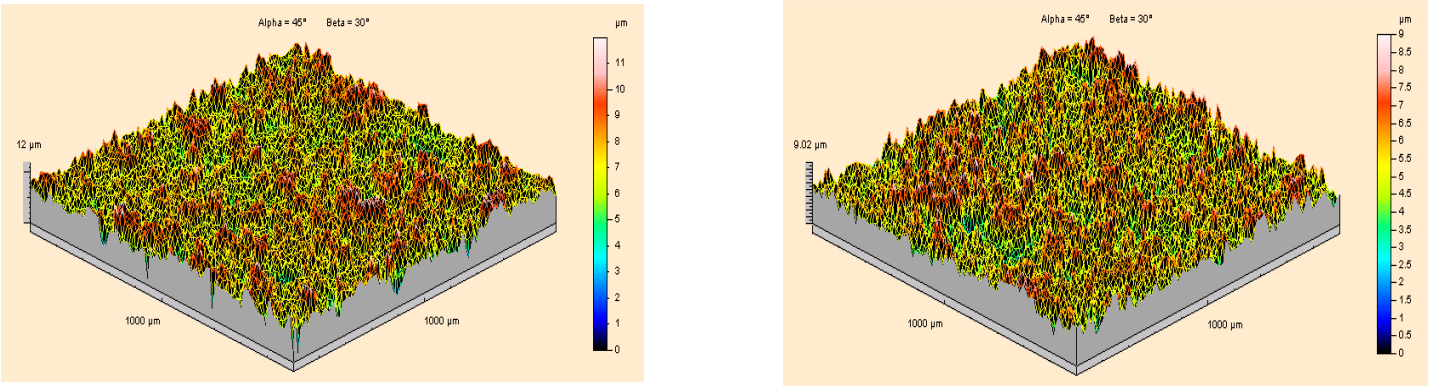

Figure 28 - 3D Square Evaluation with Microtopographer: A) Etched Sample B) Anodized Sample.

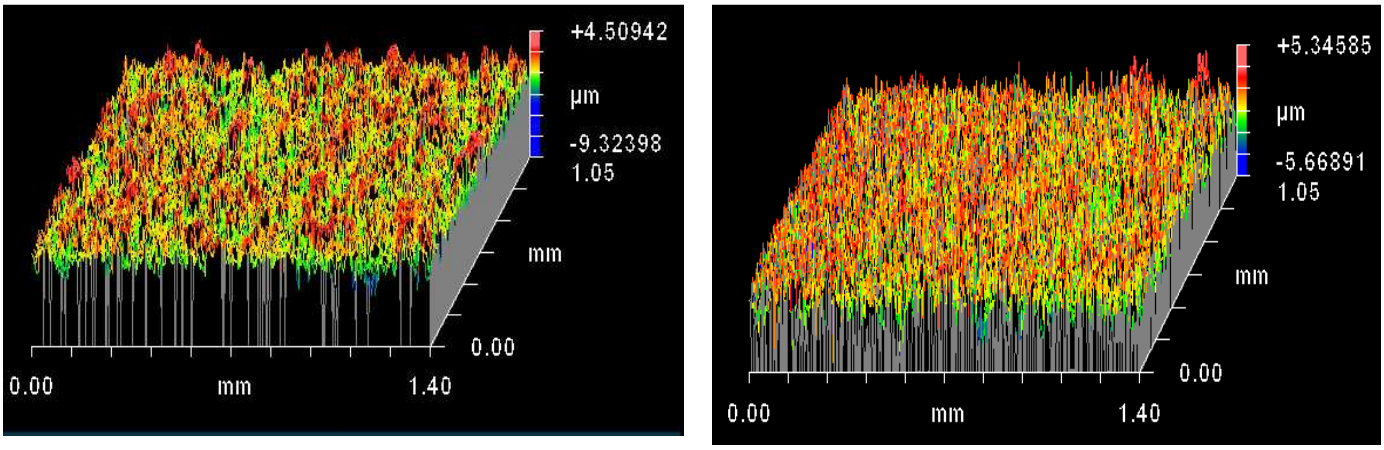

Figure 29 - 3D Square Evaluation with Interferometer: A) Etched Sample B) Anodized Sample.

Before discussing the results obtained, it is important to refer that for the Anodized samples, in order to obtain the interference fringes on the Interferometer, it was necessary to coat the samples with gold. Such procedure has been used to evaluate titanium oxides by White Light Interferometry [(54)] in order to avoid phase shift errors and wrong measurements of real topography.

After the anodization the surface morphology of titanium is completely changed and it was expected that, along with the porosity created during the anodization process, that the Ra of the Anodized samples would be different than the one of the Etched samples. However, on both techniques, a minor difference between the samples is observed indicating that the anodization process doesn't contribute to a significant variation of the average rugosity (Ra) of the surfaces. On the other hand, a slight increase of the Rz is seen on the Etched samples comparing to the Anodized samples, on the Microtopographer, but considering the standard deviation found, both types of samples are in the same range of values. With the Interferometer, the Rz is higher on the Anodized samples but again the standard deviation eliminates any difference between the samples. The results from 3D evaluation are similar to the 2D evaluation, with no significant difference between the samples, but there's a tendency to exhibit higher values than the ones from 2D evaluation. This might be due to the fact that a higher amount of material is evaluated. Also, the parameter Rz or Sz seems to be more affected than the Ra or Sa, revealing that only by 3D evaluation it may be possible to have a real perception of the vertical distance between the highest peak and the deepest valley (Sz).

In general, the results obtained with the Interferometer are consistent with the ones from the Microtopographer. The fact that for the Anodized samples it was necessary to coat the samples with gold (due to the different optical properties of the surface) to allow the feasibility of the measures on the Interferometer, one should have in mind that the coating may "mask" and induce a certain error to the measurement. But even though the techniques have their particularities, all the values are in the same range and no significant difference between the topographical properties of the samples was found. However, it is known that different surface morphologies may present similar topographical

properties [74]. Several authors have already published surface evaluation of Anodized films on titanium, both with the incorporation of calcium and phosphate or not. In Table 12 are presented the values of Ra and Rz gathered from different works. All the values were selected from samples that had the most similar preparation as the ones presented in this work, but nonetheless, differences as anodization method/solution are expected to bring variance since this variables on the process will influence the final result of the anodization (see Chapter 1) and also the use of different methods of measurement for the topographic characteristics (contact and non-contact methods) are present.

Table 12 - Ra and Rz found in scientific publications for Anodized oxide films in titanium.

Authors	Ra (µm)	Rz (µm)	Solution	Method	Measurement Method	Surface Obtained
Il Song Park (2007)[73]	0,437 (± 0,012)	2,442 (± 0,085)	B-glycerophosphate disodium salt hydrate (β-GP)	Anodic Spark Oxidation	Surface Profilometer (stylus)	Similar to Anodized Samples
Xiaolong Zhu (2004)[72]	0,4 (not referred)	Not referred	Calcium glycerophosphate (Ca-GP)	Galvanostatic mode	Surface Profilometer (diamond stylus)	Similar to Anodized Samples
Il Song Park (2006)[34]	0,53 (± 0,03)	3,57 (± 0,12)	B-glycerophosphate disodium salt hydrate (β-GP)	Anodic Spark Oxidation	Surface Profilometer (stylus)	Similar to Anodized Samples
Carlos Nelson Elias (2008)[75]	0,87 (± 0,14)	5,14 (±0,69)	Not referred	Galvanostatic mode	Laser Profilometer	Similar to Anodized Samples

The values for Ra and Rz reported in most works performed by other groups are lower regarding the ones obtained on this thesis, except for the work of *Elias et al*[75] that reports an average Ra of 0,87 µm for Anodized samples that is close to the one measured on the Anodized samples with the Microtopographer (0,83 µm).

In a biomedical implant, surface properties as the average roughness (Ra or Sa) are linked to the induction of a biological response towards the material, where surfaces with high Ra (or high Sa) seem to be more compliable for the attachment and growth of cells [76][77], improving the osseointegration process. With this in mind, it may be expected that a similar biological response will be induced by both types of samples, due to the same topographical properties. The cells are very sensible to these parameters and the biological behavior has to be evaluated in a deeper scale, at the nanometer level. Since the cells are in dimensions around 10 µm, they are very sensitive to nano features[78] on the surface of implant materials and in the case of the studied materials, the Anodized samples reveal a more complex surface than the Etched samples, that present nano features (nano-pores) that may play a role on the biological response. Figure 23 B' and A' illustrates the complex morphology of the Anodized surfaces vs. Etched surfaces. The Etched samples have peaks and valleys randomly distributed by the surface but the Anodized samples, as already discussed before, have all those pores (micro and nano pores) that will provide anchorage for the cells. Considering this, it is

possible that the anodize samples may induce a different biological response and in conjunction with the incorporation of calcium and phosphate (that are two of the basic components of bone), has an advantage over the Etched samples. Such behavior must be assessed in in-vitro tests and it's out of the frame of this master thesis.

3.1.2.2. Classification of the Samples

In biomaterials it is well known the role that the surface of materials has regarding the biological response of the human body. To improve the osseointegration of dental implants two strategies may be applied: one through improving the chemical nature of the surface (e.g. incorporation of calcium phosphate) and the other is through the modification of the surface architecture (topography) [74]. In the present work, the studied materials were modified along with both strategies, the Etched samples, with an etching treatment that modified the surface architecture and, the Anodized samples, which during anodization are subjected to a chemical modification of the surface by the incorporation of calcium and phosphorous and as well have the surface architecture modified (porous structures). However, with the intense research on biomaterials directed to the surface modifications that may improve the biological response of the materials and increase the performance of the implants, sometimes, on the scientific publications, it isn't clear the description of the surface that is being presented. In this way, *Dohan Ehrenfest et al* [74] have proposed a characterization code for osseointegrated implant surfaces based on the chemical properties of the material, the composition of the core material and its chemical or biochemical modification, and on the physical characteristics of the material, the topography at micro and nano-scale and its global architecture. On Table 13 is presented the implementation of the code on the studied samples.

Table 13 - Characterization codes for studied samples.

Surface	Chemical Characteristics		Physical Characteristics		
	Core Material (Core)	**Modification (Mod)**	**Microtopography (Micro)**	**Nanotopography (Nano)**	**Global Architecture (Archi)**
Etched Samples	C.P. Ti Grade 2	None	Rough (R) Minimal (Mi)	Smooth (R)	Fractal (F) Homogeneous (Ho)
	Core.G2Ti		Micro.R.Mi.	Nano.R	Archi.F.Ho
	Code = **Core.G2Ti/ Micro.R.Mi./ Nano.R/ Archi.F.Ho**				
Anodized Samples	C.P. Ti Grade 2	Calcium Phosphate (CaP) High Impregnation (HI)	Porous (Po) Minimal (Mi)	Smooth (S)	Non Fractal (NF) Homogeneous (Ho)
	Core.G2Ti	Mod.CaP-HI	Micro.Po.Mi	Nano.S	Archi.F.Ho
	Code = **Core.G2Ti/ Mod.CaP-HI/ Micro.Po.Mi/ Nano.S/ Archi.F.Ho**				

In this way and accordingly to *Dohan Ehrenfest et al* [74] the samples studied on this master thesis may be classified as:

Etched: **Core.G2Ti/ Micro.R.Mi./ Nano.R/ Archi.F.Ho**

Anodized: **Core.G2Ti/ Mod.CaP-HI/ Micro.Po.Mi/ Nano.S/ Archi.F.Ho**

3.2. Electrochemical Evaluation without sliding

To perform the evaluation of the tribocorrosion processes of a material, first it is necessary to characterize the electrochemical behaviour of the material in the selected electrolyte without sliding. In order to do so, it was observed the evolution of the Open Circuit Potential of the material, when immersed on artificial saliva for approximately 18 hours and also an Electrochemical Impedance Spectroscopy measurement after 5 hours.

3.2.1 Open Circuit Potential Evolution

The evolution of the potential on both Etched and Anodized samples is demonstrated on Figure 30.

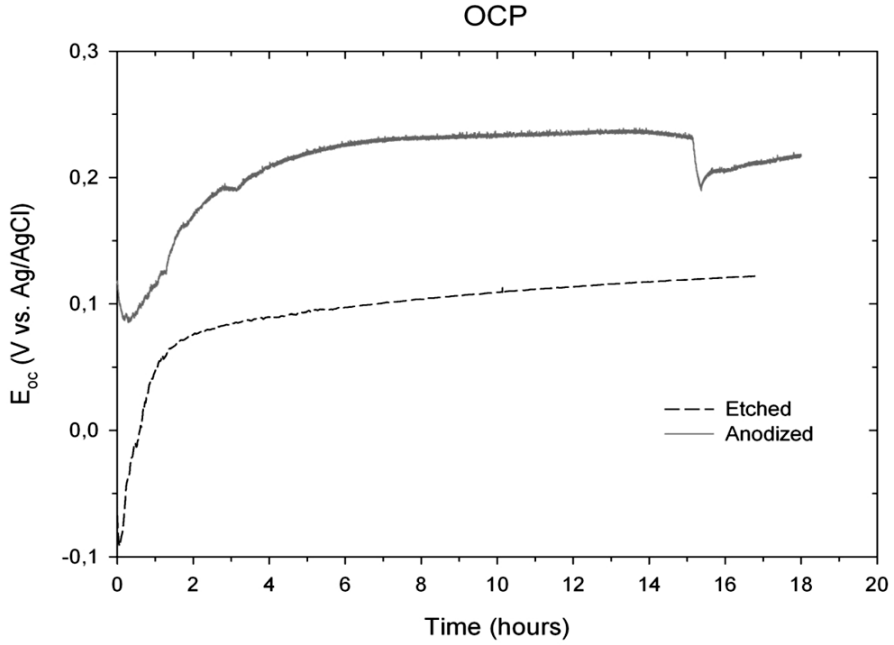

Figure 30 - Evolution of the open-circuit potential with time of an Etched and Anodized sample.

For the Etched sample, at the beginning of the test, the open-circuit potential is around – 0,9V vs. Ag/AgCl, and it is possible to notice an increase on the values of potential during the first hour, indicating that a passivation process is occurring. During this process the predominant reaction is the anodic reaction, due to the small and gradual oxidation of titanium and the reaction with the electrolyte in order to form the titanium dioxide (TiO_2) passive film. After that point, the potential has a small variation and the stabilization of the potential (< 60mV/h) is achieved at around + 0,10 V vs. Ag/AgCl. This stabilization indicates that a stable passive film is formed on the surface of the sample and that the cathodic and anodic reactions are in an electrochemical equilibrium.

Regarding the Anodized sample, after immersion on the electrolyte it presents a potential value around + 0,10 V vs. Ag/AgCl and has a positive evolution until ≈ 4 hours, where the potential starts to stabilize (< 60 mV/h) around + 0,22 V vs. Ag/AgCl. The Anodized sample has already a thick Anodized film formed on its surface, and the fact that the anodic reaction occurs is not related to the growth of a passive film, but instead, related to the interactions of the electrolyte with the Anodized

film and also to the penetration of the electrolyte inside the pores that the Anodized sample has on its surface. The porosity will provide to the material a bigger contact area with the electrolyte. As referred previously, some of these pores may cross the total thickness of the Anodized film and by this way, allow a deep penetration of the electrolyte that will react with the Anodized film and eventually with the base material (titanium), in a very particularly way due to the fact that both on composition and morphology, the Anodized film is very distinctive of the natural oxide film of titanium. Around 15 hours it is possible to visualize a rapid decrease of the potential, due to a cathodic reaction, but right after, the potential starts to increase and at the final of the test the potential is very close to the stable potential of + 0,22 V vs. Ag/AgCl.

3.2.2 Electrochemical Impedance Spectroscopy

Along with OCP, to better understand the passive state of the samples and the mechanisms occurring at the passive film/electrolyte interface, an Electrochemical Impedance Spectroscopy was performed after the stabilization of the potential. The values present on the tables are the mean values of the studied samples.

On Figure 31 is showed the Nyquist plot and on Figure 32 is represented the Bode Z plot and the Bode phase plot of an Etched sample while on Figure 33 is presented the Nyquist plot of an Anodized samples and the respective Bode Z plot and the Bode phase plot on Figure 34.

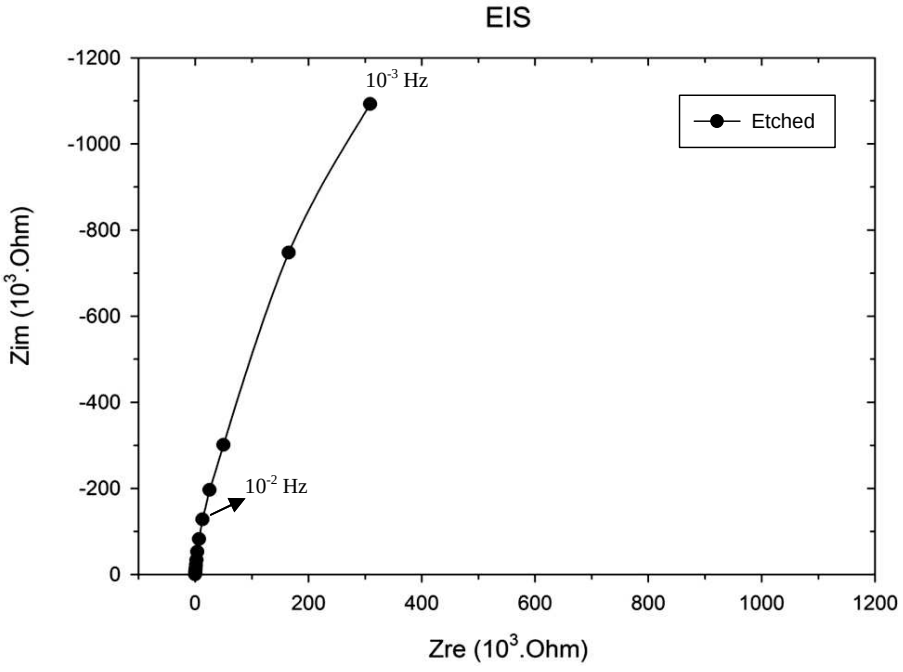

Figure 31- Nyquist plot of Etched sample.

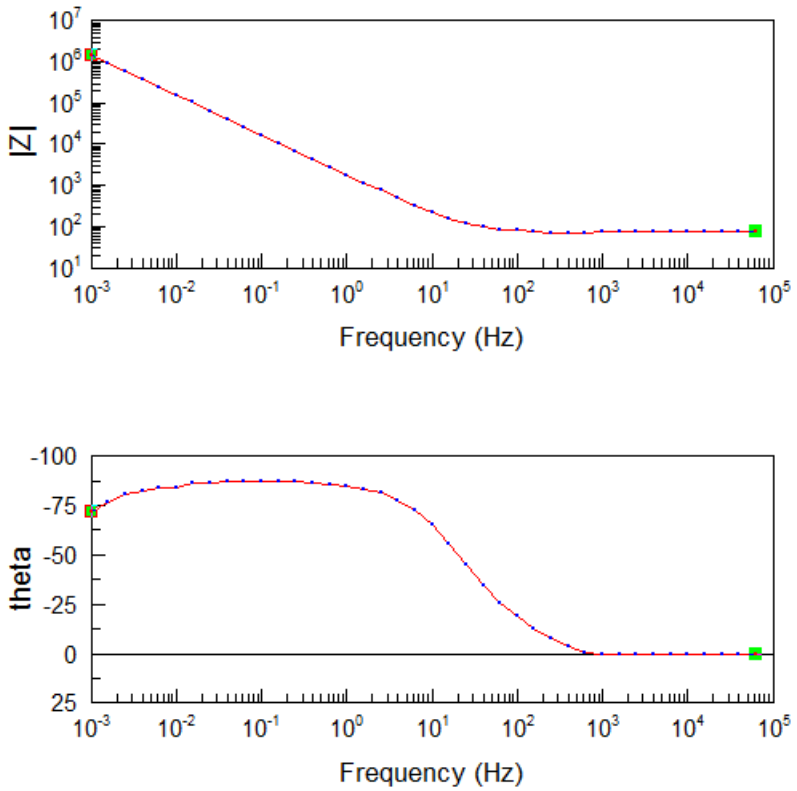

Figure 32 – Bode Z plot (frequency vs. impedance modulus |Z|) and Bode phase plot (frequency vs. phase angle) of Etched sample.

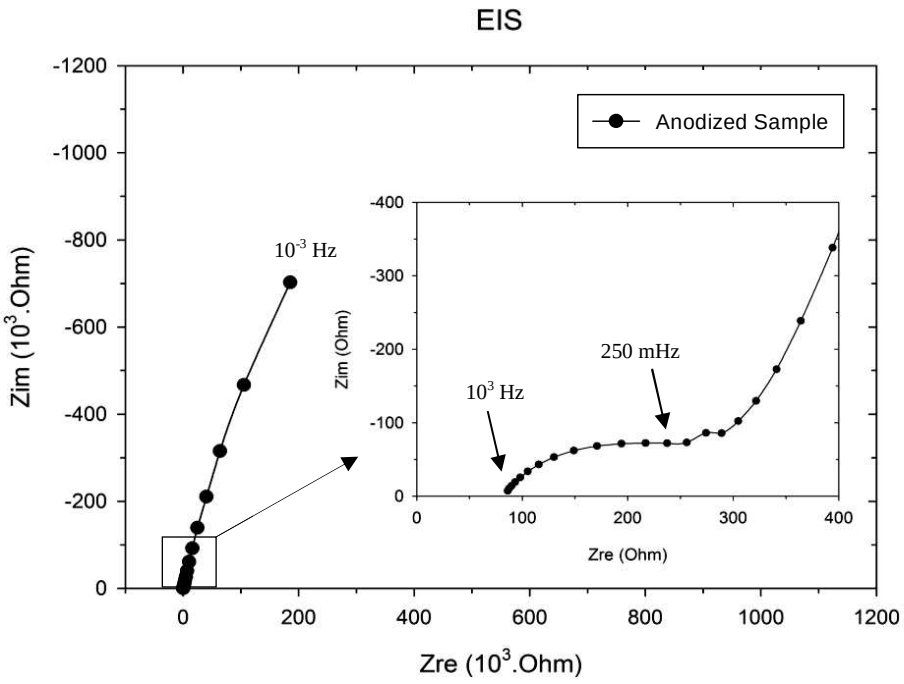

Figure 33- Nyquist plot of Anodized sample.

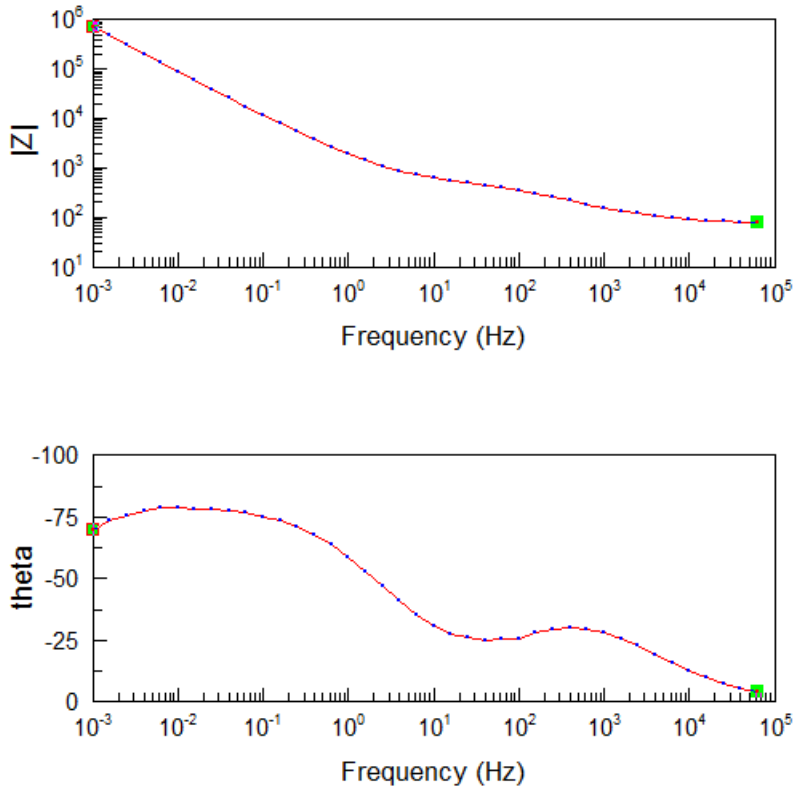

Figure 34 - Bode Z plot (frequency vs. impedance modulus |Z|) and Bode phase plot (frequency vs. phase angle) of Anodized sample.

From the fitting with the equivalent circuits presented on Chapter 2 were obtained the values of the parameters that describe the electrochemical state of the samples on the studied electrolyte (Table 14).

Table 14 – Polarization Resistance (R_p), Specific polarization resistance (r_p) and corrosion current density ($\boldsymbol{i_{corr}}$) of Etched Samples and Polarization resistance (R_{pp}) and specific polarization resistance (r_{pp}) of porous layer and Polarization resistance (R_{pb}), specific polarization resistance (r_{pb}) and corrosion current density ($\boldsymbol{i_{corr}}$) of barrier film of Anodized Samples without sliding.

Sample	A_0	*Passive Film*		
		R_p (Ω)	r_p (Ω.cm^2)	i_{corr} (A.cm^{-2})
Etched	3,3 (± 0,15)	8,08 × 10^6 (± 9,80×10^6)	2,61 × 10^7 (± 3,16×10^7)	4,41 × 10^{-8} (± 1,05×10^{-7})
Sample	A_0	*Porous Layer*		*Barrier Film*		
		R_{pp} (Ω)	r_{pp} (Ω.cm^2)	R_{pb} (Ω)	r_{pb}(Ω.cm^2)	i_{corr} (A.cm^{-2})
Anodized	3,4 (± 0,15)	4,27 × 10^2 (± 178)	1,45 × 10^3 (± 664)	7,81 × 10^6 (± 5,02×10^6)	2,62 × 10^7 (± 1,70×10^7)	1,29 × 10^{-9} (± 8,20×10^{-10})

From the values of the previous table and considering that the specific polarization resistance of the material (r_p) allow us to evaluate if the surface is in a passive state ($r_p \geq 100\,000\ \Omega.cm^2$) or in an active state ($r_p \leq 1000\ \Omega.cm^2$) [55], is possible to affirm that the surface of the Etched titanium is

covered by a passive surface film. The corrosion current density gives an idea of the dissolution of titanium through its passive film to the electrolyte and with the Faradays Law is possible to estimate a corrosion rate of 52,4 µg/year of titanium to the electrolyte, which is an evidence of the stable condition of the material on the studied conditions. In relation to the Bode representation, the impedance modulus give us an idea of the total impedance of the system evaluated (electrolyte + material) mostly due to the passivation of titanium. From the phase angle is possible to observe a large capacitive domain of the passive film of titanium ranging from 10^{1} Hz to 10^{-3} Hz. This capacitive behaviour is related to the properties of passive films that act as insulators to the dissolution of ions from the base material.

Regarding the Anodized samples, the evaluation of the electrochemical behaviour is more complex. On the Nyquist plot (Figure 33) it's possible to observe that the resistance of the Anodized film will be significant since the diagram resembles to a straight line and even at 10^{-3} Hz it doesn't show the typical curvature of the arc of circle. After, at the high frequency range, is possible to distinguish a first arc of circle until 250 Hz and then another arc of circle until 10^{-3} Hz. From this, it is already visible a contrast that the Anodized film may not show the same mechanisms regarding electrochemical reactions comparing to the natural oxide film of titanium. The morphology and the composition of the Anodized film may interfere with the electrochemical response. The presence of two arcs of circle may be due to the morphology of the Anodized film. Previously, it was possible to notice that the Anodized film is composed by layers (Figure 24) and the resistance of both porous layers may be connected to the first arc of circle while the other arc of circle is related to the resistance of the compact barrier film. The equivalent circuit for the Anodized samples presented in Chapter 2 was assumed, in order to calculate the resistance values of each component of the Anodized film. The results are presented on Table 14. The porous layer presents a specific polarization resistance of 1450 Ω.cm2 and it is relatively high in comparison with values found in literature (151 Ω.cm2 [35]) on oxide films of titanium enriched with calcium and phosphorous. The difference might result from the applied technique for the growth of the oxide (anodic oxidation vs. galvanostatic method [35]) and the concentrations of the electrolyte (0,7 mol/l CA vs. 0,2 and 0,4 mol/l [35]) that can induce a different morphology. Anyway, Krupa et al [35] refers that the resulted oxide film is composed by a superficial porous layer and an inner barrier film. The value obtained for the porous layer (R_{pp}) characterizes the resistance that the porous structure reveals against the electrochemical phenomena and is linked to the dimension of the pores (possibly from nano, to micro and macro pores) and also to the pathway (tortuosity) of the porosity of the Anodized film, all morphological features that play a role on the overall interaction of the electrolyte with the material. The barrier film has a specific polarization resistance of $2{,}62 \times 10^{7}$ Ω.cm^2 that is very similar with the one obtained for the Etched sample ($2{,}61 \times 10^{7}$ Ω.cm^2). Similarly, the Bode phase plot (Figure 34) shows also a different behaviour, with a smaller capacitive domain at 10^{3} Hz to 10^{2} Hz and another higher capacitive domain from 10^{0} Hz to

10^{-3} Hz where the first domain may be related to the superficial porous layer of the Anodized film while the second to the deeper barrier film.

This first evaluation allow the knowledge how the material reacts in contact with the artificial saliva solution at room temperature with a pH of 5,5. From the open-circuit evolutions of Etched and Anodized samples it is clear that the anodization process changes the electrochemical behaviour of titanium. While the Etched samples have a equilibrium potential of + 0,10 V vs. Ag/AgCl the Anodized samples show a more noble equilibrium potential of + 0,22 V vs. Ag/AgCl. The results of OCP indicate that the Anodized samples are less vulnerable than the Etched samples to electrochemical processes that could lead to corrosion phenomena. While this may be true, the EIS contributes with more information about the electrochemical system and verifies the mechanisms at the interface of the material with the electrolyte. Comparing both samples, the total impedance of the systems is similar and the anodization doesn't seem to improve the corrosion behaviour of titanium significantly. However, it is clear that the electrochemical interface is changed by the anodization process. Such impact is evident on the Nyquist plot, where is possible to see a difference that may proof that the morphology of the Anodized film play a role on the electrochemical reactions. Ions from the electrolyte will penetrate the Anodized porous film and interact with the film and also, ions that were dissolved from the Anodized film will migrate to the electrolyte. There is a reciprocal exchange due to the tendency to achieve an electrochemical balance. Furthermore, the chemical composition of the Anodized film will as well affect the corrosion performance of the material, in a way that the ionic impregnation with calcium and phosphate ions will modify the conductivity of the film. It is expected, since there is a wider ionic component, that the conductivity of the anodic film is from the natural oxide film of titanium and in this way, will reveal a specific electrochemical resistance that may not be related to the higher or lower dissolution rate of titanium for the electrolyte.

The application of titanium as a biomaterial, and even the improvements with superficial treatments, is not only related to its corrosion properties and one must not forget that the mechanical properties, in an application as a dental implant, will have also an important influence on the performance of the implant. In this way, the mutual effect of corrosion properties and mechanical properties is evaluated in tribocorrosion tests and a balance between both must be found in order to advance the implants industry.

3.3. Tribocorrosion Evaluation

To assess the tribocorrosion behaviour of titanium was performed continuous unidirectional sliding tests and simultaneasly was recorded the electrochemical response of the material through Open-Circuit Potential measurements and Electrochemical Impedance measurements. The influence of the normal load, of the velocity of rotation and the presence of a cell layer on the surface of the material will be presented.

3.3.1 Effect of Normal Load

3.3.1.1 Open Circuit Potential Evolution

The open-circuit potential was recorded during 3 hours before starting the continuous unidirectional sliding tests, in order to see the stabilization of the potential after immersion on the solution, during the continuous unidirectional sliding tests and for about 20 minutes after the end of the sliding tests. Three tests were performed for each condition for both samples and the typical behaviour of the evolution of the open-circuit potential of an Etched and Anodized sample is presented on Figure 35.

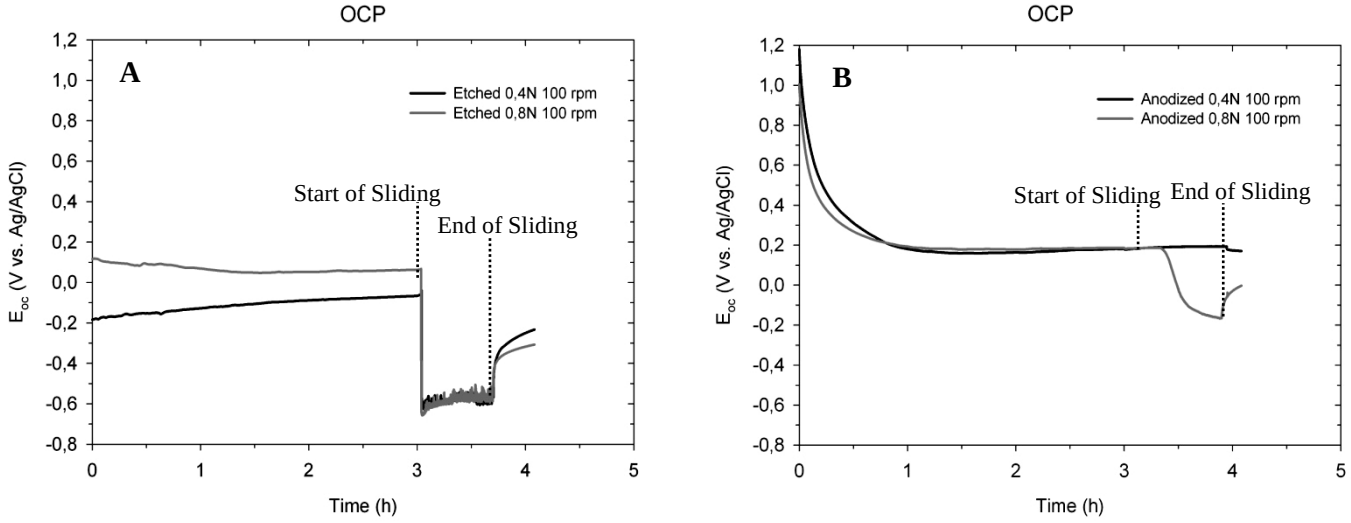

Figure 35 - Evolution of the open-circuit potential, before, during, and after continuous unidirectional sliding tests performed at 0,4N and 0,8N at 100 rpm on (A) Etched and (B) Anodized samples.

Starting with the Etched samples, first of all is possible to observe a contrast on the evolution of the potential before starting sliding. The sample tested a 0,4N has a lower stable potential (-0,1 V vs. Ag/AgCl) than the sample tested at 0,8N (+ 0,1 V vs. Ag/AgCl), differing also from the previous electrochemical study performed on the samples without sliding. Such a difference may be related to the fact that the sample tested with 0,4N was part of the first set of samples cleaned with ethanol and the sample tested with 0,8N was cleaned with hot distilled water. Before, it was presented the different morphology obtained on the samples with the different cleanings and that can be the cause of the change of the electrochemical behaviour of the samples. After, at the start of sliding, an abrupt drop on

the open-circuit potential with the same amplitude is noticed on both samples, leading the potential to more cathodic values exposing a modification of the surface state of the sliding track area on titanium. The cathodic shift on the potential is associated to the destruction and removal of the stable oxide passive film that was covering the surface, exposing an active surface that is highly reactive with the electrolyte. During sliding, the open-circuit potential remains constant and similar (≈ -0,6 V vs. Ag/AgCl) on both samples and this potential is characterized by a galvanic coupling between the worn area (active area inside the wear track) and the unworn area (passive area outside the wear track), and thus creating a mixed potential that will be dependent on the ratio active/passive area. In this case it is possible to see that the normal force didn't cause any perturbation on the open-circuit potential under friction of titanium. Such result is due to the fact that the loads applied are not substantial and the effects of the increase of the contact pressure (204 MPa for 0,4N and 258 MPa for 0,8N) are not enough to shift the potential to more cathodic values. Then, when the sliding is ended, the open-circuit potential of titanium starts to increase revealing an anodic shift that on passivating metals, like titanium, is associated to the re-formation of the oxide passive film on the surface of the material. Here is possible to notice differences between the tested samples. At first, the rate at which the potential decreases on loading and increases on the unloading of the ball is different. On loading an abrupt modification of the potential occurs due to the sudden mechanical destruction of the passive film while on unloading, the repassivation rate is slower and the increase of the potential is dominated by the reaction mechanisms of the oxidation of the material in the electrolyte. Then, at the end of the test the open-circuit potential of the sample tested at 0,4N reaches a more noble potential than the sample tested at 0,8N, -0,2 V vs. Ag/AgCl against -0,25 V vs. Ag/AgCl respectively. Here, the difference on the final potentials is mainly related to the ratio of worn and unworn areas as also the resulting galvanic coupling between the active wear track and the remaining passive surface. With the increase of the normal force is expected that the area of worn surface will increase, and in this way, the active surface that is exposed to the electrolyte is superior and to repassivate that area and to the potential achieve higher values will take more time. The aspects related to the evolution of the wear track area will be exposed on Chapter 3.4. This effect of the evolution of the active area could also be noticed on the values of the open-circuit potential under continuous unidirectional sliding, since it influences the galvanic coupling created, leading the potential to more cathodic values with a higher ratio active/passive area, as shown in the work of Ponthiaux et al [79], but in the present study such variation is not evident on Figure 35. In this way, the increase of the active area due to the increase of the normal force wasn't important enough to shift the potential to more cathodic values. One should also consider that the effect on the recovering of the potential may also be related to some mechanical effects, like elasto-plastic deformation or load-induced phase transformation, since the contact pressures on each tested load were different (204 MPa for 0,4N and 258 MPa for 0,8N). Regarding the Anodized samples, after immersion on the electrolyte, the potential reveals a cathodic tendency where the potential decreases through time, from a value between + 1,18 V vs. Ag/AgCl and + 1 V vs.

Ag/AgCl, reaching a steady state of approximately + 0,2 V vs. Ag/AgCl after ≈ 1 hour. This value is in agreement with the electrochemical evaluation of the samples without sliding. The cause for, at the beginning of the test, the samples reveal such an anodic potential wasn't found, but could be related to the infiltration of ethanol to the pores during the cleaning before test. Still this wasn't confirmed. When sliding starts, the potential remains stable and continues at + 0,2 V vs. Ag/AgCl in both samples. No cathodic shift arises from the mechanical contact due to the destruction of the surface oxide passive film. The fact that the anodization provides a thicker porous film to titanium is behind this behaviour under mechanical solicitation. The anodization creates a thicker three layered Anodized film (Figure 24), a superficial layer with pores of larger diameter, an intermediary layer with pores of smaller diameter and a compact inner layer without porosity. In addition, on the composition of the Anodized film, not only the anatase phase of dioxide titanium is present but also the rutile phase is, providing better mechanical properties to the Anodized film. In this way, the results indicate that the Anodized passive film can resist to the initial mechanical contact with both loads and that with friction there is no significant destruction of the passive film. Meanwhile, approximately at 3,3 hours the sample tested at 0,8N reveals a shift on the behavior and the potential starts to decrease while the sample tested at 0,4N remains with the potential stable. At the beginning of the cathodic shift, the potential drops rapidly and then starts to stabilize and when sliding ends (≈ 4 hours), a sudden increase is observed, and the potential keeps raising to more positive values to a final potential of 0 V vs. Ag/AgCl at the end of the test. The sample tested with 0,4N, at the end of sliding, shows a slight variation on the potential but still continues with the potential at + 0,2 V vs. Ag/AgCl. The shift displayed by the sample tested at 0,8N is a result of fatigue of the Anodized film. Such phenomenon is associated to materials that are subjected to repeated loading and unloading cycles. A continuous unidirectional sliding test subjects the tested material to such conditions and with 0,8N, at about 1667 cycles the Anodized film reaches a limit and starts to give in and to expose deeper layers beneath the Anodized film, which in turn will start to be in contact with the sphere and be subjected to removal of material. This removal causes the exposition of active material to the electrolyte leading to the consequent decrease of the potential. Similarly the sample tested at 0,4N eventually could present the same cathodic shift, but due to the lower normal force, to achieve such result it would be necessary to increase the number of cycles, or in other words, the number of loading and unloading cycles to damage the Anodized film. More insight on the wear track surface and wear mechanism of the Anodized samples is presented on Chapter 3.4.

The tribocorrosion behaviour of both samples is different. It's obvious that the anodization process brings improvements not only to the electrochemical interface of the material but also to the mechanical response under sliding. On the open-circuit potential evolution, the Anodized samples have overcome the Etched samples not only on the electrochemical point of view but also on the mechanical point of view, since it's possible to confirm that the Anodized samples have a higher resistance against the mechanical loading of a counterbody on its surface. When sliding starts, the

Anodized film remains protective for the surface against dissolution processes contrarily to the Etched samples where the passive film is instantaneously removed and the active material exposed to the electrolyte.

3.3.1.2 Electrochemical Impedance Spectroscopy

An impedance measurement was done under continuous unidirectional sliding. The obtained impedance plot (Nyquist plot) for Etched and Anodized samples is presented in Figure 36 and the Bode Z plot and the Bode phase plot of Etched samples on Figure 37 and for Anodized samples on Figure 38.

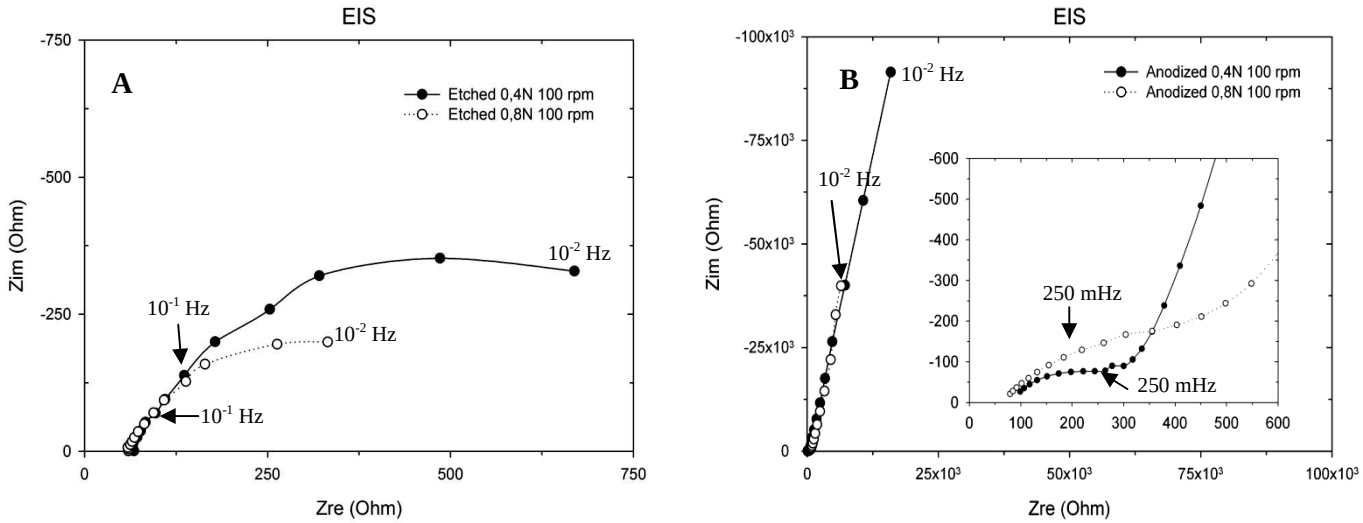

Figure 36 - Electrochemical impedance spectra measured at the mean open-circuit potential value during continuous unidirectional sliding tests performed at 0,4N and 0,8N at 100 rpm on (A) Etched and (B) Anodized samples.

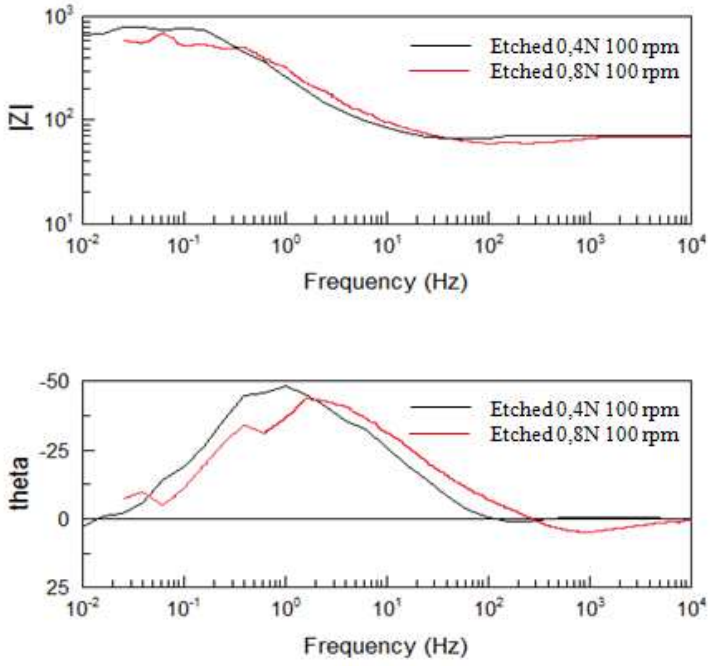

Figure 37 - Bode Z plot (frequency vs. impedance modulus |Z|) and Bode phase plot (frequency vs. phase angle) during continuous unidirectional sliding tests performed at 0,4N and 0,8N at 100 rpm of Etched Sample.

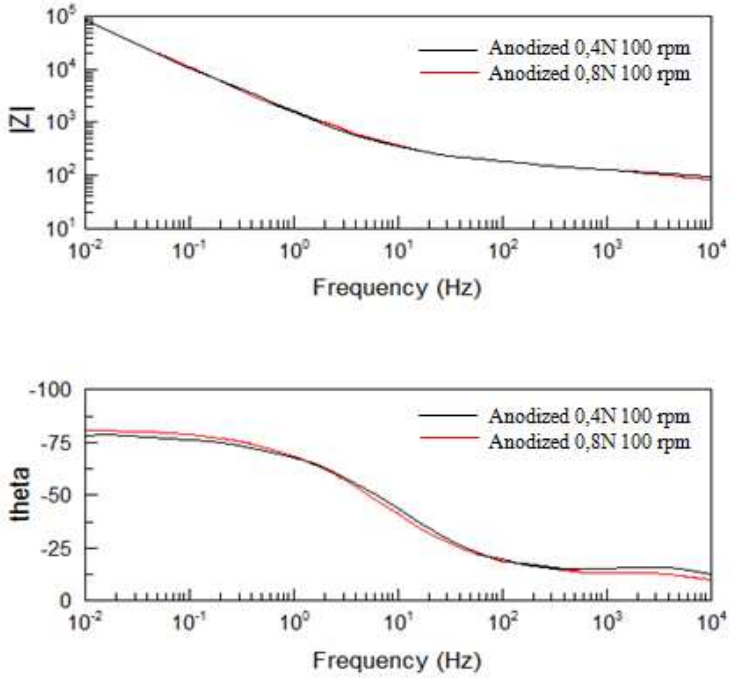

Figure 38 - Bode Z plot (frequency vs. impedance modulus |Z|) and Bode phase plot (frequency vs. phase angle) during continuous unidirectional sliding tests performed at 0,4N and 0,8N at 100 rpm of Anodized Sample.

From the Nyquist plot (A) under sliding it's possible to calculate a polarization resistance under sliding (R_{ps}) assuming that the equivalent circuit for the Etched samples, stated on Chapter 2, is suitable. The value of R_{ps} obtained by the fitting, due to the fact that the sample is subjected to sliding, is in fact a combination of two polarization resistances connected in parallel. The first is related to the sliding track area (active area) and the second one to the area outside the sliding track (passive area). In order to deconvulate both polarization resistances, on Chapter 2 and based on the protocol *"A methodology for the assessment of the tribocorrosion of passivating metallic materials"* are exposed certain assumptions. Due to the fact that the small period between two successive contact events (T_r = 0,6) incapacitates the surface to completly repassivate after a contact event, it is assumed that the sliding track area is in a continuous active electrochemical state (corrosion) and it is possible to consider that the area of the sliding track is equal to the area of the active surface ($A_{tr} = A_{act}$) and is possible to obtain the values that characterize the active surface. The values obtained for the R_{ps}, for the specific polarization resistance under sliding (r_{act}) and the corrosion current density under sliding (i_{act}) are presented on Table 15. The values present on the tables are the mean values of the studied samples.

Table 15 - Sliding track area, polarization resistance, specific polarization resistance and corrosion current density of Etched samples at open-circuit potential under continuous unidirectional sliding at 0,4N and 0,8N at 100 rpm.

	A_{tr} (cm^2)	R_{ps} (Ω)	r_{act} ($\Omega.cm^2$)	i_{act} ($A.cm^{-2}$)
0,4 N	0,215 (± 0,12)	$57,8 \times 10^2$ ($\pm 7,73 \times 10^2$)	$31,4 \times 10^2$ ($\pm 24,1 \times 10^2$)	$2,59 \times 10^{-5}$ ($\pm 3,57 \times 10^{-5}$)
0,8 N	0,249 (± 0,14)	$9,06 \times 10^2$ ($\pm 3,20 \times 10^2$)	$2,16 \times 10^2$ ($\pm 0,049 \times 10^2$)	$11,5 \times 10^{-5}$ ($\pm 2,57 \times 10^{-5}$)

By comparing the values of Table 14 (without sliding) with the ones of Table 15, a difference on the condition before and under sliding is seen. It is apparent that under sliding there is a significant degradation of the protective surface film in the sliding track on titanium. This degradation is proved by the considerable decrease of the value of polarization resistance. In the same way, by comparing the values of Table 15 also a decrease is seen from the sample tested at 0,4N to the one tested at 0,8N. Such effect is visible on Figure 36 where the Nyquist plot for the sample tested with higher load seems to reveal a smaller arc of circle that in turn will result in a lower polarization resistance. The lowest specific polarization resistance under sliding is of $2,16 \times 10^2\ \Omega.cm^2$ for the sample tested at 0,8N and in this way is evident that with the increase of the load, the surface oxide passive film under sliding is more damaged and less protective for the surface of the material. Such effect is confirmed by the higher current density ($11,5 \times 10^{-5}\ A.cm^{-2}$) for the sample tested at 0,8N revealing a higer dissolution rate. However, in the overall, the samples in their active state are quite similar. In addition, the Bode Z plot and the Bode phase plot (Figure 37) confirms the effect of the normal force in the decrease of the protection provided by the surface oxide passive film. It is evident that the capacitive domain of the passive film has been affected, indicating that the properties of the film are not the same before sliding and under sliding.

Likewise in Figure 37 (B) the Nyquist plot of the impedance measured under friction for the Anodized samples is present as well the Bode plot (Figure 38). However, the characterization of the electrochemical state of the Anodized samples under friction couldn't be made using the same methodology applied for the ecthed samples. On the Etched samples was used the protocol presented on Chapter 2, which has the objective of studying the influence of the destruction and growth of the passive film (5-10 nm in thickness) of a metal on the total wear, when the material is exposed to mechanical solicitations as sliding. The anodization results in the increase of the thickness of the Anodized film to the order of the micrometers, being the first disadvantage. Secondly, for the correct application of the protocol, it is assumed that an active wear track is present on the tribocorrosion process, which will be characterized by a different electrochemical state when in comparison with the unworn area. This electrochemical state is characterized by EIS under sliding, resulting in an impedance under sliding that is a mixed impedance of the unworn and worn area, as already referred, and in order to characterize electrochemically the state of the worn surface, certain relations are assumed in order to make the deconvolution of the electrochemical values that characterize the

unworn area and the worn area. As an active wear track isn't obtained when testing the Anodized samples on the studied conditions (for more insight on the wear track of Anodized samples consult Chapter 3.4), the equations of the protocol that able the deconvolution of the impedances aren't fitted to the evaluation of the Anodized samples. The equations are present on Chapter 2. At last, as the impedance under sliding was schedule to start 15 min after the beginning of sliding, part of the impedance measurement was made during the gradual cathodic shift present on Figure 35 B, where the system wasn't electrochemically stable. Anyway, an evaluation of the changes of the system may be done with the observation and the comparison of the Nyquist plots and Bode plots obtained for the Anodized samples under friction. This methodology will be applied whenever is necessary to evaluate the conditions of the Anodized film under sliding.

The Bode plot (Figure 38), on this case, doesn't show any difference between the sample tested at 0,4N and at 0,8N. The evolution of the total impedance and of the phase angle is very similar in both cases. On the other hand, the Nyquist plot of Figure 36 B shows a difference between the samples tested at 0,4N and at 0,8N, especially on the high frequency range. The high frequency range is related to the outer porous layer of the Anodized film and by the plot it appears that when the load is increased the polarization resistance of the porous layer will increase. This would not be consistent with the fact that at 0,8N it's visible a cathodic shift of the open-circuit potential at ≈ 3,3 hours related to the destruction of the Anodized film. In this way, to evaluate the impedance under friction one should try to locate the impedance during the evolution of the open-circuit potential, to see if it was before or after the cathodic shift. The impedance measurement starts before the cathodic shift but the last three or two points are measured during the shift, but as the potential varies very slowly, the influence of the destruction of the Anodized film is not visible on the impedance. To eliminate the possibility that it could be a difference between the properties of the samples, the impedance before sliding on both samples was compared. Here, the increase of the loop at the high frequency range was already noticed. As the anodization process is a technique that is very sensible to modification of the parameters or preparation of samples, it is possible to obtain a certain variation on the Anodized film properties from sample to sample. This fact invalidates that the change on the loop under sliding is due to the difference of the normal force imposed on the surface of the sample under sliding. This variation is a result of a discrepancy on the reproducibility of the anodization process. Even so, the electrochemical impedance measurements performed confirmed the superiority of the Anodized samples and such tests show the potential of the anodization process as a surface treatment to improve the performance of the implant material. However, a more precise evaluation of the electrochemical impedance on the Anodized samples is necessary to better understand the mechanisms of reaction of the Anodized film with the surrounding electrolyte as well, regarding the anodization process itself, it should be guaranteed the reproducibility of the process.

As a surface modification for a biomaterial with applications in a dental implant, the anodization process proves its potentiality against the artificial saliva. The studied conditions of

electrolyte as artificial saliva at a pH of 5,5 may simulate the first stages of implantation of the material on the patient, since after the procedure the pH of the surrounding environment for the dental implant is of 5,5 and increases only after 2 or 3 weeks and also some saliva may remain on the contact after the surgery. In the meantime, the implant may be subjected to several electrochemical reactions with the environment and with the performed tests until now, it's possible to observe that the anodization process provides a certain reinforcement on the surface of titanium against those reactions.

The next set of tests, where the effect of velocity and the presence of a cellular layer on the surface of the material are studied, will give the opportunity to observe others aspects related to the implant material and the anodization process.

3.3.2 Effect of Velocity

3.3.2.1 Open Circuit Potential Evolution

In order to be able to compare the mechanical wear the same number of mechanical contacts (N = 7200) than the first set of tests done at 100 rpm was defined. In this part of the work it was only possible to perform one test for each condition due to the time that each test takes. The open-circuit potential was recorded during 3 hours before starting the continuous unidirectional sliding tests, in order to see the stabilization of the potential after immersion on the solution, during the continuous unidirectional sliding tests and for about 20 minutes after the end of the sliding tests. As the decrease of velocity to 2 rpm increases to ≈ 60 hours the duration of sliding, the comparable portion of potential to the first tests at 100 rpm corresponds to a window of time of 0,7 hours. Figure 39 shows the evolution of the open-circuit potential at 100 rpm and 2 rpm for both tested normal forces on the Ecthed and Anodized samples on the comparable window of time.

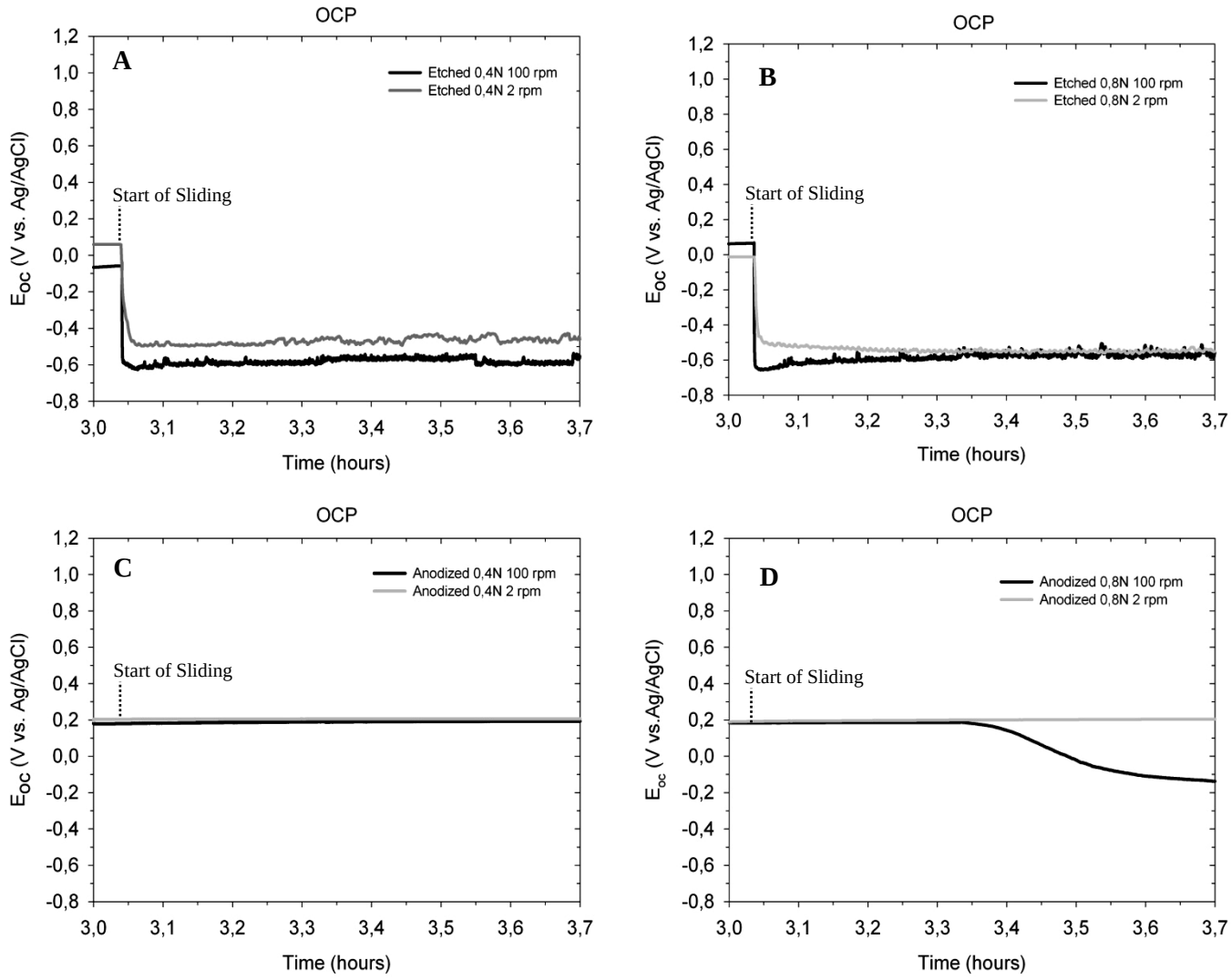

Figure 39 - Evolution of the open-circuit potential under continuous unidirectional sliding tests performed at 0,4N ((A) - (C)) and 0,8N ((B) - (D)) at 100 rpm and 2 rpm on Etched and Anodized samples.

For the Etched samples, on the moment when the mechanical contact occurs and sliding starts, it's visible that on both normal loads, the potential has a lower cathodic shift at 2 rpm than at 100 rpm, showing a less negative value of potential. The potential under sliding at 100 rpm is of - 0,6 V vs. Ag/AgCl on both normal loads and at 2 rpm is of - 0,4 V vs. Ag/AgCl at both normal loads, with a tendency to decrease after few cycles to - 0,6 V vs. Ag/AgCl when the normal load increases to 0,8N. At lower velocities the potential of titanium seems to reveal more anodic values. The velocity of sliding is related to the time between two successive contact events and in a passivating material, after a contact event that results on the removal of the surface oxide passive film and exposes active surface, the material will have the tendency to repassivate again the active surface. The open-circuit potential under sliding records the evolution of the potential in both this phenomena and is characterized by an equilibrium potential of destruction and repassivation of the surface oxide film. In this way, the tendency of repassivation will be affected by the velocity of the counter-body and the frequency of the contact events. The studied velocities are of 100 rpm (1,67 Hz) and 2 rpm (0,032Hz), being the latter fifty times slower than the first. The samples tested at 2 rpm have only a small part of active area exposed to the electrolyte, that immediately after the passage of the ball, will start to repassivate and has a longer period of time for repassivation than the ones tested at 100 rpm. In that period of repassivation, the material is not subjected to mechanical destruction of the surface oxide film and the ratio active/passive area decreases, leading the potential to more anodic values and a galvanic coupling that is not as strong as at 100 rpm. As a result, the open-circuit potential under sliding of the samples tested at 2 rpm reveal a more anodic value. Considering now the Anodized samples (Figure 39 C and D), at 0,4N is shown the same tendency at both velocities, maintaining the potential at + 0,2 V vs. Ag/AgCl. The change of velocity (frequency) of sliding doesn't seems to affect the integrity of the Anodized film. The surface remains electrochemically stable and the Anodized film provides a continuous protection to titanium against the electrolyte. In contrast, it is possible to see a change on the potential of the sample tested at a higher load (0,8N) and faster velocity. When the sample is tested at 100 rpm (graphic C), after about 1667 cycles (has already has been described) the Anodized film reaches a limit and starts to show cathodic values, but when tested at 2 rpm the potential remains stable. This fact shows that the integrity of the Anodized film may somehow be directly related to the number of contact events (cycles) and not to the velocity (frequency) of sliding.

The complete evolution of the open-circuit potential of the Etched samples tested at 2 rpm is presented on Figure 40.

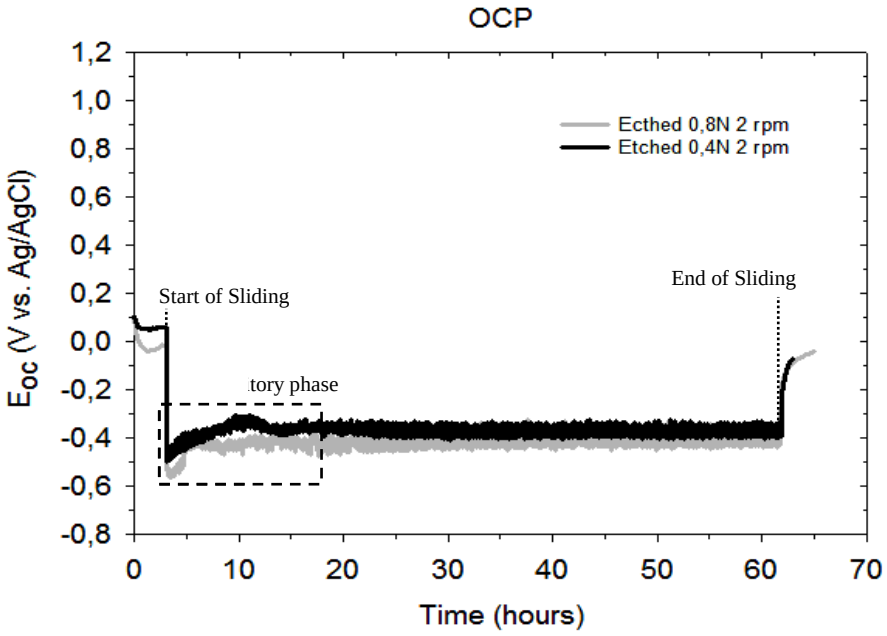

Figure 40 - Evolution of the open-circuit potential, before, during, and after continuous unidirectional sliding tests performed at 0,4N and 0,8N at 2 rpm on Etched samples.

Before sliding the open-circuit potential of the sample tested at 0,4N follows the expected evolution and the sample tested at 0,8N has a minor diference of - 100 mV on the stable potential (0 V vs. Ag/AgCl). At the time of the mechanical loading and the beginning of sliding, the typical cathodic shift due to the sudden destruction of the surface oxide film is evident on both samples, has already discussed. During the first cycles of sliding a certain evolution of the potentials is seen until their stabilization at ≈ 20 hours. While on Figure 35 A after the beginning of sliding the potential doesn't seems to have a transitory phase, on Figure 40 it's possible to observe such phase, where the potential has a certain evolution after sliding started. In this phase the surface oxide film is being slowly removed by the ball (at a lower frequency than at 100 rpm) and the surface of the material reacts with the electrolyte to repassivate the surface with a different reaction kinetic. Eventually, the surface of the material will accommodate to the cycles of destruction/repassivation and reach a equilibrium potential under sliding, that is characterized by the galvanic coupling between the potential of the active area of the wear track and the potential of the remaining passive area. Also, a difference on the potential under sliding is observed on the samples tested at 2 rpm. While the sample tested at 0,4N shows a stable potential under friction of – 0,35 V vs. Ag/AgCl the one tested at 0,8N is stable at -0,4 V vs. Ag/AgCl. Such effect is not due to the normal force, since from what can be seen in Figure 35 of section 3.3.1.1 of Chapter 3.3, it has been already exposed that the potential under sliding of titanium is not affected by the increase of the normal force. In fact, before sliding the samples had already a - 0,1 V difference on the equilibrium potential that will also influentiate the values recorded under sliding. In this way is possible to assume that both samples show a similar open-circuit potential under sliding of

approximately -0,4 V vs. Ag/AgCl. At the end of sliding the potential shifts to more anodic values due to the oxidation of titanium and the repassivation of the surface, with the formation of a new surface oxide passive film. At first, both samples reveal the same kinetics of the oxidation reaction due to the fact that the lines of the potential are almost overlapped and seem to start to stabilize at 0 V vs. Ag/AgCl. But if the potential would be measured for a longer period after the end of friction, the sample tested at 0,4N would reveal a more anodic potential (more positive potential) due to the lower effect of the galvanic coupling induce by the lower ratio of active/passive area.

The complete evolution of the open-circuit potential of the Anodized samples tested at 2 rpm is presented on Figure 41.

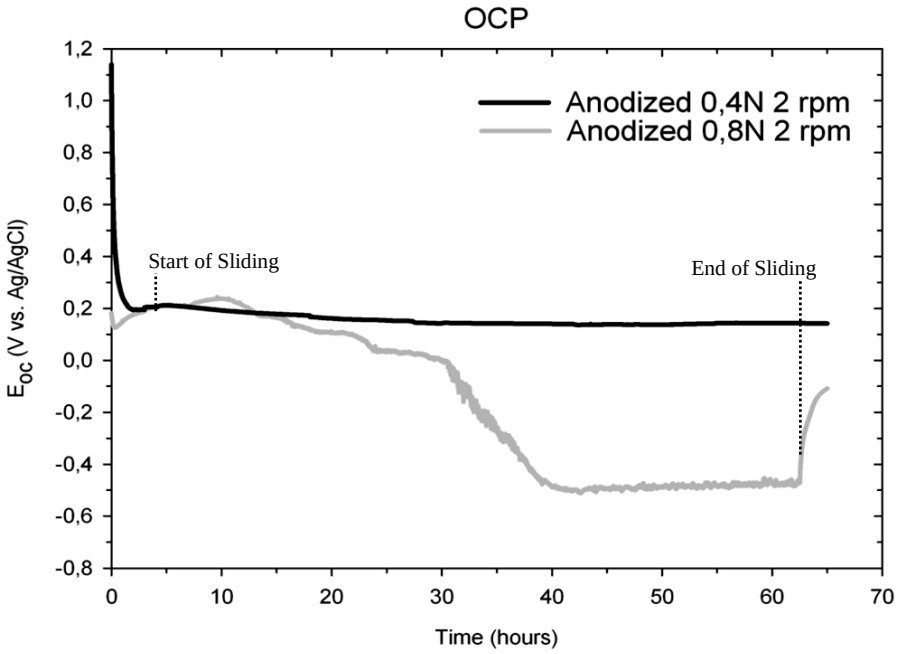

Figure 41 - Evolution of the open-circuit potential, before, during, and after continuous unidirectional sliding tests performed at 0,4N and 0,8N at 2 rpm on Anodized samples.

The velocity (frequency) of sliding was decreased by 50 fold at 2 rpm. In this way, also the amount of time that the samples will be subjected to mechanical load is changed, increasing from 1h10m at 100 rpm for 60h (2 and ½ days) at 2 rpm, giving the opportunity to observe how the Anodized film reacts to longer expositions of mechanical solicitations. After immersion on the electrolyte the potential shows an evolution until reaching a stable potential of + 0,2 V vs. Ag/AgCl. Such potential is in agreement with the previous results. When sliding starts, the potential maintain its tendency and again the Anodized film seems to be resistant against the mechanical contact and keeps protecting the surface of titanium. The values of potential of the sample tested at 0,4N doesn't show any variation and even after the end of sliding, the potential is stable at + 0,2 V vs. Ag/AgCl. By its side, the sample tested at 0,8N has a different tendency. At ≈ 7 hours the potential starts to drift and then shows a trend to gradually decrease at 15 hours. It is interesting to see that at this time the sample has been subjected to approximately 1800 cycles, a value that is not too far from the one obtained on

the test at 100 rpm (1667 cycles) for the cathodic shift. This may be evidence that the Anodized film is sensible to cyclic loading and has a critical point of stability. After, at ≈ 30 hours a more important cathodic shift is evident until the potential stabilizes at – 0,4 V vs. Ag/AgCl. Here the electrochemical interface between the material and the electrolyte has changed, and the values suggest that the integrity of the Anodized film may have been compromised. This is confirmed by the fact that the same potential is demonstrated by the Etched samples tested at the same velocity (2 rpm). This is evidence that the Anodized film is no longer providing protection against the electrochemical dissolution of titanium to the electrolyte, since the potential measured is representative of the active surface of the Etched titanium. Here, and after the evaluation of the wear track, was possible to confirm that the Anodized film has been completely damaged and removed from the surface, allowing the infiltration of electrolyte and the occurrence of electrochemical reactions, characteristic of corrosion phenomena. The wear track morphology that corroborates such analysis is discussed on Chapter 3.4. This cathodic potential is maintained until the end of sliding, when the potential starts to reach more positive values (anodic shift) and at the end of the test is at a potential of -0,1 V vs. Ag/AgCl.

The change of the velocity of sliding allowed the opportunity to see the mechanical resistance of the studied Anodized film as well the electrochemical response of the material. As it was referred, the sliding time increased from 1h10min to 2 and ½ days, giving a secure window of time where it was possible to see the evolution of the resistance of the Anodized film to sliding and compare it to the Etched titanium. It was interesting to see that at the beginning, the Etched samples had a transitory phase where the potential drifted until stabilization. Is possible to confirm that the reactivity of the surface of titanium is high and it tries to adapat itself to the constant removal of the oxide film that protects the surface. On the Anodized samples, for instance, that transitory period isn't observed since the anodization provides already a surface that is resistant, from the first moment, against the mechanical solicitations. Notwithstanding what has been said, with the tests at 2 rpm was possible to remark that even with the good mechanical properties and good contact surface, the Anodized film, sooner or later, will start to reveal weak points and give in to the degradation of its integraty. As the Anodized film is a stratified structure, the gradual drop of the potential was awaited. The real exposure of the base material, titanium, occurred only at ≈ 42h of constant sliding (load/unloading).

3.3.2.2 Electrochemical Impedance Spectroscopy

An Electrochemical Impedance Spectroscopy was performed during sliding at 2 rpm. The Nyquist plots on Figure 42 show the impedance spectra of the Etched and Anodized samples tested at both loads and velocities. Figure 43 presents the Bode plot for the Etched samples and Figure 44 the Bode plot of the Anodized samples. From the fiting with the equivelent circuit, the values that characterize the electrochemical state of the wear track of the Etched samples are presented on Table 16.

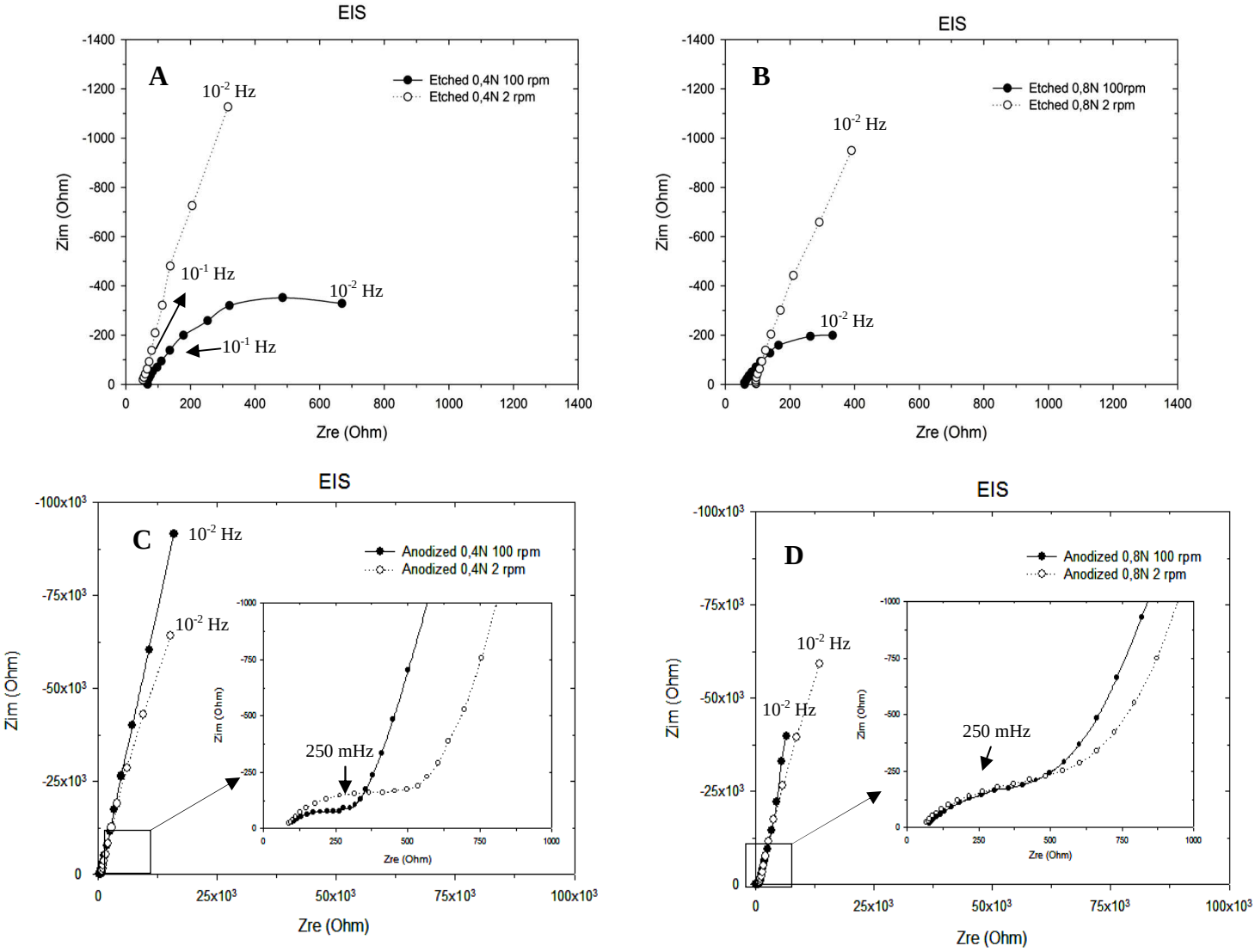

Figure 42 - Electrochemical impedance spectra measured at the mean open-circuit potential value during continuous unidirectional sliding tests performed at 0,4N ((A) - (C)) and 0,8N ((B) – (D)) at 100 rpm and 2 rpm on Etched and Anodized samples.

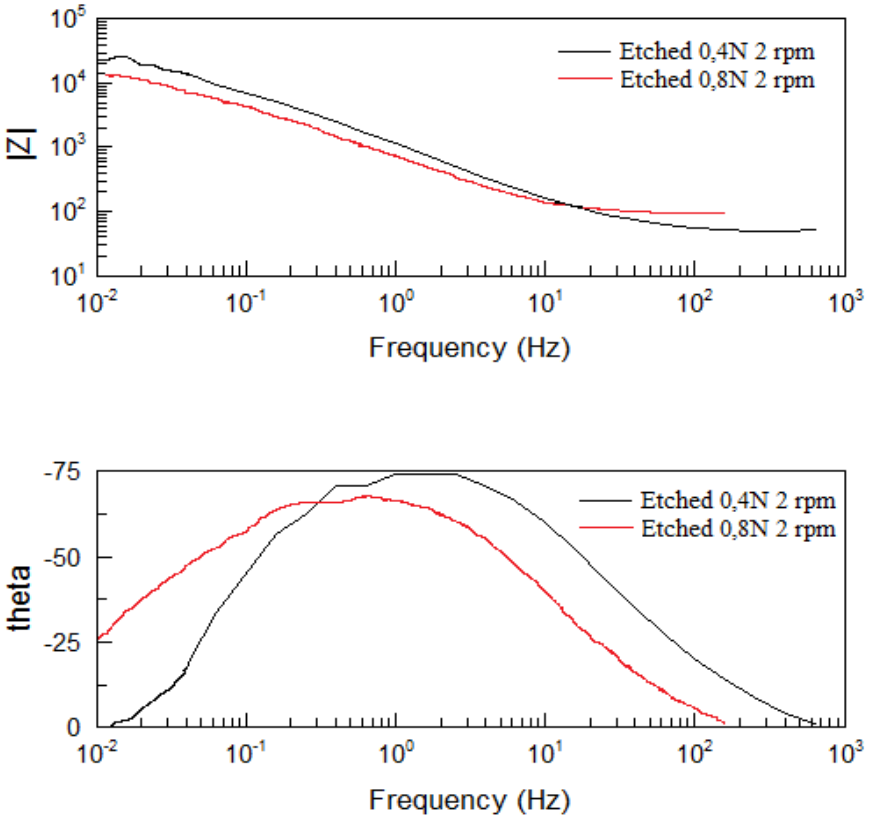

Figure 43 - Bode Z plot (frequency vs. impedance modulus |Z|) and Bode phase plot (frequency vs. phase angle) during continuous unidirectional sliding tests performed at 0,4N and 0,8N at 2 rpm on Etched Samples.

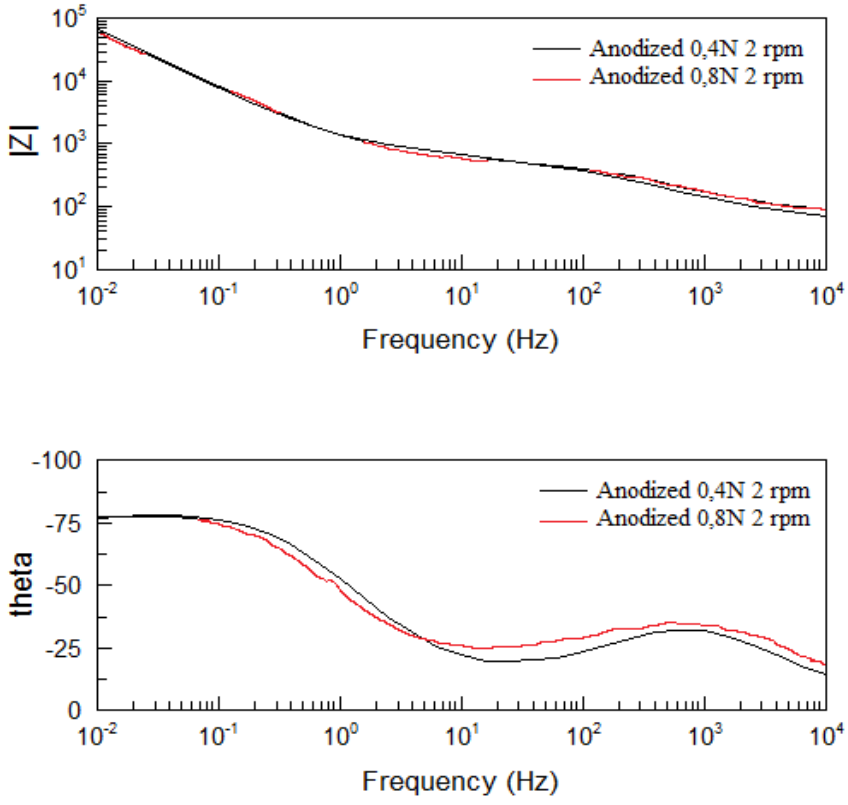

Figure 44 - Bode Z plot (frequency vs. impedance modulus |Z|) and Bode phase plot (frequency vs. phase angle) during continuous unidirectional sliding tests performed at 0,4N and 0,8N at 2 rpm on Anodized Samples.

Table 16 - Sliding track area, polarization resistance, specific polarization resistance and corrosion current density of Etched samples at open-circuit potential under continuous unidirectional sliding at 0,4N and 0,8N at 100 rpm and 2 rpm.

		A_{tr} (cm^2)	R_{ps} (Ω)	r_{act} ($\Omega.cm^2$)	i_{act} ($A.cm^{-2}$)
100 rpm	0,4 N	0,215 (± 0,12)	$57,8 \times 10^2$ ($\pm 7,73 \times 10^2$)	$31,4 \times 10^2$ ($\pm 24,1 \times 10^2$)	$2,59 \times 10^{-5}$ ($\pm 3,57 \times 10^{-5}$)
	0,8 N	0,249 (± 0,14)	$9,06 \times 10^2$ ($\pm 3,20 \times 10^2$)	$2,16 \times 10^2$ ($\pm 0,049 \times 10^2$)	$11,5 \times 10^{-5}$ ($\pm 2,57 \times 10^{-5}$)
2 rpm	0,4 N	0,281	$1,76 \times 10^4$	$4,54 \times 10^3$	$5,20 \times 10^{-6}$
	0,8 N	0,312	$1,47 \times 10^4$	$4,61 \times 10^3$	$5,21 \times 10^{-6}$

From Figure 42 A and B and if one considers the results at 2 rpm, the impedance curves aren't different in terms of the arc of circle that they describe. In opposition to the tendency showed on the samples tested at 100 rpm, the normal force doesn't seem to affect the value of the polarization resistance under sliding (R_{ps}). Also, the Bode Z plot (Figure 43) shows that the two studied systems aren't so different and their total impedance is relatively similar. On the phase angle, the stabilization of the capacitive domain of the samples is well defined and the protection provided by the passive film doesn't seems affected by the load, as the Nyquist plot already indicates.

It's clear the fact that the increase of the load implies a greater influence to the impedance diagram when the samples are tested at 100 rpm than at 2 rpm. The arc of circle clearly decreases its width when the load increases at 100 rpm but at 2 rpm such effect is not noticed (Figure 42 A and B). This results, where the normal force doesn't affecte the R_{ps} at lower velocities, might be due to the effect of the galvanic coupling on the impedance at 2 rpm. The galvanic coupling is dependent on the ratio active/passive area and greater is this ratio higher is the galvanic coupling and its effect on the corrosion currents. At 2 rpm only a small part of the surface of titanium is trully depassivated and exposed to the electrolyte. By this, in conjunction with a superior window of repassivation time, the ratio active/passive area is not as important as the same ratio at 100 rpm and, even with the increase of the load, at 2 rpm, it doesn't affect the galvanic coupling that in its turn would affect the corrosion currents measured during the impedance. A better characterization of the electrochemical state of the Etched samples is given by Table 16. It's possible to comprove the significant decrease of the polarization resistance under sliding at 100 rpm than at 2 rpm, displaying the sensitivity of the passive film to higher velocities of sliding. The R_{ps} of the samples tested at 2 rpm, with a normal load of 0,8N is only slightly lower than the one of the sample tested at 0,4N. In the same way, the values for the corrosion current density are very similar, giving the idea that even considering the different normal force that is being applied both samples are, in fact, being subjected to the same rate of dissolution of titanium to the electrolyte. It's possible to say that both samples are electrochemically reacting at the same rate.

Respecting the Anodized samples, both the Nyquist (Figure 42 C and D) as the Bode plot (Figure 44) reveal no difference on the impedance results for the Anodized samples tested at 2 rpm. On the Nyquist plot the impedance spectra is similar for both normal forces, even at the high

frequency range. On the samples tested at 2 rpm, the Nyquist plots before sliding were checked to see if the properties of the Anodized films were similar, and the sample tested at 0,4N had a minor loop at the high frequency range than the one observed during sliding. The loop of the sample tested at 0,8N was similar before and during sliding. Thus, at the high frequency range there has been a modification of the electrochemical interface at the outer porous layer of the Anodized film with a normal load of 0,4N, with a tendency to increase the polarization resistance of the porous layer. A similar effect as been already described by *Souza et al* [37], where it's discussed the effect of the sealing of the porosity on Anodized samples on the resistance of the porous layer, and the results revealed that an increase is observed with the sealing. On the characterization of the wear track at 0,4N is discussed that the Anodized film is not destroyed but instead deformed and the pores are covered by plastic deformation of the outer porous layer. For more insight on the wear track is advised the consultation of Chapter 3.4. In this way, the effect on the impedance may clearly be derived from the "sealing" of the pores. The results of the Bode plot (Figure 44) reveal a similar behaviour on both samples. In general, doesn't provide any additional information considering the effect of decreasing the velocity. However, as only one test was made at 2 rpm, more experiments are necessary to verify the tendency and exclude the possibility of dispersion of data.

One should have in mind that it isn't possible to apply the deconvolution of the impedances under sliding on the Anodized samples, with the applied protocol on this thesis. In this way, to evaluate the effect of velocity in terms of EIS on the Anodized samples, the spectra before sliding of each pair of samples (0,4N 100 rpm vs. 0,4N 2 rpm and 0,8N 100 rpm vs. 0,8N 2 rpm) displayed on Figure 42 C and D were compared. It was possible to observe that before sliding, the pairs of samples had similar spectra and any difference visible under sliding would be from the effect of the different velocity. In general, from Figure 42C and D, the Anodized films are not affected by the velocity of sliding. The impedance spectra are almost a straight line, revealing that electrochemicly the material is protected by a very strong film. Meanwhile, at the high frequency range of the samples tested at 0,4N, one may observe that at 100 rpm the amplitude of the loop is smaller than at 2 rpm. It appears that the velocity has some effect on the high frequency range of the Anodized film. Considering the previous assumption of the "sealing" of the pores with the plastic deformation of the Anodized film, the fact that two types of loops are observed at different velocities may be related to the time required to "seal" the pores and the damaged imposed on the Anodized film by it. At 100 rpm the resistance of the outer porous layer will be smaller due to the fact that the counterbody is sliding much faster than at 2 rpm. The tendency to obtain the plastic deformation needed to cover the pores its easily reached at 100 rpm, and when the impedance is performed, several pores will be already covered. However, at the same time, at 100 rpm the Anodized film is more damaged and more extended cracks than at 2 rpm may be already present, allowing the infiltration of the electrolyte to deeper layers of the Anodized film, decreasing the resistance. At 2 rpm the same may be obtained, but only after several cycles.

In a dental implant, considering that the patient reached a successful osteointegration of the implant, it will be fixed on the jaw and positively will remain like that all life. However, if loosening problems starts to arise, micromovements of the dental implant on the jaw will start to induce pression and wear on the surface of the material, due to the loads of mastication during meals, for instance. These extended cycles of load could be misimulated by this slow velocity and in this way obtain a better knowledge of how the Anodized film respond to a long exposure of slow loading cycles. On the other hand, it was also attractive to see that at 2 rpm the polarization resistance of the porous layer increased maybe due to some “sealing” effect and lower presence of cracks created during sliding. This associated to the fact that the film at 0,4N revealed extensive mechanical resistance during all test, may be a good starting point to expose some suggestions to the medical community like, for instance, the development of a new chirurgical procedure where, at the moment of insertion of the implant on the patient, if it were applied a new technique that had a major control on the torsion and load necessary to insert the implant, the surface of the implant would be less requested and as the results show, will remain protective against dissolution or even improve its resistance. Also, now related to the anodization process, the study of organic and biocompatibility sealings that may improve the resistance against electrochemical reactions may be one of the directions to turn, in order to advance even further on the performance of the superficial treatment.

3.3.3 Effect of Cell Layer

As an implant material with a potential application on dental implants, the effect of a layer of osteoblast cell on the tribocorrosion behaviour was also evaluated. The preparation of the samples may be consulted on Chapter 2 and the tribocorrosion conditions are maintained as the previous tests. The fact that the samples had a layer of biological material on the surface of the samples, the horizontality of the surface in relation to the counterbody could not be 100% satisfied.

3.3.3.1 Open Circuit Potential Evolution

Due to the contribution of the cell layer on the open-circuit evolution and the difficulty in having always the same exactly biological conditions on the surface of the material, the data obtained for all samples will be presented instead of one plot that represents a general behaviour of the biomodified sample.

Figure 45 displays the results of the OCP measurements on the bioEtched samples at both loads.

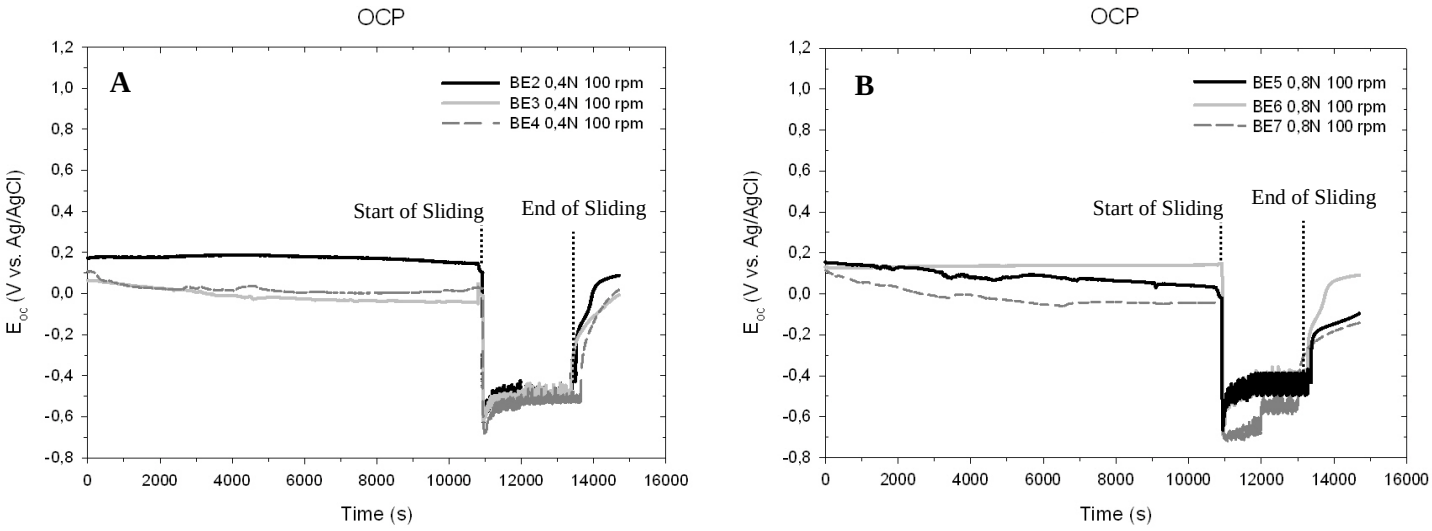

Figure 45 - Evolution of the open-circuit potential, before, during, and after continuous unidirectional sliding tests performed at 0,4N (A) and 0,8N (B) at 100 rpm on BioEtched samples.

Before sliding, on both images A and B, the open-circuit potentials of the samples vary between samples of the same group. At 0,4N BE2 has a potential that is very stable since the immersion on the electrolyte, around + 0,2 V vs. Ag/AgCl. It is a value superior than the expected (+ 0,1 V vs. Ag/AgCl) and similar to the potential of the Anodized samples. BE3 and BE4 show a lower potential that is close to 0,0 V vs. Ag/AgCl. At 0,8N (Figure 45 B) one of the samples has a stable open-circuit potential of + 0,1V vs. Ag/AgCl (BE6) while the others samples reveal a small cathodic tendency until nearly 0,0 V vs. Ag/AgCl, as well. The effect of the cell layer on the evolution of the open-circuit potential before sliding is not clear, since both effects of increasing and decreasing the potential were observed (Figure 35 shows the evolution without cells). The uncertainty on knowing

exactly if actually a significant cell layer was present on the surface of the sample is also another aspect that influences the evaluation of the results. Afterwards, the EIS evaluation of the samples may be more clear to show the influence of the cell layer. When sliding starts, at 0,4N the same drop on the potential is seen in all samples and the same potential under friction as on the regular Etched samples is registered, around - 0,6 V vs. Ag/AgCl. The samples tested at 0,8N reveal some dispersion on the potentials registered under friction. Sample BE7 follows the same tendency as the regular Etched samples with an open-circuit potential under friction of - 0,6V vs. Ag/AgCl while samples BE5 and BE6 have a potential around - 0,4V vs. Ag/AgCl. Since the cellular layer may be easily removed from the surface of the material with sliding, it is expected that the potential under sliding will be similar to the ones recorded without cells. However, while this is true for the samples tested at 0,4N, at 0,8N is observed that only one sample (BE7) follows the expected tendency and sample BE5 and BE6 show a potential similar to the one obtained when the regular Etched samples were tested at 2 rpm (- 0,4V vs. Ag/AgCl). In this situation, the variables are the impossibility of checking the horizontality of the sample before the test and the presence of biological material on the unworn area. Even that the counterbody removed the surface film and a wear track was visible on all length of the path of the counterbody, probably at same locations, the passive film was not removed entirely and only a superficial layer of the passive film was affected and removed by sliding. In this way, the surface remained semi-passivated and the potential was maintained at higher values. Also, it may be an effect of the different surface state that the remaining unworn area of the sample has, due to the cell culture. With this, the electrochemical behaviour of the unworn area might be different from the unworn area on the regular Etched samples and influence the potential recorded during sliding. At the end of sliding, on both images A and B, an increase of the potential is measured until the end of the test, implying the repassivation of the active wear track by the oxidation of titanium.

The plots obtained with the tests of the bioAnodized samples are shown on Figure 46.

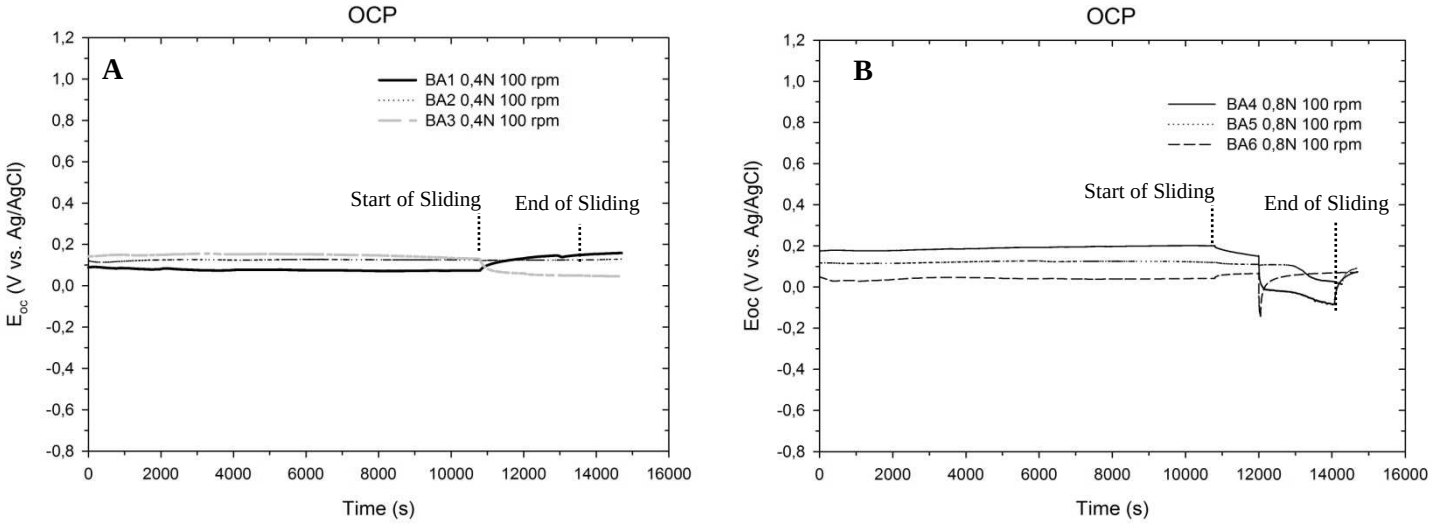

Figure 46 - Evolution of the open-circuit potential, before, during, and after continuous unidirectional sliding tests performed at 0,4N (A) and 0,8N (B) at 100 rpm on BioAnodized samples.

Considering that the open-circuit potential of the regular Anodized samples on artificial saliva is of + 0,2V vs. Ag/AgCl, in general, before friction the bioAnodized samples reveal a lower potential. The samples tested at 0,4N have a open-circuit potential near + 0,1 V vs. Ag/AgCl, and on the samples tested at 0,8N, sample BA4 is the only one that don't seems affected by the cell layer (+ 0,2V vs. Ag/AgCl) but sample BA5 has a lower open-circuit potential of + 0,1V vs. Ag/AgCl and BA6 has a potential very close to 0 V vs. Ag/AgCl. Again the electrochemical reactivity of the surface of the material changed with the cell culture, with a tendency to induce more cathodic values of open-circuit potential. On the Anodized samples the interpretation of the effect of the cellular culture is more difficult, since the anodization provides a complex morphology to the samples. The porosity present on the Anodized samples may allow the penetration of culture medium to the Anodized film and in fact, instead of measuring the effect of a cell layer, the difference measured on the potential is due to the infiltration of the culture medium to deeper levels of the film and its interaction with the Anodized film. This uncertainty is overcome with a control measurement, where a sample without cells is left the same time immersed on the culture medium and then the evolution of the open-circuit potential is observed. With sliding, a response of the potential is seen to the mechanical loading, but it is not constant and regular for all samples. All possible behaviours are seen, the potential or increases (BA1), maintains (BA2) or decreases (BA3) its values when loaded with 0,4N. It is known that without cells, at this load, the Anodized film remains protective at the mechanical loading and the potential continues stable at + 0,2 V vs. Ag/AgCl during all period of sliding. In this way, the variation seen on the potential might result from some influence that the cell culture had on the sample. It is possible that during culture, not only the cells spread on the surface (Figure 47) and the culture medium infiltrate the pores, but also some cells may interact with them and change the electrochemical interface.

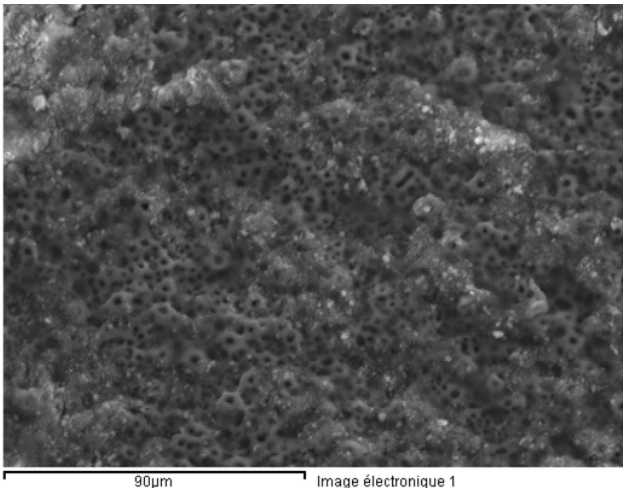

Figure 47 - Surface of BioAnodized Sample (750x).

On chapter 3.4 it is possible to see more micrographs of the surface of bioAnodized samples (Figure 74) with cells on the surface and how they remain on the top of the pores. However, more tests

are necessary to clarify what really happens on the bioAnodized samples at 0,4N. With the increase of the load, the open-circuit potential has also a different tendency than on the regular Anodized samples. Already at the moment of loading and beginning of friction with 0,8N, is seen a response on the potential from the samples that wasn't seen before. Samples BA4 and BA6 change their potential, while BA5 keeps the potential stable at + 0,2V vs. Ag/AgCl. The interesting aspect of samples BA4 and BA6 is that both show a cathodic shift at the same time (≈ 12000s) and if the number of cycles is calculated, this shift appears at ≈ 1667 cycles. If one recalls, it is the exact same number of cycles from which the same cathodic shift appeared on the regular Anodized samples tested at 0,8N. This observation allows one to confirm that until this point the Anodized film is protective and maintains its integrity but after it, the electrochemical interface is modified and the sample is subjected to corrosion phenomena. The shift on BA4 reveals a gradual decrease of the protection of the Anodized film, which may be related to the increase number of passages of the counterbody. On the other hand, the shift on BA6 is sudden and then the potential starts to rise, as if the Anodized film has been breached momentarily and then sealed by a repassivation process. As the potential reached the same value as before sliding (≈ 0 V vs. Ag/AgCl), the film was not affected by the passages of the counterbody and probably the defect occurred on an area outside the wear track. But the previous assumption could not be comproved by SEM and the wear track revealed the usual morphology for an bioAnodized sample tested at 0,8N. In the meantime, sample BA5 eventually shows the same shift, only at ≈ 12500s, in a more subtle evolution. This fact may be related to the horizontality of the sample in relation to the counterbody. At the end of sliding, BA4 and BA5 demonstrate the anodic shift of oxidation of the base material exposed to the electrolyte.

3.3.3.2 Electrochemical Impedance Spectroscopy

An impedance measurement was performed after the stabilisation of the potential before sliding, to see if the cell layer modified the mechisms at the electrochemical interface. The obtained impedance plot (Nyquist plot) for the BioEtched samples and the one of the regular Etched sample is presented in Figure 48.

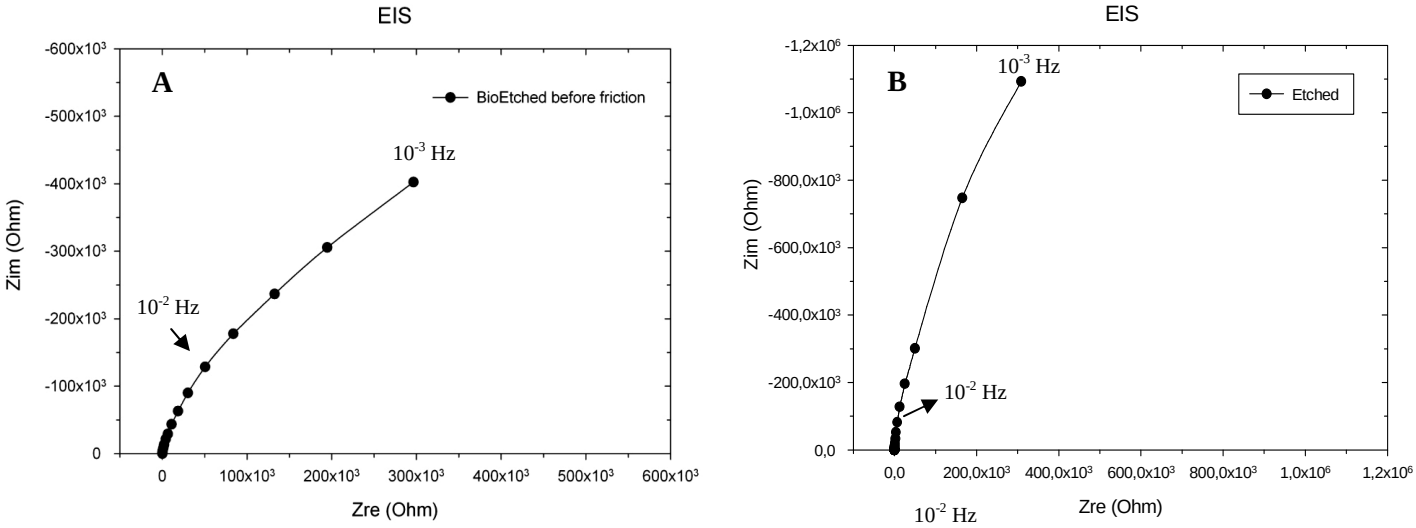

Figure 48 - Electrochemical impedance spectrum measured at the mean open-circuit potential value on BioEtched samples (A) and on the regular Etched samples (B).

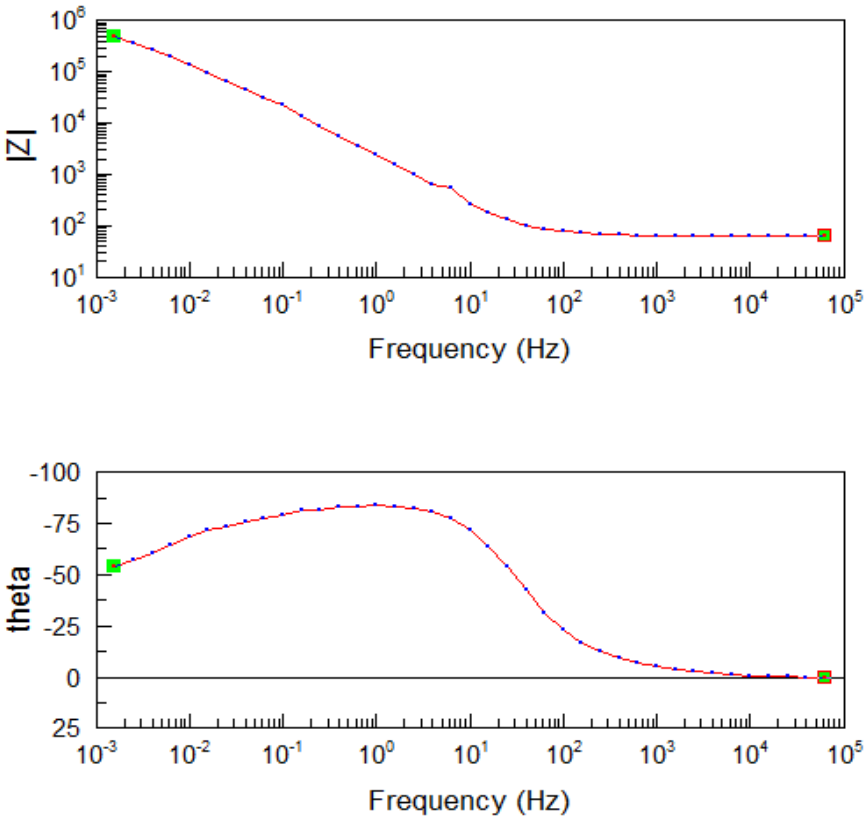

Figure 49 - Bode Z plot (frequency vs. impedance modulus |Z|) and Bode phase plot (frequency vs. phase angle) on BioEtched Samples.

The impedance spectrum of the bioEtched sample is different from the one of the regular Etched samples. The amplitude of the arc of circle appears to be lower and in consequence the polarization resistance of the passive film of the bioEtched samples will be smaller. By fitting with an equivalent circuit for the Etched samples presented in Chapter 2, the polarization resistance (*Rp*) and the values of the specific polarization resistance (*rp*) and the corrosion current density (i_{corr}) for the bioEtched sample were calculated and presented on Table 17.

Table 17 - Specific polarization resistance and corrosion current density of BioEtched sample without sliding.

A_0 (cm^2)	R_p (Ω)	r_p (Ω.cm^2)	i_{corr} (A.cm^{-2})
3,15 (± 0,10)	$3{,}47 \times 10^5$ ($\pm 2{,}74 \times 10^5$)	$1{,}10 \times 10^6$ ($\pm 8{,}88 \times 10^5$)	$5{,}55 \times 10^{-8}$ ($\pm 7{,}24 \times 10^{-8}$)

As suspected, the *Rp* of the bioEtched sample is smaller in comparison to the one of the regular Etched sample present on Table 14 ($8{,}08 \times 10^6$ Ohm). Even so, the r_p value obtained confirms the presence of a passive film on the surface of the material, but the cellular culture changed the properties of the passive film. As a consequence, it is not as protective for the surface of the material as the one of the regular Etched samples. That protection may also be evaluated by the corrosion current density, which is superior for the bioEtched samples leading to a higher amount of dissolution of elements to the electrolyte (217 µg/year).

An impedance measurement was done under continuous unidirectional sliding. The obtained impedance plot (Nyquist plot) for bioEtched samples tested at both loads is presented in Figure 50 and in Table 18 the average values obtained for the R_{ps}, for the specific polarization resistance under sliding (r_{act}) and the corrosion current density under sliding (i_{act}), calculated with the same methodology as in the regular Etched samples. As well the Bode plot is displayed on Figure 51.

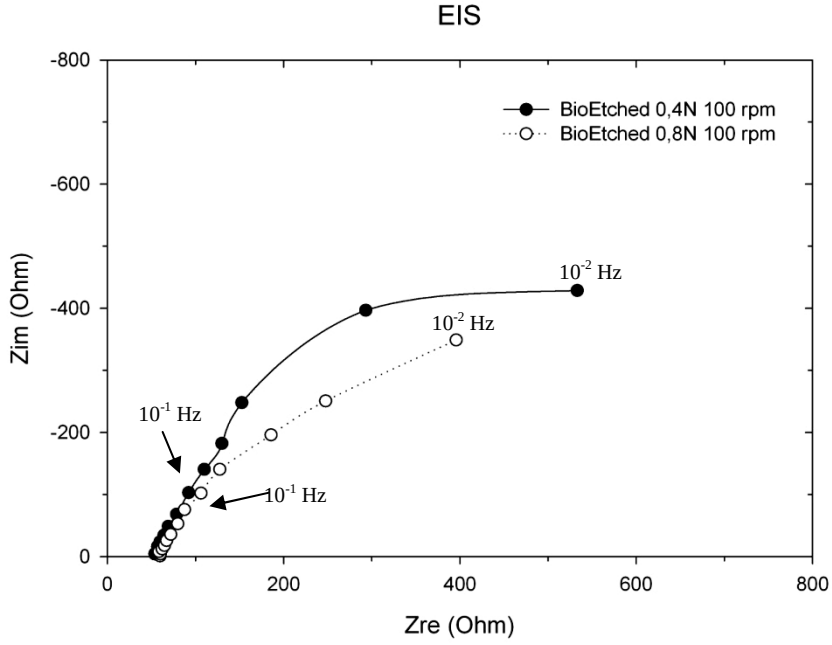

Figure 50 - Electrochemical impedance spectra measured at the mean open-circuit potential value during continuous unidirectional sliding tests performed at 0,4N and 0,8N at 100 rpm on BioEtched samples.

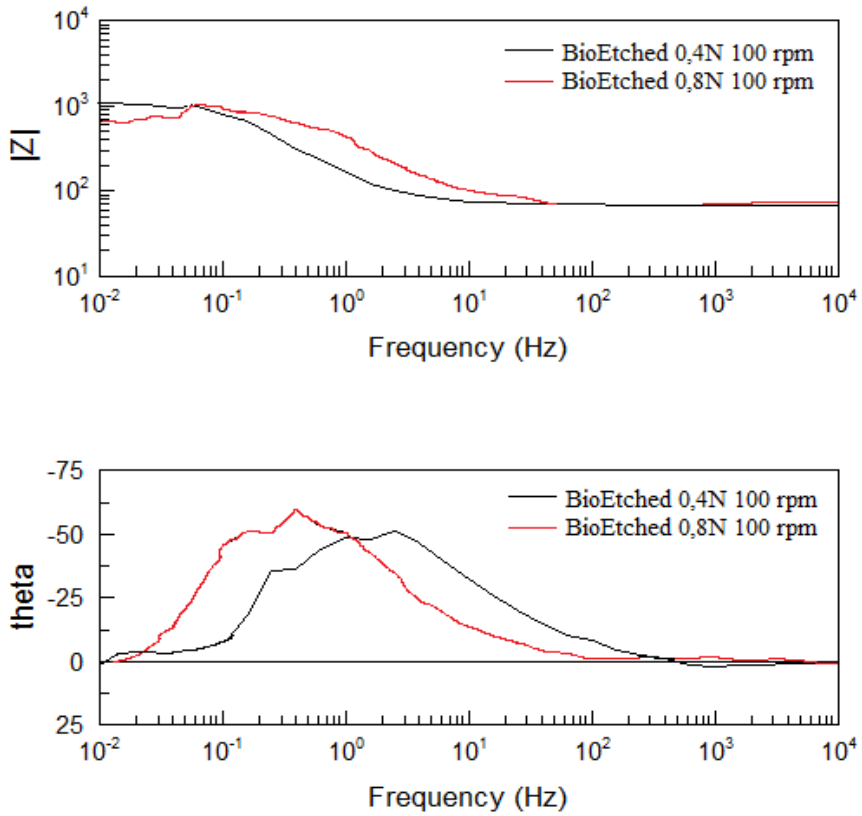

Figure 51 - Bode Z plot (frequency vs. impedance modulus |Z|) and Bode phase plot (frequency vs. phase angle) during continuous unidirectional sliding tests performed at 0,4N and 0,8N at 100 rpm on BioEtched Samples.

Table 18 - Sliding track area, polarization resistance, specific polarization resistance and corrosion current density of BioEtched samples at open-circuit potential under continuous unidirectional sliding at 0,4N and 0,8N at 100 rpm.

	A_{tr} (cm^2)	R_{ps} (Ω)	r_{act} (Ω.cm^2)	i_{act} (A.cm^{-2})
0,4 N	0,263 (± 0,11)	$9{,}65 \times 10^2$ ($\pm 1{,}71 \times 10^2$)	$7{,}73 \times 10^2$ ($\pm 4{,}03 \times 10^1$)	$5{,}39 \times 10^{-5}$ ($\pm 1{,}55 \times 10^{-5}$)
0,8 N	0,321 (± 0,14)	$8{,}58 \times 10^2$ ($\pm 3{,}06 \times 10^2$)	$2{,}54 \times 10^2$ ($\pm 7{,}66 \times 10^2$)	$9{,}61 \times 10^{-5}$ ($\pm 3{,}54 \times 10^{-5}$)

As seen on the regular Etched samples, sliding and increase of the normal force imposes a decline on the corrosion performance of the material. Both polarization resistances under sliding are lower than the one obtained before sliding (Table 17) with the sample tested at 0,8N showing the lowest value. With the deconvolution of the impedances (see Chapter 2) and calculation of r_{act} it is possible to observe that the corrosion current density for the bioEtched sample tested at 0,8N is relatively higher. The corrosion reactions are more present on the sample tested at 0,8N. Comparing the EIS data of the bioEtched samples (Table 18) with the EIS data of the regular Etched samples under sliding (Table 15), it's possible to state that the presence of the cell layer induced a general decrease on the electrochemical parameters evaluated. The difference between the conditions of the different loads it's more significant without the cellular layer. So, again, it is remarkable that the cellular layer will influence the electrochemical mechanisms on the interface electrolyte/sample.

The electrochemical impedance spectrum of the bioAnodized samples before sliding and the Bode Z plot and Bode phase plot are present on Figure 52A and Figure 53, respectively.

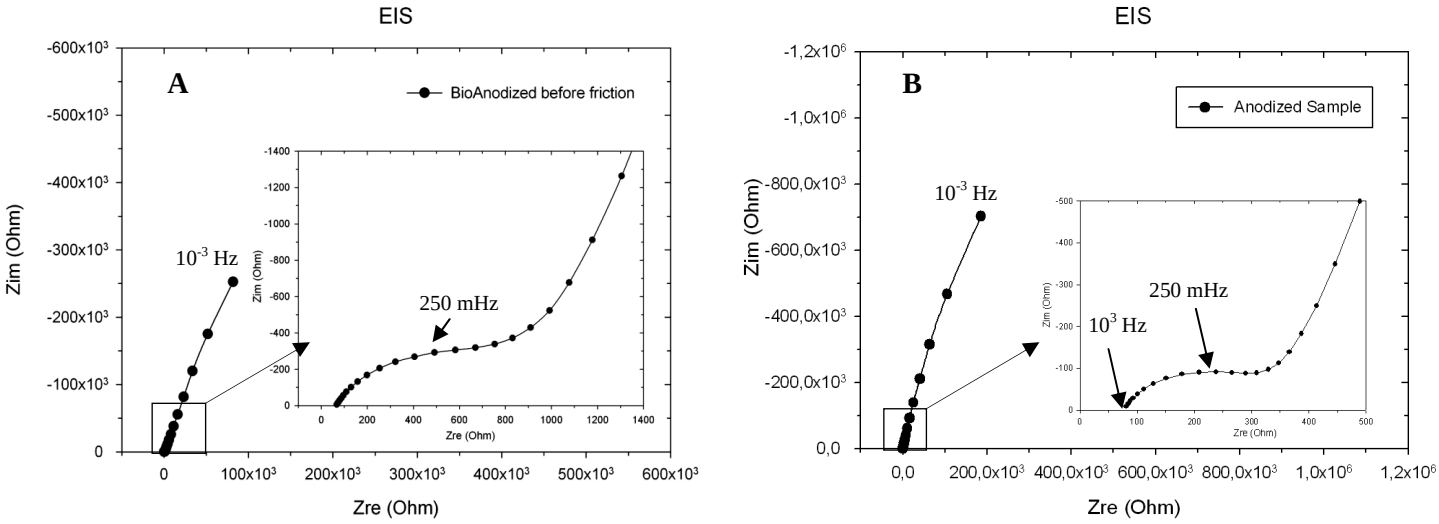

Figure 52 - Electrochemical impedance spectra measured at the mean open-circuit potential value on BioAnodized samples (A) and regular Anodized samples (B).

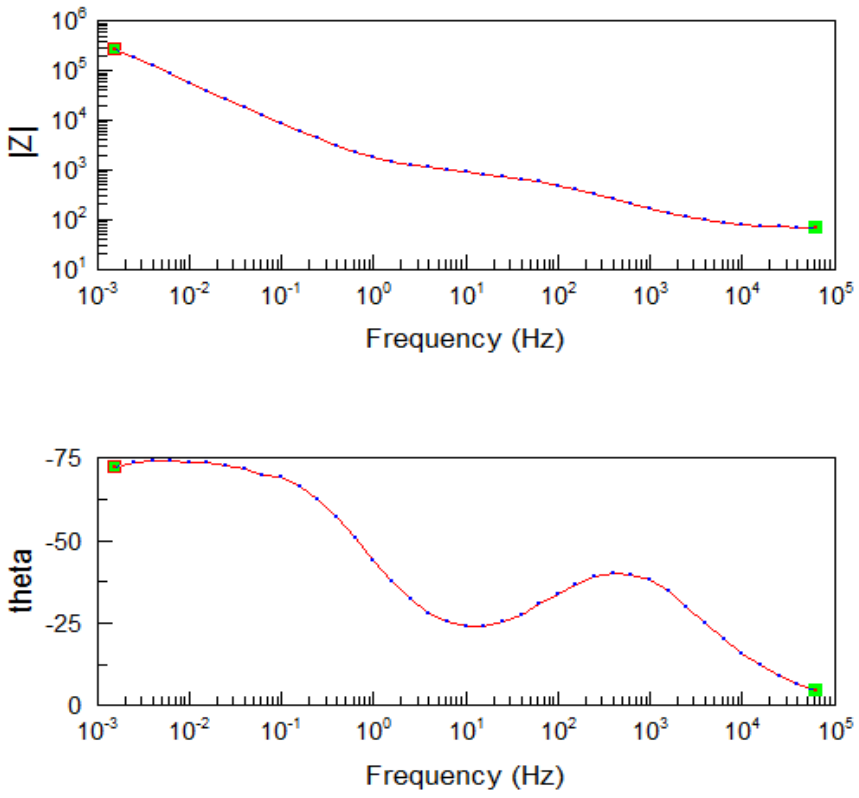

Figure 53 - Bode Z plot (frequency vs. impedance modulus |Z|) and Bode phase plot (frequency vs. phase angle) on BioAnodized Samples.

In general, the same type of spectrum is obtained with the bioAnodized samples. The Nyquist plot shows at the high frequency range a first arc of circle and then another arc until the last frequency measured (10^{-3} Hz). As already discussed, this behaviour is due to the complexity of the Anodized

film and its interactions with the electrolyte, where the first arc is related to the porous layer and the second to the barrier layer. However, if this plot is compared to the one of Figure 33, it's noticed that the first arc seems to have a higher magnitude on the bioAnodized samples than on the regular Anodized, while the polarization resistance, by its side, seems to have decreased. The Bode phase plot shows the two capacitive domains characteristic of the Anodized films.

To characterize the properties of the bioAnodized samples, the equivalent circuit for the Anodized samples presented in Chapter 2 was assumed. The average values obtained for the tested samples are present on Table 19.

Table 19 - Polarization resistance (R_p) and specific polarization resistance (r_p) of porous layer and Polarization resistance (R_b) and specific polarization resistance (r_b) of barrier film on BioAnodized sample without sliding.

A_0 (cm^2)	*Porous Layer*		*Barrier Film*		
	R_{pp} (Ω)	r_{pp} ($\Omega.cm^2$)	R_{pb} (Ω)	r_{pb} ($\Omega.cm^2$)	i_{corr} ($A.cm^{-2}$)
3,4 (± 0,01)	$9{,}95 \times 10^2$ ($\pm 4{,}68 \times 10^2$)	$3{,}40 \times 10^3$ ($\pm 1{,}60 \times 10^3$)	$2{,}21 \times 10^6$ ($\pm 4{,}12 \times 10^6$)	$7{,}55 \times 10^6$ ($\pm 1{,}41 \times 10^7$)	$2{,}54 \times 10^{-8}$ ($\pm 3{,}02 \times 10^{-8}$)

Indeed the cellular layer had an influence on the impedance response of the Anodized film. An increase on the resistance of the porous layer is seen with a specific polarization resistance of $3{,}40 \times 10^3$ $\Omega.cm^2$ vs. $1{,}45 \times 10^3$ $\Omega.cm^2$ on the regular Anodized film. On the work of *Yu et al* [80] it's evaluated the in vitro corrosion resistance of TiO_2 nanotube layers in solutions with proteins. The morphology of the surfaces is not the same as in this work, but the nanotubes will provide as well porosity to the surface of the material. When the material was tested in solution with proteins, it was seen that the proteins had the tendency to cover the tubes and in consequence, the resistance of the outer tube layer increased. As a new structure (cellular layer) was present on the surface of the Anodized samples and due to their natural tendency of spreading and growing, the cells will cover the pores of the Anodized surface and prevent the infiltration of medium and decrease the electrochemical reactions as well. This might be a first evidence of the effect of the cell layer on the surface of the Anodized film and a future study on the EIS behaviour of cell culture on Anodized samples would be interesting to conduct. Regarding the polarization resistance of the barrier film, it reveals a lower value against the regular Anodized sample showing that the corrosion performance of the barrier film decreased. It may be an effect of the interaction of the barrier film with the culture medium, due to the infiltration before the samples covered the pores.

An impedance measurement was done under sliding to evaluate the effect of the cellular layer on the impedance under friction. Figure 54 and Figure 55 represent the impedance results in the form of Nyquist plot and Bode plot, respectively.

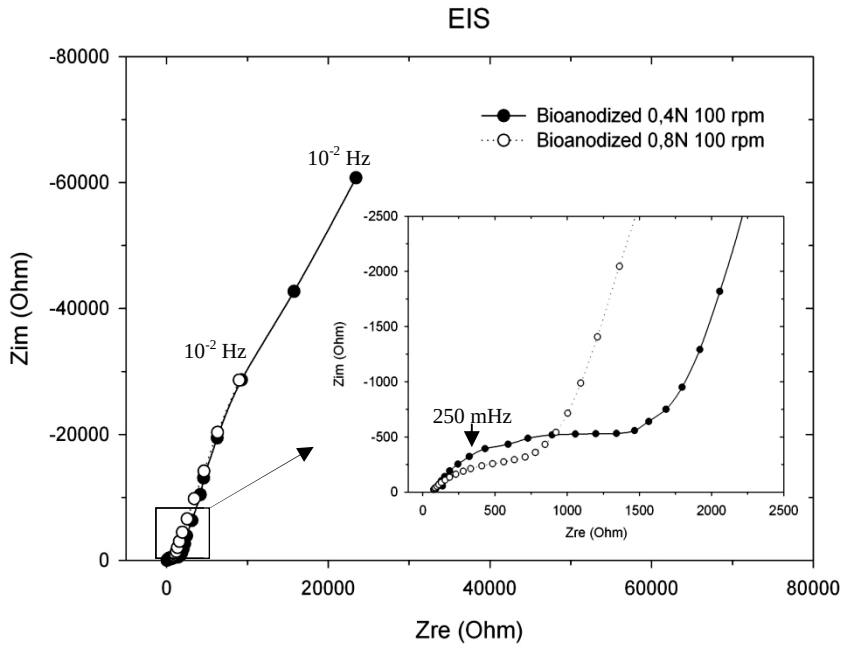

Figure 54 - Electrochemical impedance spectra measured at the mean open-circuit potential value during continuous unidirectional sliding tests performed at 0,4N and 0,8N at 100 rpm on BioAnodized samples.

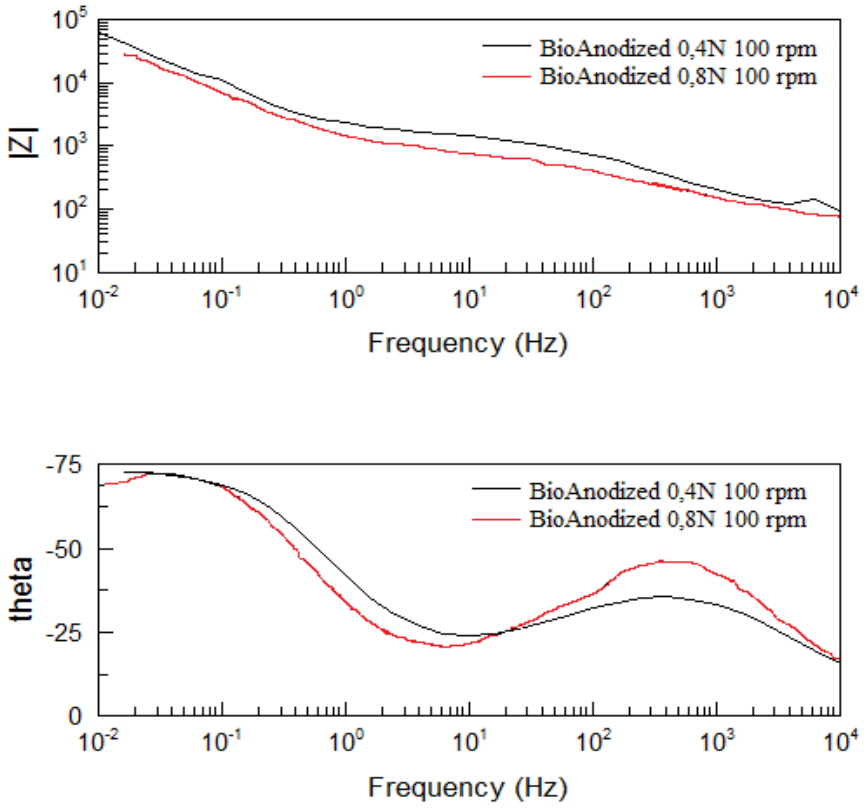

Figure 55 - Bode Z plot (frequency vs. impedance modulus |Z|) and Bode phase plot (frequency vs. phase angle) during continuous unidirectional sliding tests performed at 0,4N and 0,8N at 100 rpm on BioAnodized Samples.

On the evaluation of the impedance of the Anodized film, is important to be sure that all the samples have the same electrochemical tendency before friction, in order to validate the comparison during friction. Unfortunately, the first set of samples tested at 0,4N reveal a higher polarization

resistance for the outer porous layer before sliding than the samples tested at 0,8N. Table 20 shows the average values of the R_p of the bioAnodized samples and the set of samples tested at 0,4N has a higher R_p.

Table 20 - Polarization Resistance of Outer Porous Layer of BioAnodized samples.

Samples	R_p before sliding(Ω)
Set at 0,4N	$10{,}7 \times 10^2$
Set at 0,8N	$9{,}23 \times 10^2$

This fact influences the behaviour under sliding bringing a variance to the system that changes the evolution of the results. In this way it isn't possible to perform a comparison under sliding between the samples tested at 0,4N and 0,8N. In the meanwhile, it was explored if on the same sample the impedance diagram changed, before and during sliding. At the high frequency domain the loop before and during sliding remained the same and the common result to all samples is that the loop at low frequencies, that is related to the resistance of the barrier layer, decreased.

The rehearsal of testing Etched and Anodized samples with a layer of osteoblastic cells wasn't 100% a success but revealed helpful information and already showed some interesting results. The cellular cultures are very sensible to the environmental conditions and the biomodified samples weren't exception. The fact that the tests were performed on artificial saliva at pH of 5,5 and room temperature, wasn't the best conditions to evaluate the tribocorrosion properties of the samples with biological cells alive on the top of them. A great variability on the samples was found. It is true that with a cellular layer on the surface of the samples, the electrochemical interface would be changed. Such result was already seen, since in all samples, bioEtched and bioAnodized, there is a tendency to show different values of the electrochemical parameters as the polarization resistance. On the Etched samples the effect of a cell layer may be negative, with the decrease of the R_p but on the Anodized, due to the morphology of the film and the covering of the pores, actually the R_p of the porous layer may increase and in this way diminish the electrochemical dissolution of titanium. In the future, different test conditions, like increase number of culture days or using the culture medium on the tribocorrosion test, may improve the environmental conditions for the cells as well will provide more realistic information. At the end of this thesis will already be presented some measurements with these suggestions, as a preliminary study.

When the conditions are optimized, it will be interesting to address the effect of the cellular layer on the electrochemical response of the surface as well on the mechanical response. This would be an important stage of tests for the anodization system, since it is the ultimate simulation of the real conditions of application for the dental implant.

3.4. Wear Mechanism and Wear Quantification

To attempt to define the wear mechanism present on the studied samples, SEM sessions were performed on each tested sample and for the wear quantification, microtopographical analysis were made on the wear tracks in order to obtain the volume of material removed by mechanical action. The tribocorrosion parameters were calculated accordingly to the protocol referred on Chapter 2 and the importance of each component of the wear, the mechanical wear and the corrosion wear, will be assessed.

3.4.1 Wear track of Etched Samples at 100 rpm and 2 rpm

The wear tracks on the Etched samples were well defined and uniform along all tracks. The change of the velocity of sliding didn't affect the morphology of the wear track. On Figure 56 are presented micrographs of the wear tracks on Etched samples tested with 0,4N and 0,8N.

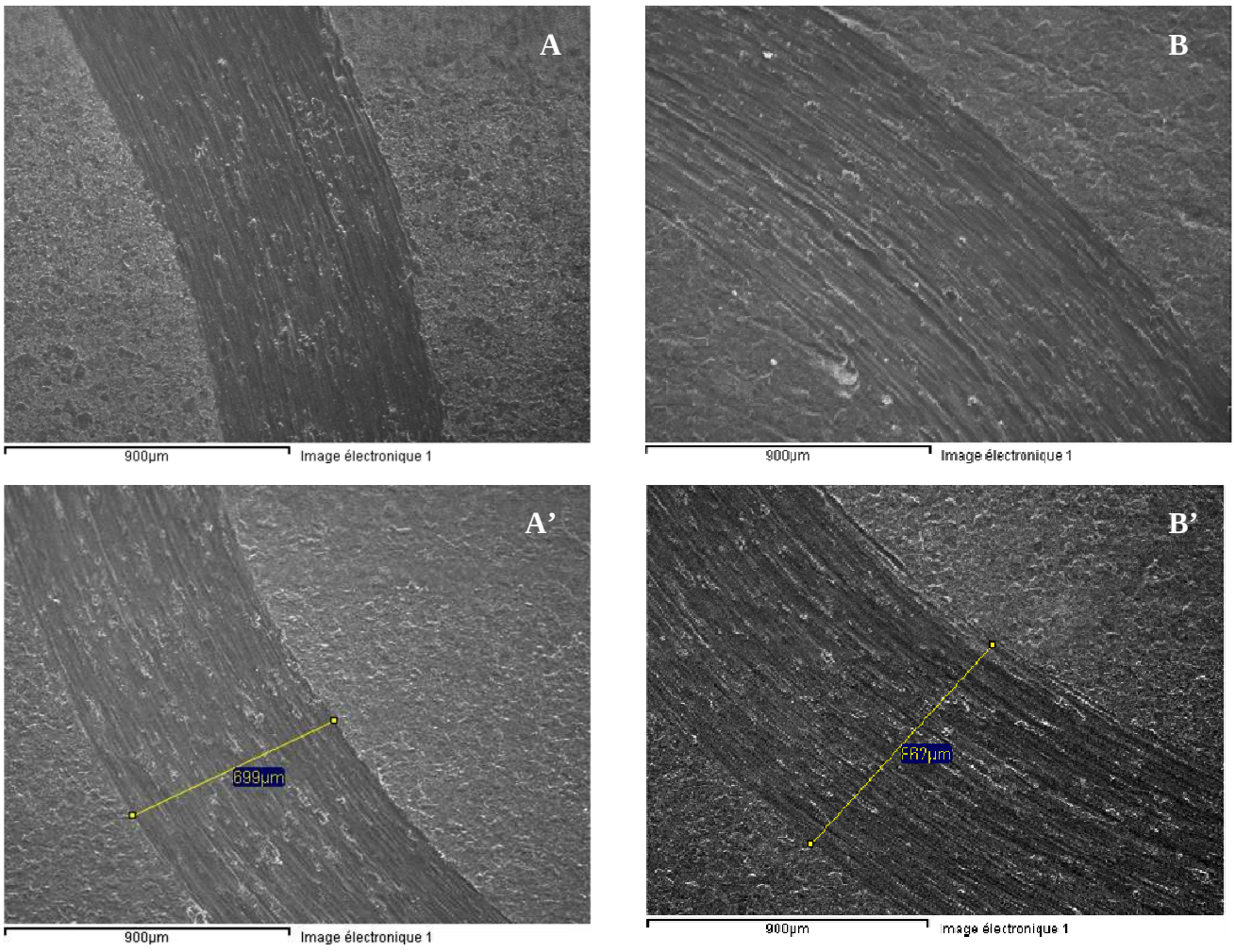

Figure 56 - Wear track of Etched Samples tested at 0,4N (A and A': 75x) and 0,8N (B and B': 75x).

With the presented micrographs it is clear the identification of the worn area and the unworn area, which are related to the active area and the passive area, respectively. Micrographs A and A' are

representative of the samples tested at 0,4N while B and B' are representative of the samples tested at 0,8N. From A' and B' it is possible to prove the increase of the width of the wear track with the increase of the normal force (699 µm for 0,4N and 862 µm for 0,8N), which in turn increases the exposed active area. Images at higher magnification are presented on Figure 57 to illustrate the morphology and wear mechanisms of the wear track.

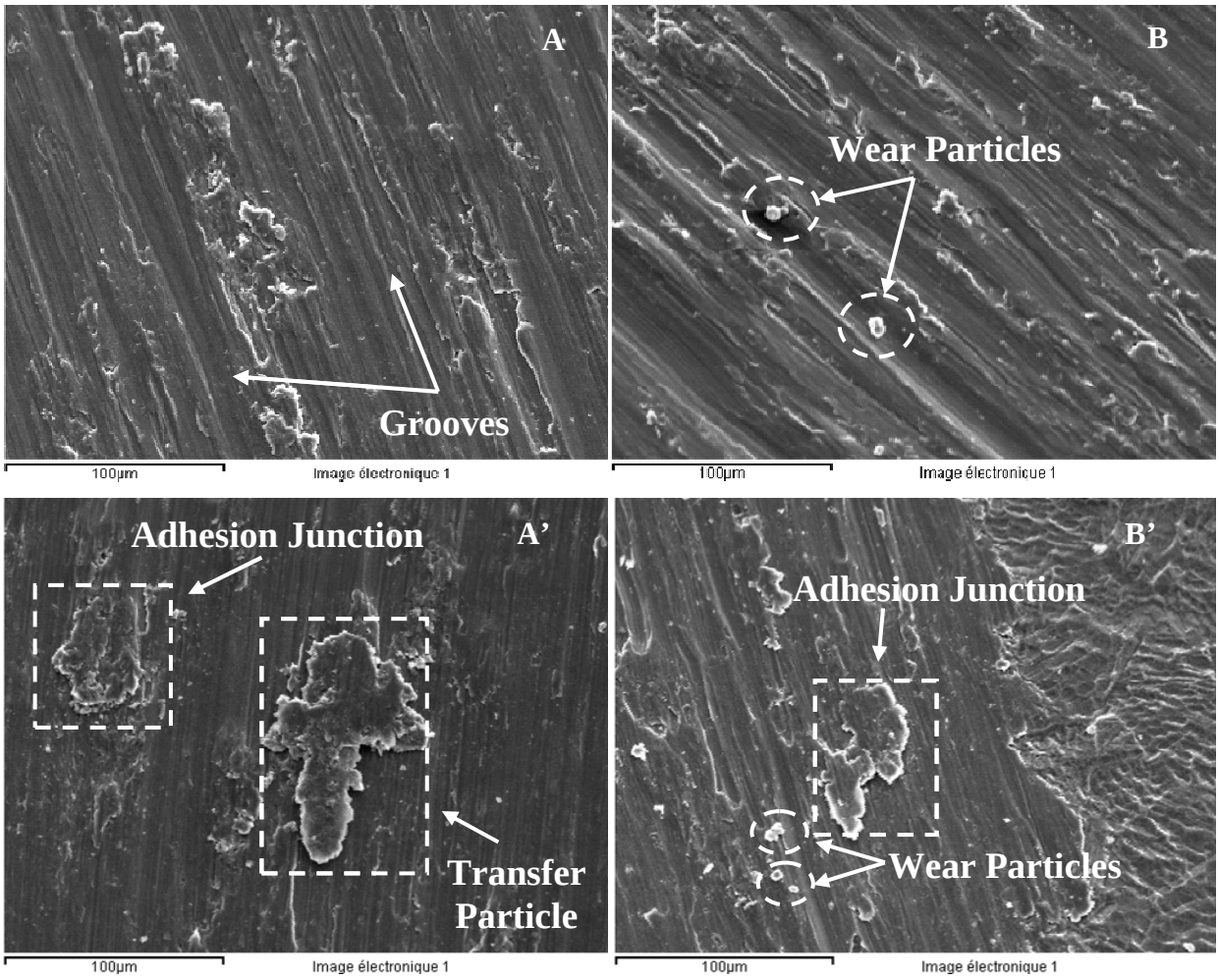

Figure 57 – Wear track morphology of Etched Samples tested at 0,4N (A and A': 350x) and 0,8N (B and B': 350x)

On both tested loads the morphology of the wear track is similar. It is evident the damaging imposed by the rubbing of the counterbody on the surface of the material, with the creation of grooves and scratches on all width of the wear track. By comparing Figure 57 A and B, it gives the impression that the grooves are more pronounced on image B, where also is possible to identify some wear particles. Such effect may be related to the increase of the normal force, and will be further explored on the discussion of the wear mechanism of the Etched samples. Similarly, adhesion junctions are present on both samples and a transfer particle is identified on image A' and on Figure 58. This last figure shows a groove that seems to result from the transfer particle.

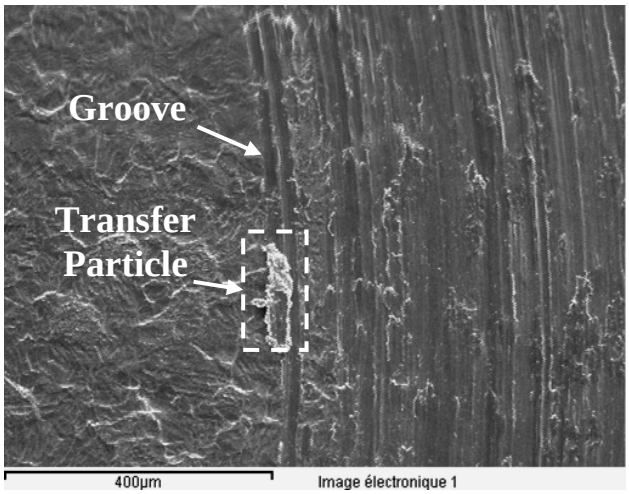

Figure 58 - Abrasive transfer particle and respective grooves on wear track of Etched sample (150x).

The chemical evaluation performed on the wear track, through EDS, revealed that the only component found was titanium (Figure 59) and apparently no material transfer occurred from the counterbody, on both tested loads.

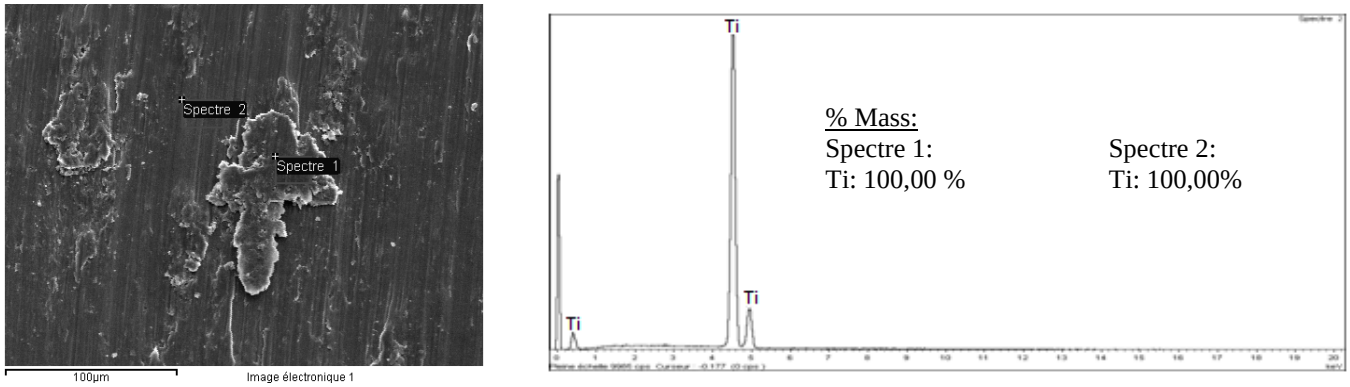

Figure 59 - EDS analysis of the wear track of Etched samples: A) 0,4N.

Concerning the wear particles, Figure 60 A shows the agglomeration of particles on the inner borders of the wear track. Here it is possible to have an idea of the high number of particles created during sliding. Figure 60 B is a micrograph on the middle of the wear track. It is possible to see that the wear particles have the same configuration that on the borders, small particles, and even some of them may agglomerate to form bigger particles. The EDS results (Figure 61) of the evaluation of two particles reveal high amounts of titanium and oxygen (due to the oxidation of the particle by the electrolyte) and some aluminium.

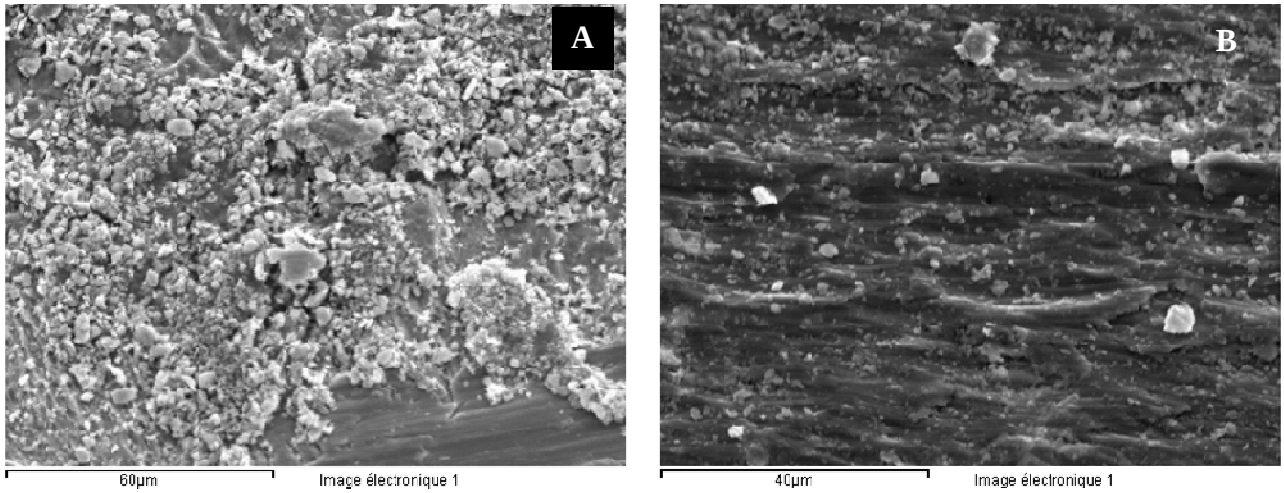

Figure 60 - Wear particles in the wear track of Etched sample A) 1000x B) 1500x.

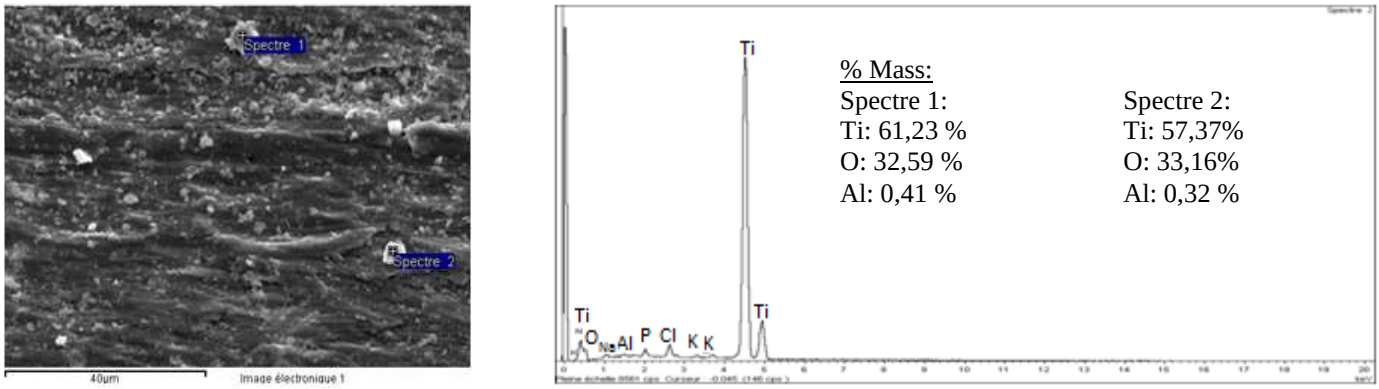

Figure 61 – EDS analysis of the wear particles of Etched samples.

If these particles remain on the tribological interface and are not dissolved on the electrolyte, they may oxidize and interact with the tribological contact.

After the tribocorrosion tests of the Etched samples, as the counterbody revealed a grey spot on the point of contact, SEM analysis was performed on the counterbody to see what changed on the surface. Figure 62 display micrographs of the alumina ball before and after friction.

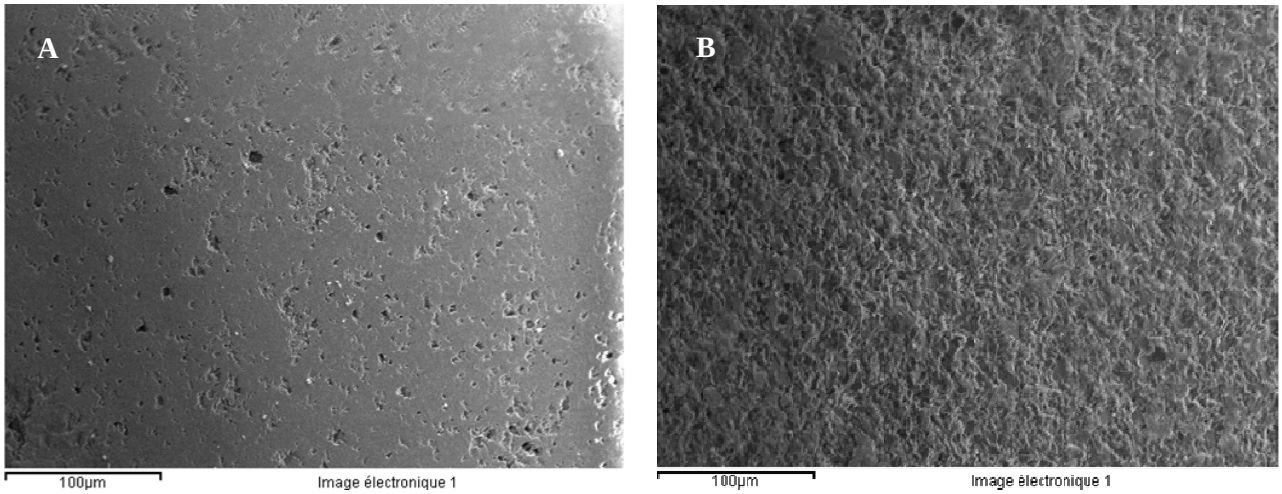

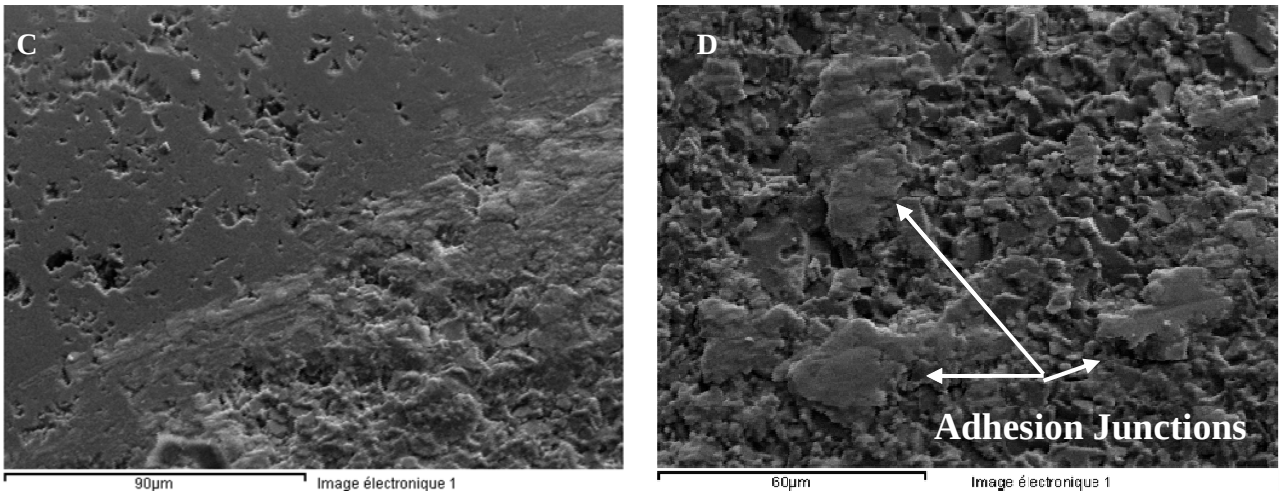

Figure 62 - Alumina Ball: A) Before friction (350x) B) After friction (350x) C) Border (750x) D) Middle of grey spot (1000x).

It is clear the change on the surface morphology of the counterbody. Before friction the surface of the counterbody is smooth while after it seems to be rough. On image C is possible to see the border between the two morphologies of the surface of the counterbody. It seems that a deposit of material is on the surface of the counterbody. That deposit is characterized by several particles attached between them (image D) and also is possible to identify adhesion junctions that may have form between the counterbody and the Etched sample. The EDS analysis (Figure 63) revealed that the composition of the surfaces before and after friction is different, showing transfer of material from the sample to the counterbody.

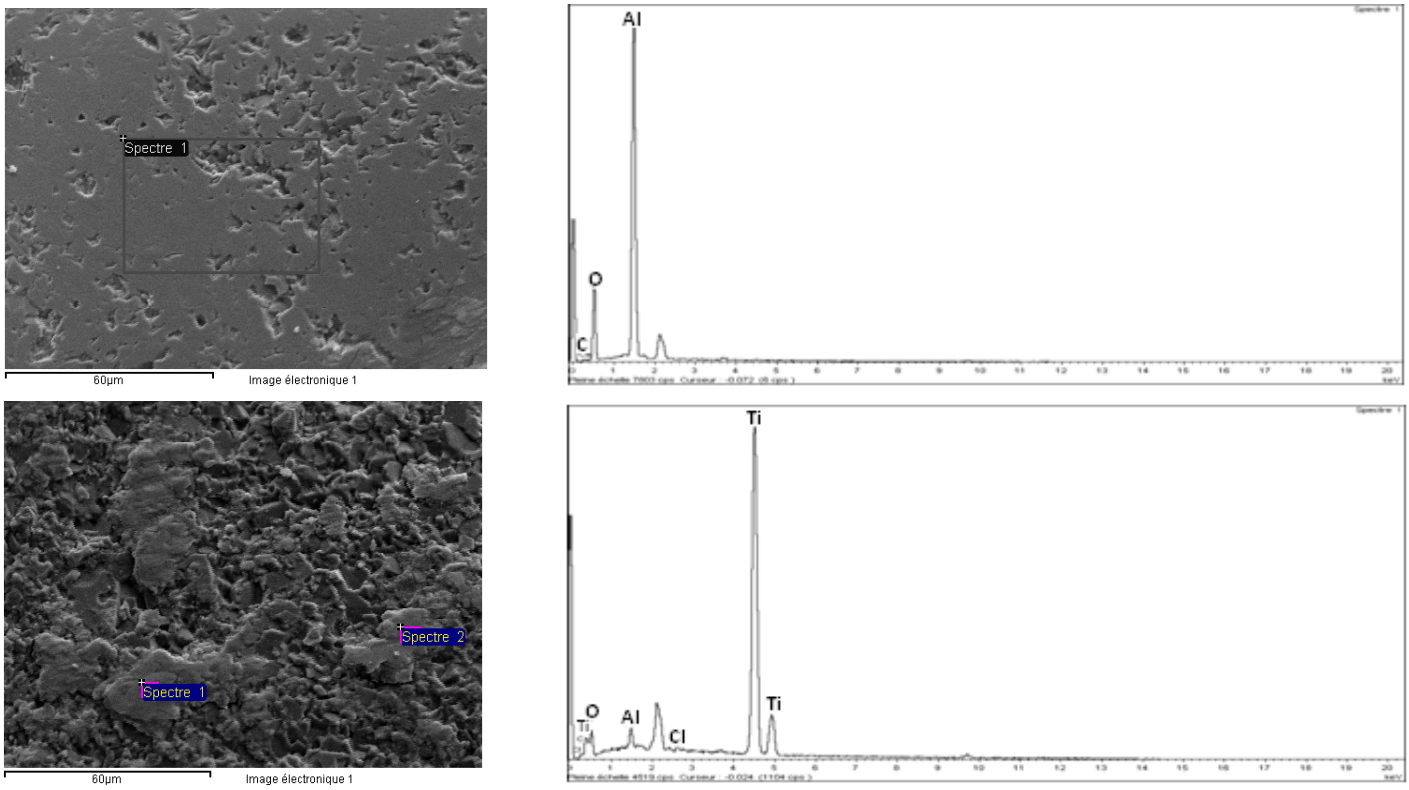

Figure 63 - EDS analysis of the counterbody: A) Before friction B) After Friction.

Wear Mechanisms of Etched Samples

Concerning the wear mechanism on the Etched samples, the figures that illustrate the obtained wear tracks reveal the same mechanisms for both loads and both velocities. Abrasive wear and adhesive wear are the two mechanisms present when an alumina ball is slide against Etched titanium in the studied conditions.

Abrasive wear is common when a harder material is slide against a softer material, and the asperities of the harder material will penetrate on the softer one and remove material. The formation of wear particles (third body particles) may increase the abrasion of the surface and a typical abraded surface is characterized by several grooves in the direction of sliding. Figure 57 A and B exemplify well such mechanism, where some grooves are aligned with the direction of sliding and few wear debris are found. These wear debris are third body particles, and their importance and relevance on the tribocorrosion behaviour of a material has been stated [(42)]. On the Etched samples, as is showed on Figure 60, several wear particles that are ejected from the surface remain on the tribological interface and are oxidized by the electrolyte and act as third body particles, being responsible for the abrasion grooves and contribute to the increase of the amount of wear. In addition, when the normal force is increased to 0,8N, the grooves became more pronounced (Figure 57 B), evidence of the role of the wear debris on the wear. Also, if these wear particles will be oxidized and dissolved on the electrolyte, a current will be measured electrochemically, contributing to the corrosion wear. Here is an example of the synergism present on tribocorrosion, which will be discussed further ahead. In addition, the third body particles may also attenuate the contact pressure by increasing the contact area on the tribological interface.

After, the adhesion mechanism is supported by the structures present on Figure 57 A' and B' as well by the transfer of material from the surface of the sample to the counterbody (Figure 62). Adhesion is due to inter-molecular forces that will create an adhesion junction between the surface of the material and the counterbody. Afterwards, with sliding, the junction breaks and material is transferred. On Figure 57 A', ductile broken junctions are visible on the wear track and on Figure 62 D on the counterbody. At the same time, due to these junctions, a transfer film was produced on the counterbody. This film may have abrasive action on the surface, since it may produce transfer particles that are generally harder than the substrate (work hardening due to sliding) and able to produce grooves in the surface. Figure 57 A' shows such a particle and Figure 58 shows another transfer particle found on an Etched sample, with the respective groove created by it behind. The adhesive wear will also modify the interface between the material and the counterbody, since the counterbody will be covered by metal and the contact will start to reveal some similarity with metal-to-metal contact.

3.4.2 Wear track of Anodized Samples at 100 rpm

The wear track of the Anodized samples is very distinctive in relation to the wear track of the Etched samples. The difference has its bases on the fact that the Anodized samples have an Anodized film on the surface of the samples that has different properties than the surface oxide film of the Etched samples. On both tested conditions (0,4N and 0,8N) the resulting morphology of the wear tracks was uniform along its length. Figure 64 shows different micrographs of the wear track of Anodized samples tested at 0,4N and 0,8N.

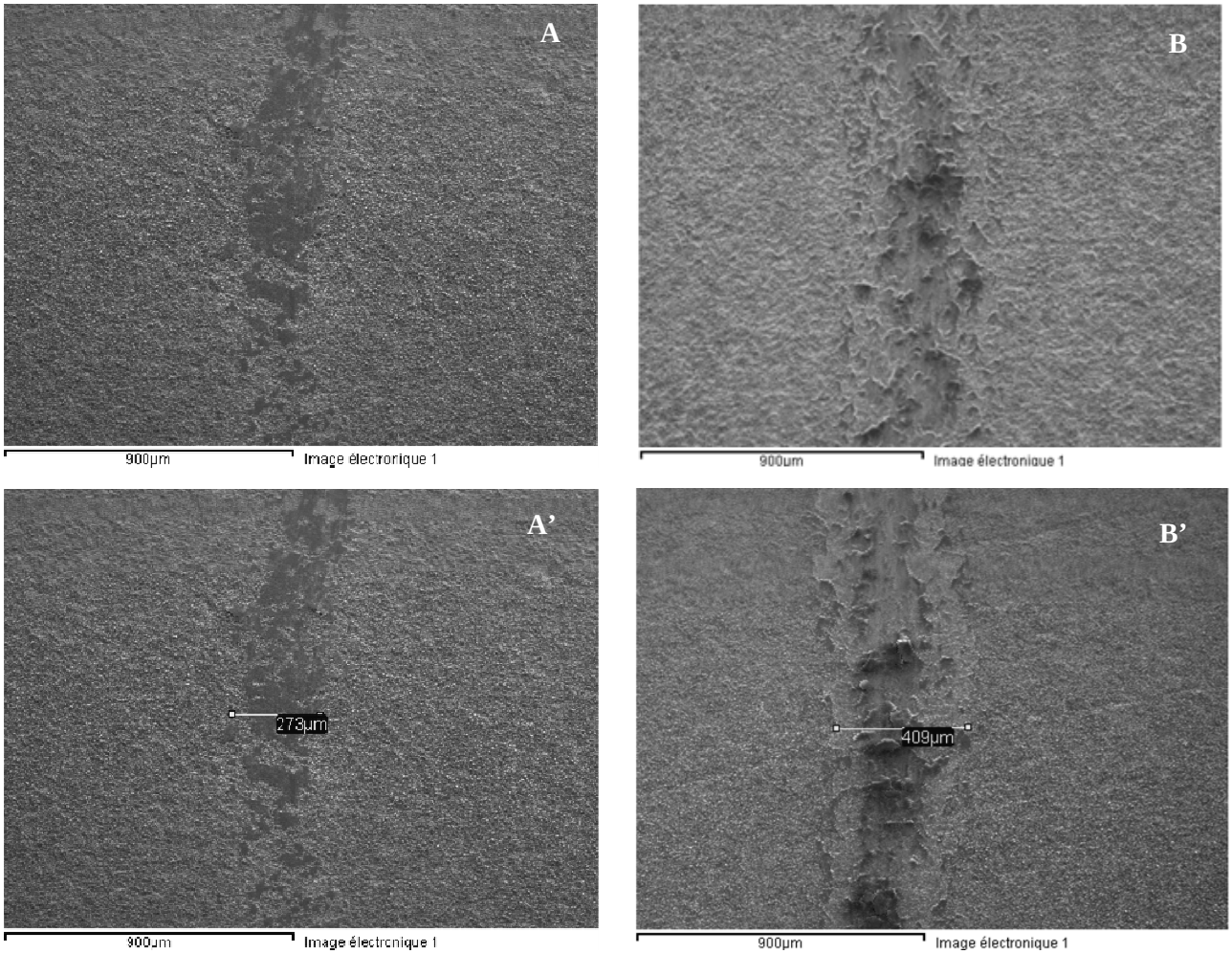

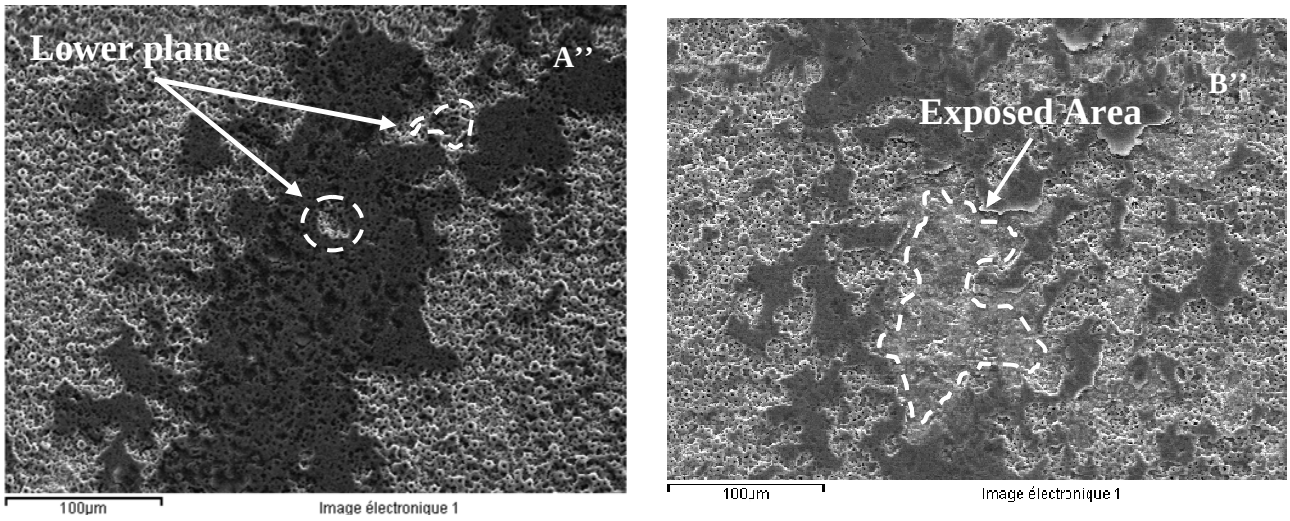

Figure 64 - Wear track of Anodized Samples tested at 0,4N (A and A': 75x and A'': 350x) and 0,8N (B and B': 75x and B'': 350x).

The identification of the worn and unworn area is possible from image A and B and it's possible to visualize a different morphology between both wear tracks on the same images. The wear track that results from the test at 0,8N shows proof of a more accentuated destruction of the outer porous layer and, as expected, an increase of the width of the wear track is seen with the increase of the load on images A' and B' (273 µm for 0,4N and 409 µm for 0,8N). However, on the Anodized samples, the limits of the wear track are not as well defined as on the Etched samples, due to the properties of the Anodized film, making impossible a precise measurement of the width.

The resulting wear track for 0,4N is characterized by the pressing of the outer porous layer of the Anodized film, where the pores with the greatest height are affected by the passage of the ball and will be pressed in the direction of the movement. Consequently, with the increase of passages, it will result on the coverage of some of the pores mainly by the plastic deformation of the superficial porous layer but also, with less importance, by some worn material that composed the higher pores. This last component has less importance, since by the images, the wear track of the Anodized film at 0,4N doesn't reveal evidence of intense material removal. At higher magnification, in Figure 64 A'', it is seen the plastic deformation caused by the passage of the ball, pressing the pores and tapping them. As well, is visible that some zones inside the wear track were not affected by the passage of the ball, due to the fact that they are in lower planes. These lower planes are consequence of the waviness of the Anodized film. More information can be obtained with Figure 65 and Figure 67 on the wear tracks produced at 0,4N.

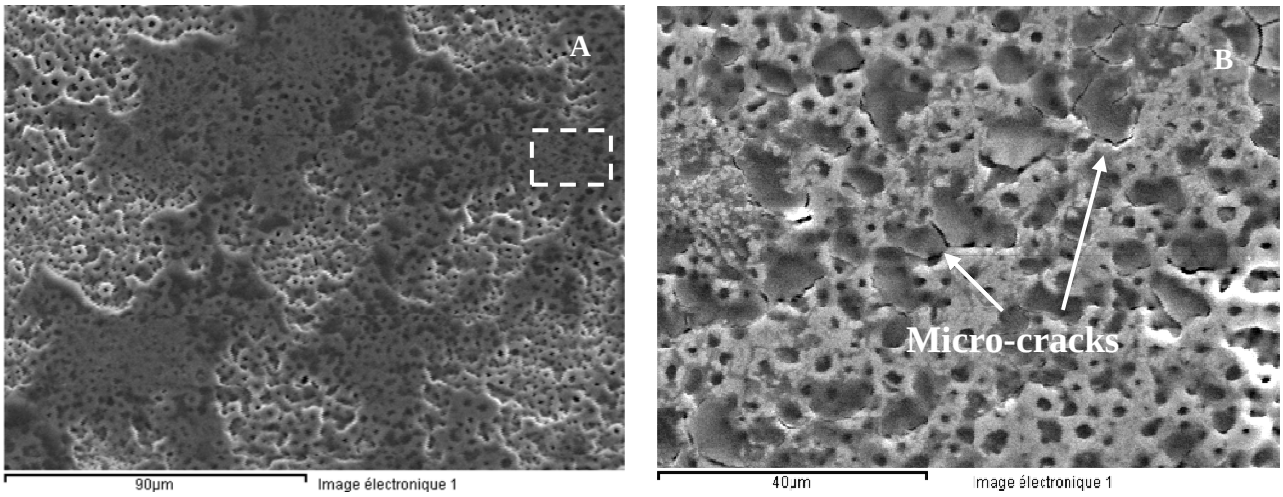

Figure 65 - Wear track of Anodized Samples tested at 0,4N (A: 750x and B: 1500x).

At 0,4N, in zones where the ball pressed the Anodized film, it is possible to identify pores that maintain their structure even if some of the pores in the neighborhood were destroyed (Figure 65 A). After, it is interesting that in certain zones where the film was more pressed by the sliding, like the one identified on image A, at higher magnifications (Figure 65 B), is possible to find micro-cracks on the Anodized film. This is evidence that the integrity of the Anodized film starts to decline. EDS analysis was performed on the pressed zones, and a variance on the quantity of the elements that compose the Anodized film was observed. The evaluated zones and the corresponding spectra are presented on Figure 66.

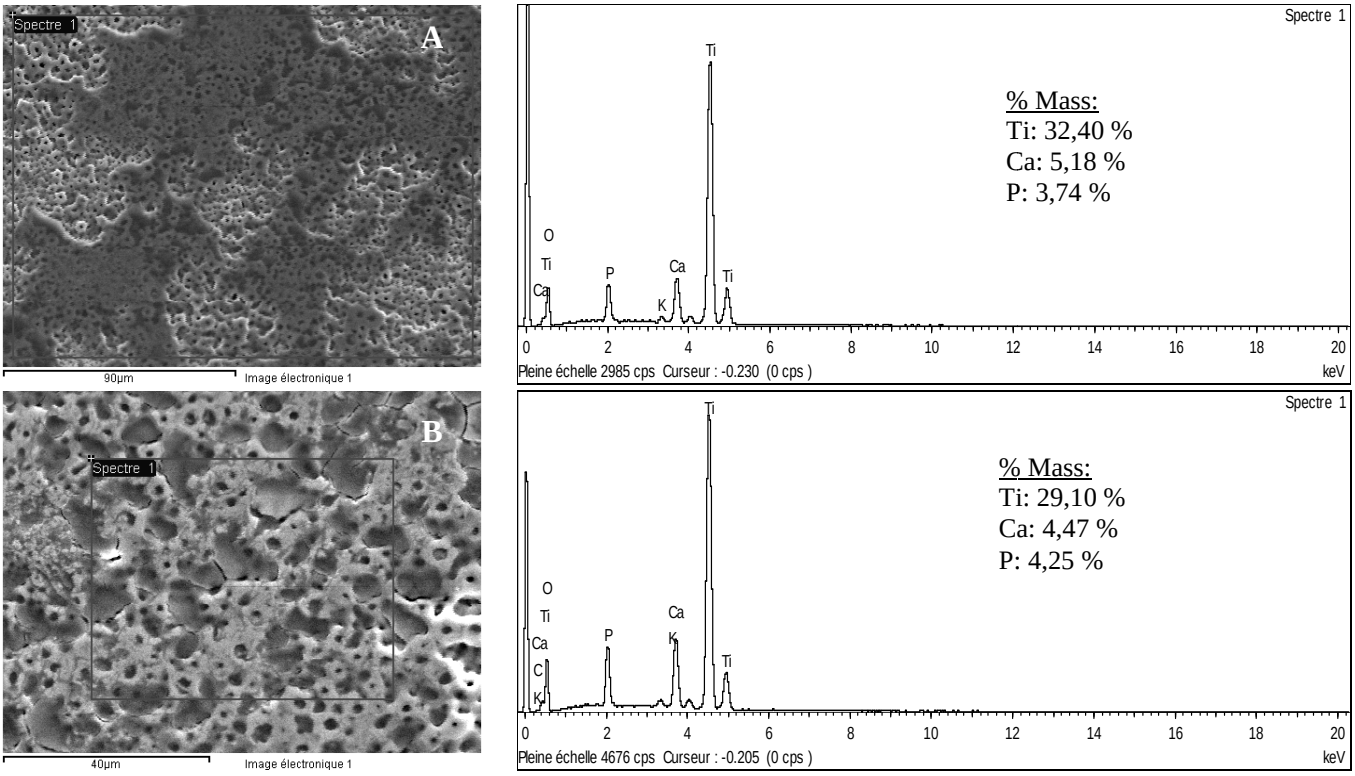

Figure 66 - EDS analysis of wear track of Anodized sample tested at 0,4N.

All the major components that are basic of the Anodized film are present on the chemical evaluation. The mass percentage of titanium and calcium decreases from A to B while phosphorous increases. In the overall, a small variation is seen on the chemical composition with a tendency to, in zones more affected, obtain lower values.

On the wear track produced with 0,8N, in Figure 64 B'', an area where it seems that the superficial layer of the Anodized film has been removed (exposed area) is visible. The damaging imposed by 0,8N is clearly more significant. Figure 67 A shows the typical damaging on the wear tracks of 0,8N, and in addition, several cracks and wear debris are visualized. The cracks result from the damaging imposed by the ball during sliding, but is important to refer that the chamber where the sample is in the SEM equipment is subjected to a vacuum, that may amplify the extent of the cracks. So, the "real" cracks are most likely less extent, but nevertheless are representative of the degradation and of the wear that sliding imposes on the material. The debris are consequence of the pull out of material from the Anodized film and may remain on the interface between the ball and the sample or get dispersed on the solution.

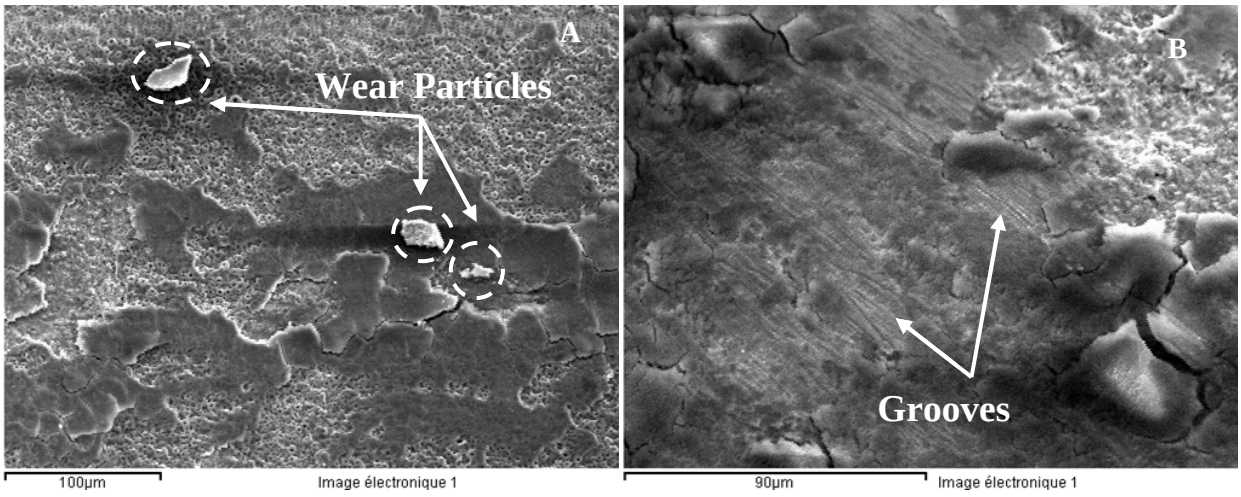

Figure 67 - Wear track of Anodized Samples tested at 0,8N (A: 350x and B: 750x).

Figure 67 B illustrates a zone of the wear track where the porosity has all been removed. It isn't possible to identify pores and the multilayered structured Anodized film, in this specific area, has been completely removed. In fact, some grooves start to arise on the wear track, unseen until now on the wear tracks of Anodized samples, indicating that the surface exposed has a different nature and the sliding affects it in another way. From the EDS analysis on the debris (Figure 68), both have similar constitution and are generated from the Anodized film. The chemical constitution of the zone without pores on the wear track (Figure 68 B) reveals a high content on titanium and a small presence of calcium and phosphate.

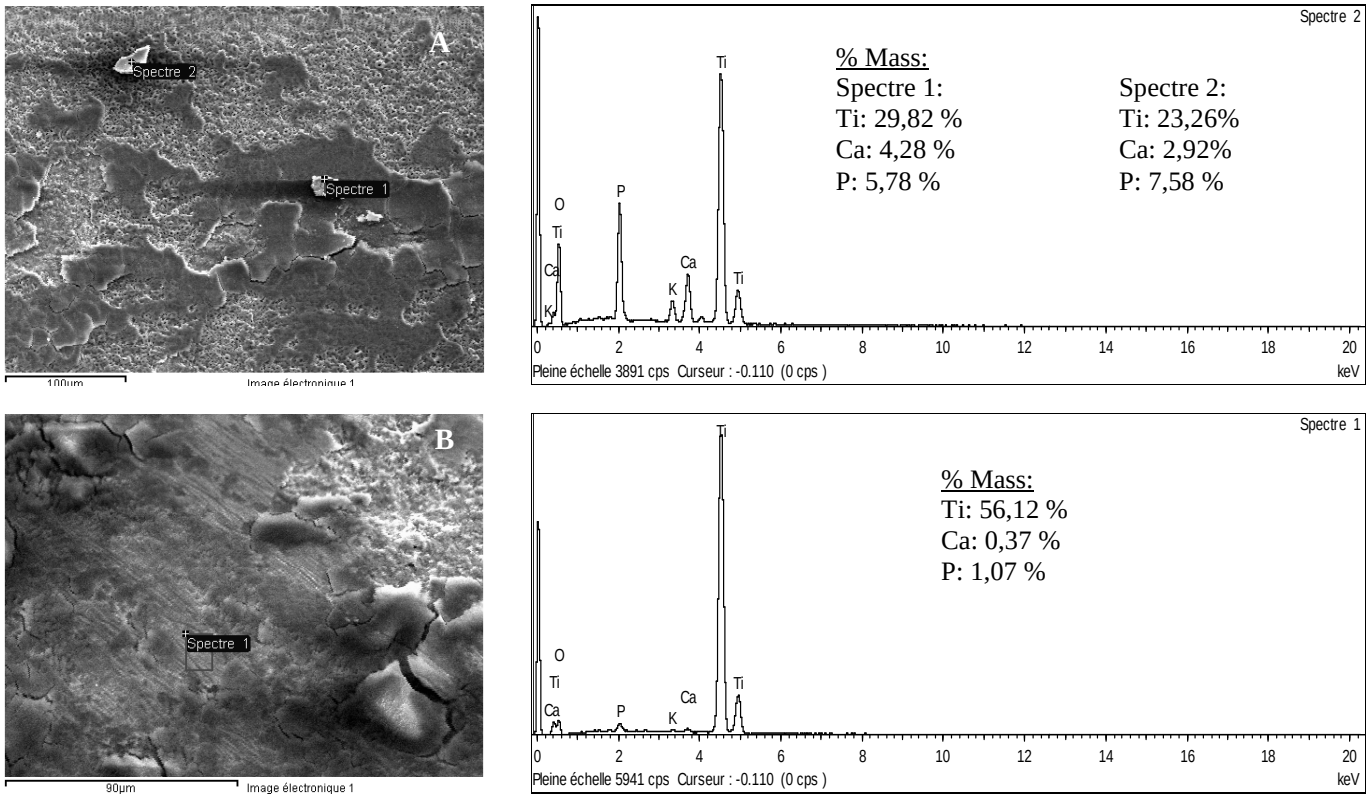

Figure 68 - EDS analysis of wear track of Anodized sample tested at 0,8N.

On the counterbodies used to test the Anodized samples it wasn't identified any grey point, sign of material transfer, so the balls were not observed at SEM.

3.4.3 Wear track of Anodized Samples at 2 rpm

The wear tracks of the Anodized samples tested at 2 rpm are relatively different from the ones at 100 rpm. The ones tested at 0,4N show the same morphology of the wear track, with the pores pressed and with a diminutive destruction of the Anodized film. The same zones without contact, on the middle of the wear track, are visible as well. The main difference is the increase of the width of the wear track to 309 µm from 273 µm at 100 rpm with the same load. These observations are supported by Figure 69 A and A''. The wear track that resulted from the samples tested at 0,8N at 2 rpm is extremely different from the one tested at 100 rpm. Figure 69 B revels a morphology distinct from the one of Figure 64 B, displaying a wear track where the Anodized film was completely removed resembling the wear track of an Etched sample (Figure 56 B) as well with a width of the wear track very similar (862 µm vs. 840 µm) of a Etched sample. On image B'' is impossible to identify any trace of porosity and only adhesion junctions, typical of the wear mechanism of the Etched samples, are visible. The micrograph of image B'' shows the border between the unworn and worn area. Here is visible the porosity of the Anodized film and on the intermediary zone between the unworn and worn area, the destruction of the Anodized film is evident.

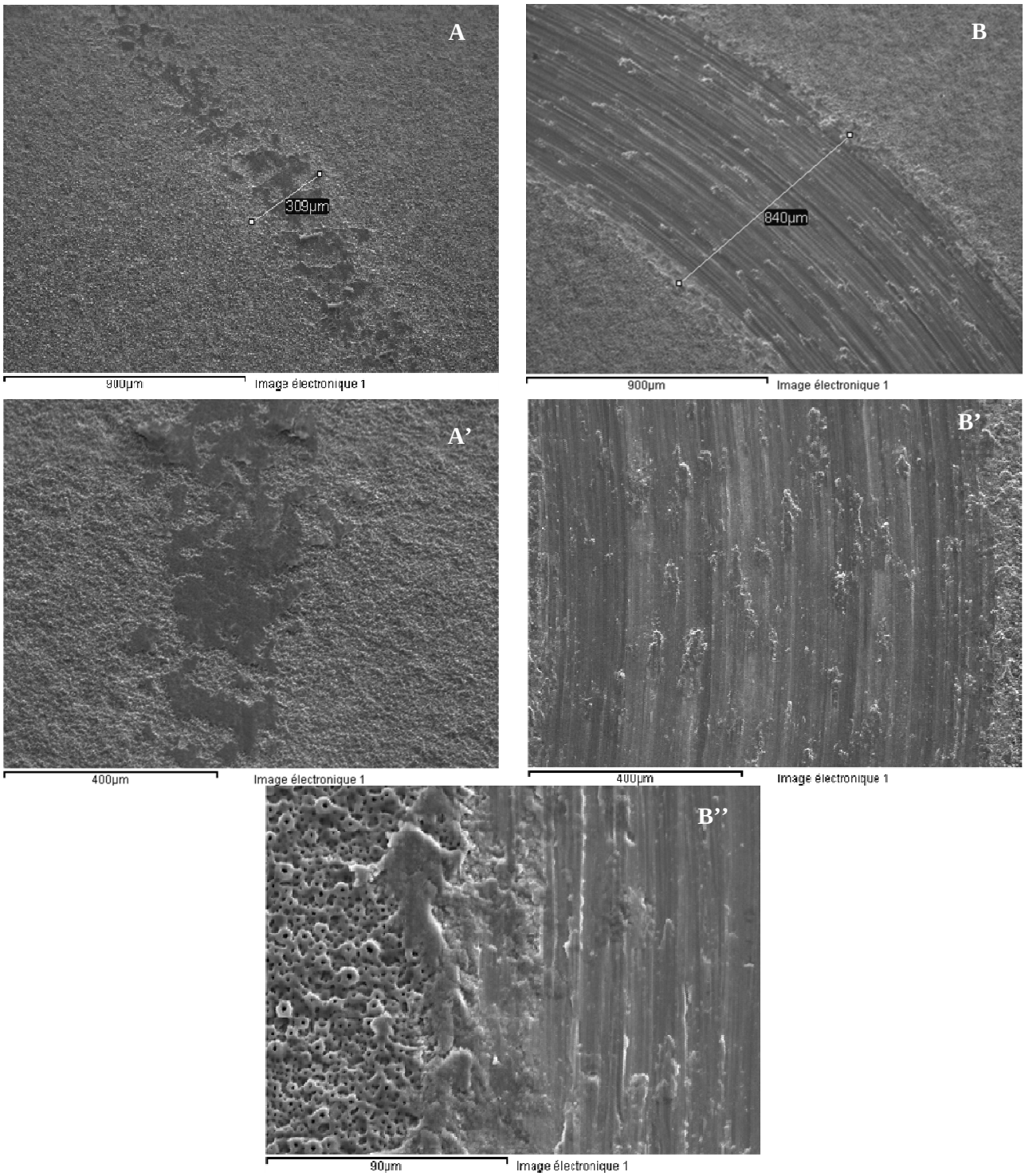

Figure 69 - Wear track of Anodized samples tested at 2 rpm at 0,4N (A and A") and 0,8N (B and B"): A) 75x B) 75X A') 150x B') 150x B'') 750x.

The EDS analysis of the unworn, intermediary and worn area (Figure 70) shows a gradient concerning the amount of elements found. The content in titanium increases towards the worn area and the content in calcium and phosphate decreases. On the worn area the small traces of phosphorous and calcium is not significant and the majority of titanium is due to the base material where the anodization process was performed.

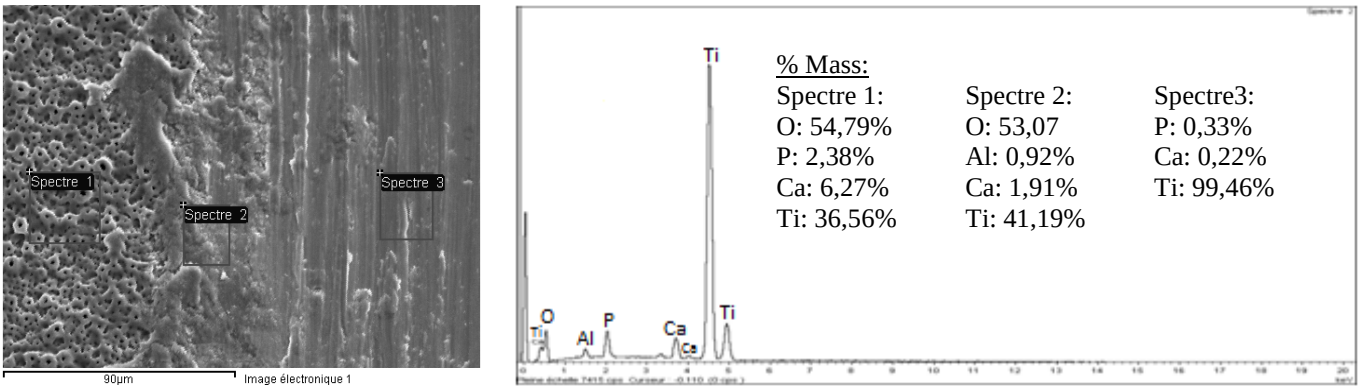

Figure 70 - EDS analysis of wear track of Anodized sample tested at 0,8N at 2 rpm.

Wear Mechanisms Anodized Samples

Regarding the Anodized samples, the wear mechanism that the figures report is fatigue wear and abrasive wear. Fatigue wear is characteristic of tribological contacts where high local stresses are repeated a large number of cycles and wear particles are created by fatigue propagated cracks. A crack starts to form on a local weak point and starts to propagate at each loading cycle and eventually will separate from the surface and create a wear particle. The electrochemical results of the Anodized samples (Figure 35 B and Figure 41) and the SEM pictures of the wear track of the Anodized samples (Figure 65 and Figure 67) indicate the presence of such mechanism. From the electrochemical results is possible to retain that only after a certain number of cycles, more precisely ≈ 1667, the Anodized film starts to display the cathodic shift on the potential, characteristic of a change on the electrochemical state of the surface and related to the dissolution of material to the electrolyte. At 0,4N the load is not strong enough to deeply affect the Anodized film, but even so, it already starts to show some weak points that gave origin to cracks (Figure 65 B). The fatigue wear is more explicit on the samples tested at 0,8N where several cracks and wear particles are observed on the wear track. One should not forget the influence of the vacuum on the cracks, already referred. Meanwhile, not only this wear mechanism is present. On Figure 67 B, due to the action of the higher normal force, the Anodized film was completely removed and naked areas were exposed. Here it was possible to identify grooves, characteristic of abrasive wear. EDS analysis (Figure 68) on those naked areas revealed a high content of titanium, which means that the base surface of titanium was exposed to the electrolyte and to the counterbody. This finding is consistent with the cathodic drop visualized on the potential of the Anodized samples tested at 0,8N at 100 rpm. At last, along with the mechanical degradation by sliding comes the electrochemical interaction (corrosion) of the material with the electrolyte. This interaction is discussed in more detail on Chapter 3.3 but nevertheless it must be referred on the wear evaluation, since it also intervenes on the degradation and wear of the material.

A contrast on the wear tracks of the Anodized samples tested at different velocities was found. At 0,4N the wear mechanism remained the same but at the same time, the width of the wear track

increased for the test at 2 rpm. This effect may be due to the increase of time of sliding (1h10 vs. 60h) that will change the wear track and, as the velocity is slower, the sliding will create a vibrational effect that may interfere with the width of the wear track. At 0,8N the most significant difference was observed, since an evolution of the wear mechanism was seen and the width of the wear track doubled from 409 µm to 840 µm at 100 rpm and 2 rpm, respectively. The results previously shown regarding the wear track of the Anodized samples tested at 2 rpm revealed that the Anodized film was completely removed from the surface, since on the wear track only titanium was found. In this way, one may assume that the counterbody, from a certain moment of the tribocorrosion test at 2 rpm, started to slide against the base surface of titanium due to the integral destruction of the Anodized film and the wear mechanisms shown are, along with fatigue wear, abrasion and adhesion due to the change of the properties of the contact. The similarity of the width of the wear track of the Etched samples tested at 0,8N (at both velocities) and the width of the Anodized sample tested at 0,8N at 2 rpm, contributes to the assumption previously expressed.

3.4.4. General increase on the width of the wear track

Regarding the results that were previously presented, one common remark for both types of samples is the increase of the width of the wear track with the increase of the normal force. The increase of the active area was of 23% for the Etched sample, when the normal force tested was augmented to 0,8N, but has was seen before, such increase didn't affected the open-circuit potential of the Etched samples during sliding in comparison to the potential showed with the lower load. For the Anodized samples the increase on the wear track was of 50% with the increase of the load. On both samples the same tendency was observed and normally, in the point of view of tribocorrosion, this increase is related to the augmentation of active material exposed to the electrolyte. However, due to the distinct nature and morphology of the surfaces on this work, such assumption may only be completely suitable for the Etched samples. Combining the electrochemical results of the Etched samples under sliding (Figure 35) and Figure 56 A' and B', it's clear that the electrochemical state of the surface was modified and that an active area was exposed with sliding. On the other hand, the electrochemical results of the Anodized samples under friction (Figure 35 B) and Figure 64 A' and B' doesn't show a change on the electrochemical behavior and the formation of an "active" surface under friction. At least during around 1100 cycles. The fact is that the Anodized samples, when friction starts, will have the surface changed by the contact of the ball but there will be no exposition of bare titanium to the electrolyte. Only after several cycles, and only with a normal force capable of destroying the Anodized film, will be possible to say that there is an "active" surface of titanium exposed to the electrolyte. Therefore, when evaluating the tribocorrosion behaviour of a surface treatment, as an anodization process, one should have in mind that the concept of active area may not fit entirely to describe the phenomena that are occurring.

3.4.5 Wear track of Biomodified Samples

The biomodified samples were regular Etched or Anodized samples that were subjected to a cell culture of MG63 osteoblastic cells. The cells were on the incubator during 3 days before the tribocorrosion tests. More details on the biomodified samples are found on Chapter 2. Also, due to the fact that these samples had a cell layer on the surface, the horizontality of the samples was not 100% correct, due to the method used to verify the horizontality that obliged the direct contact of a bubble leveller with the surface of the samples. Even so, most of the samples revealed a uniform wear track.

3.4.5.1 Wear track of BioEtched samples at 100 rpm

The wear track that resulted from the tests with the bioEtched samples was uniform, for both loads. No major differences were found between the morphology of the wear track on regular Etched samples and the one obtained with the bioEtched samples (Figure 71 A). However, due to the fact that the samples were subjected to a cell culture, along the wear track was possible to identify some structures that were not present on the regular Etched samples. Figure 71 shows images of the middle of the wear track of bioEtched samples and illustrates the structures mentioned before.

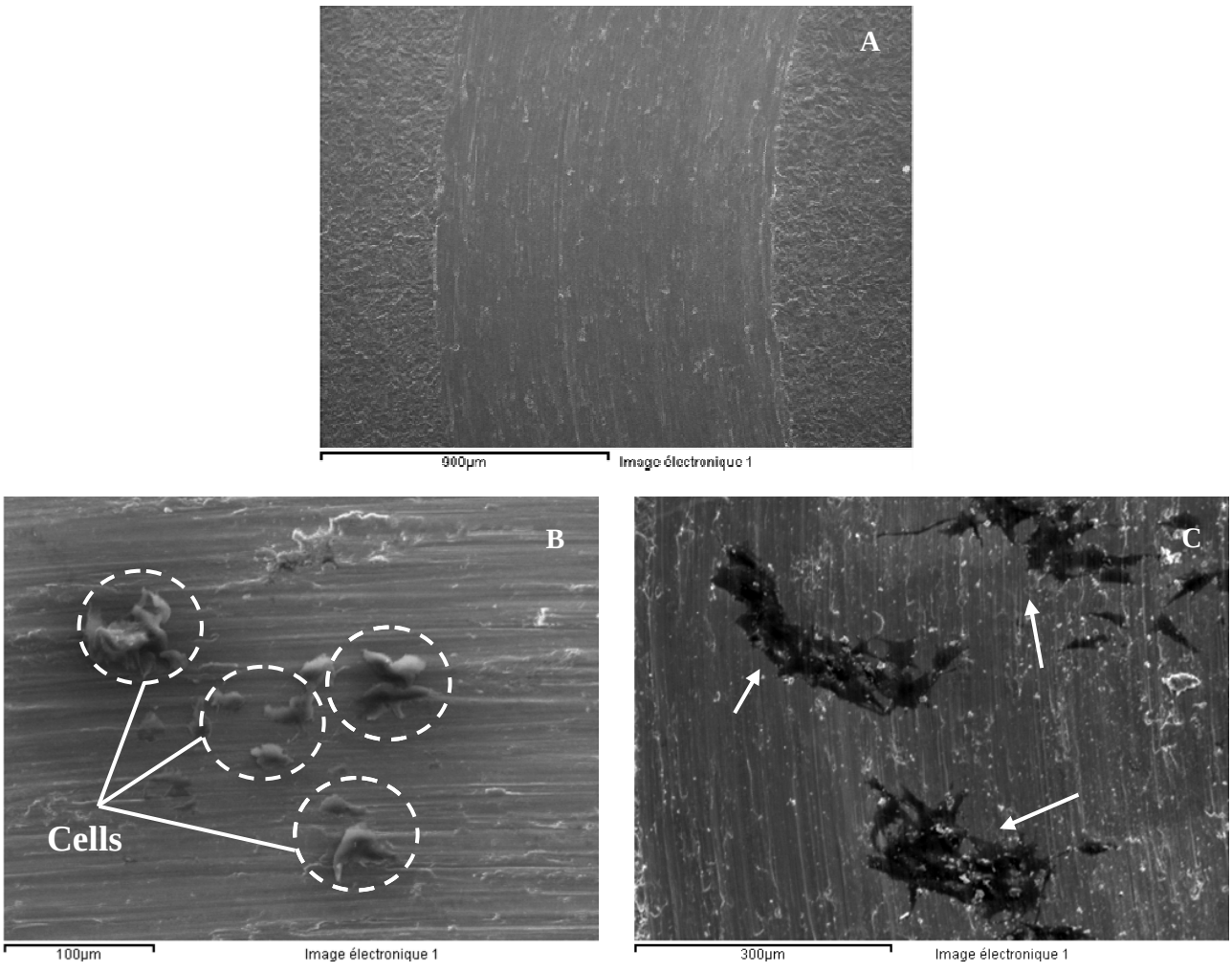

Figure 71 – Wear track of BioEtched samples: A) 75x B) 350x C) 200x. The arrows indicate cells on the wear track.

As the last figure demonstrates, these structures may not be related to wear particles, since their morphology is quite different from the one that the wear particles have. In the case of image B, the structures seem to be well defined with roundy borders. Also some seem to be joined together. By the other hand, on image C, it is possible to differentiate these structures with the wear particles (white points), which are relatively small comparing to the structures. The structures reveal some cytoplasmic protrusions, which are characteristic of biological cells. EDS analysis enabled to see the chemical composition of the structures (Figure 72). Besides the significant amount of titanium, normal due to the sliding and the degradation of the surface of the sample, also carbon was found in significant quantities that may be related to the cellular tissue that was on the surface of the sample. However as the system disturbed completely the structure of the cells with sliding, it is important to highlight that these values are representative of the evaluation area and several factors may play a part on the presented numbers.

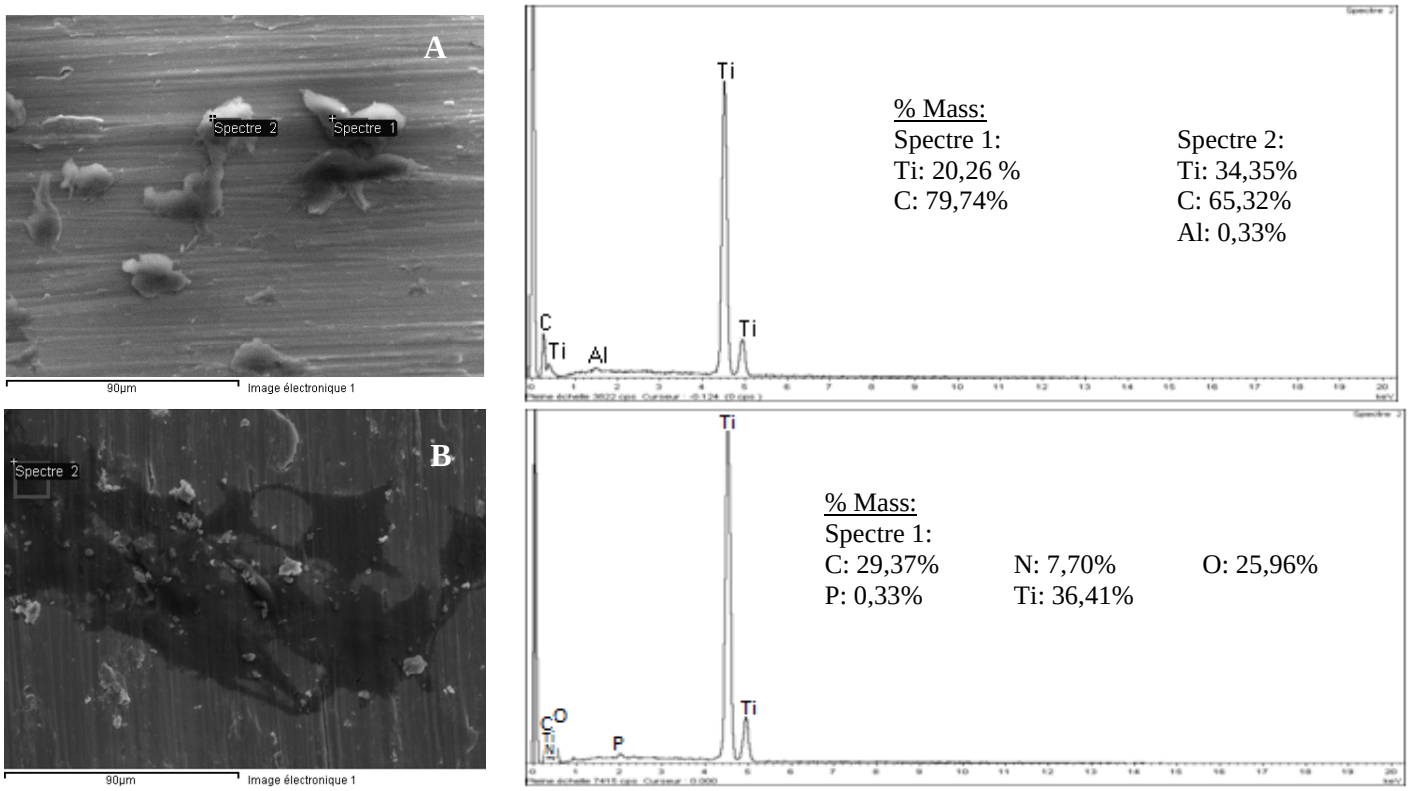

Figure 72 - EDS analysis of biological tissue on the wear track of BioEtched samples tested at 0,4N and 0,8N.

3.4.5.2 Wear track of BioAnodized samples at 100 rpm

The wear track that resulted from the tests with the bioAnodized samples was uniform, for both loads. No major differences were found between the morphology of the wear track on regular Anodized samples and the one obtained with the bioAnodized samples. But, in the same way as the bioEtched samples, some new structures are in evidence on the micrographs that illustrate the bioAnodized wear track.

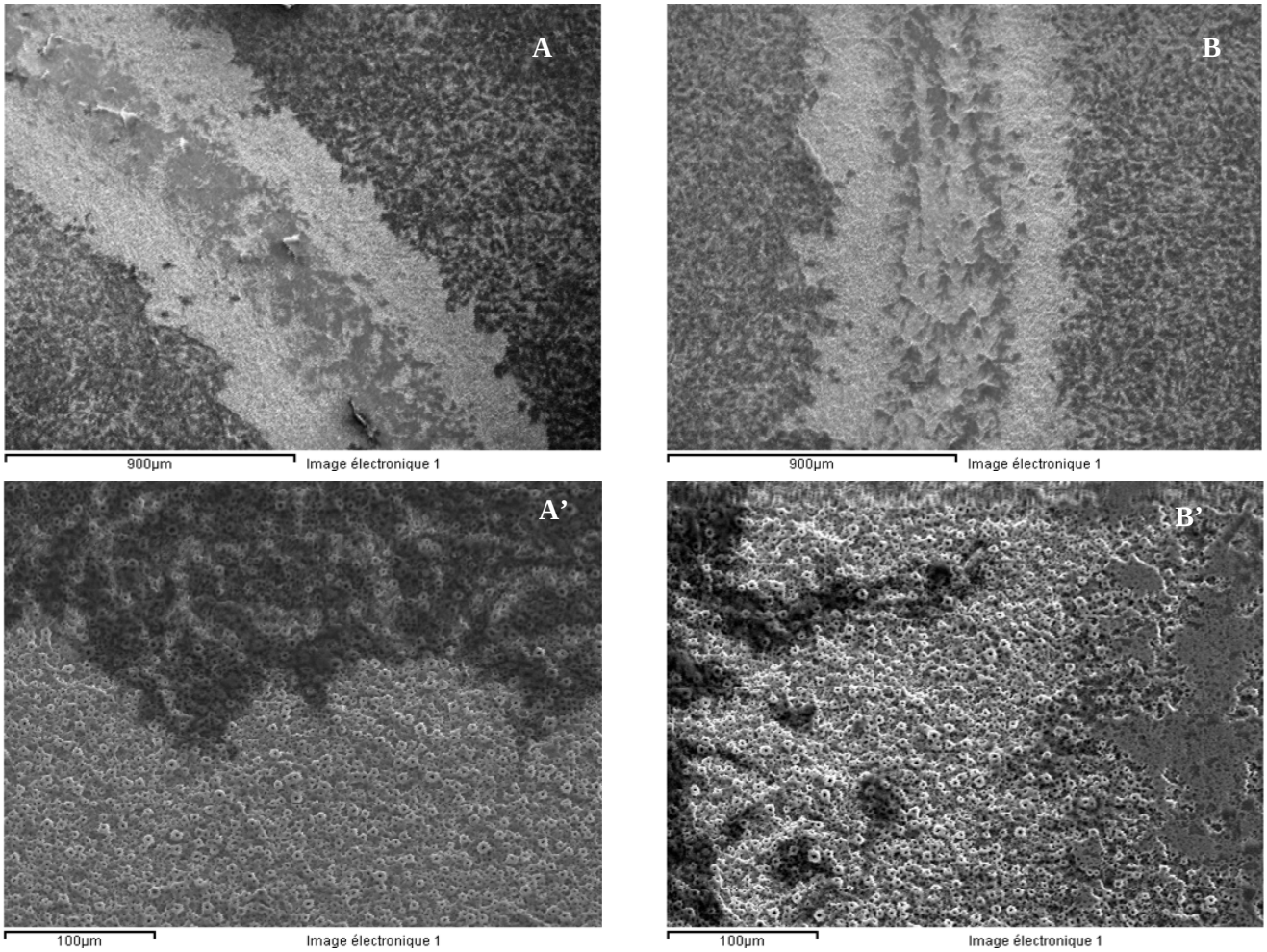

Figure 73 - Wear track of BioAnodized samples tested at 0,4N (A and A') and 0,8N (B and B'): A) 75x A') 350x B) 75x B') 350x.

If a comparison between the images A and B of Figure 73 and images A and B of Figure 64 is made, it is clear that the wear track morphology have the same tendency for each load but on the meantime, on the bioAnodized samples it seems like the width of the wear track has increased, as well a new dark structure is evident. The wear track and its vicinity appear to have something of different in relation to the rest of the surface of the sample.

On the zone were the ball was sliding, the Anodized film seems to be affected in the same way as on the regular Anodized samples but also, the vicinity of the wear track was modified. On images A' and B' of Figure 73, and specially on image B', it's possible to observe that the pores were not deformed by the normal force applied by the ball, suggesting that no direct contact between the ball and that zone was present, but even so, the passage of the ball removed a layer of the darker structure that was placed on the surface of the Anodized film. This reveals that the wear track on the bioAnodized samples may be more elaborated then on the regular ones. The observation of that structure allowed some clearance on its morphology and composition. Figure 74 are micrographs on the darker structure present on the surface of the bioAnodized samples.

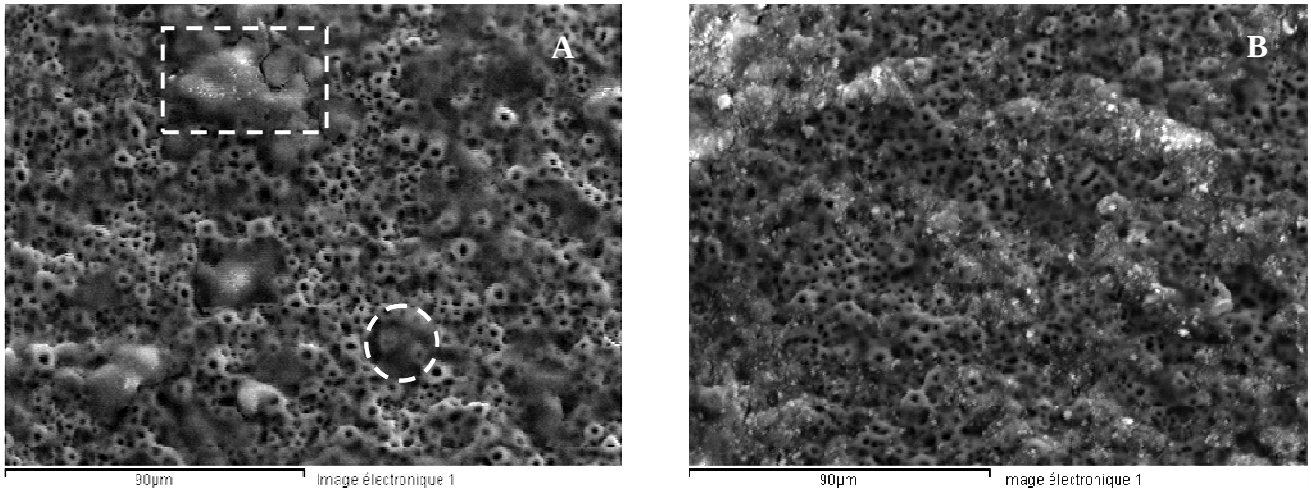

Figure 74 - Darker zone present on the surface of the BioAnodized Samples: A) 750x B) 750x. The square and the circle indicate cells covering the pores of the Anodized film.

Image A shows a surface that is composed by the pores of the Anodized film and also by some structures that are on the top of the pores, covering them. The structures are well spread all over the surface and, some of the pores are completely covered (rectangle) while others are still visible (circle) under those structures. Image B shows the same morphology on a different zone. It's safe to assume that these covering structures are cells, since the samples were subjected to cell culture. The EDS results trace elements as calcium, phosphorous, potassium and carbon that are related to the constitution and the metabolism of the cells. However one should not forget that the cleaning of the samples may leave some residues and also the rest of the elements may be from the contamination of the medium and the action of sliding.

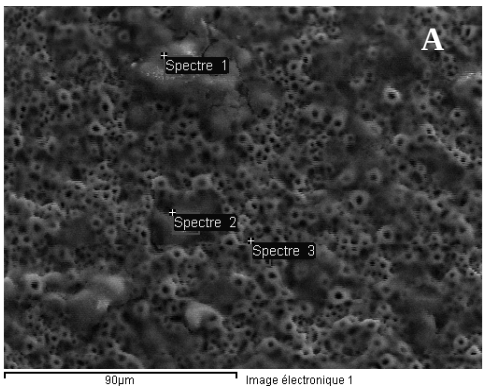

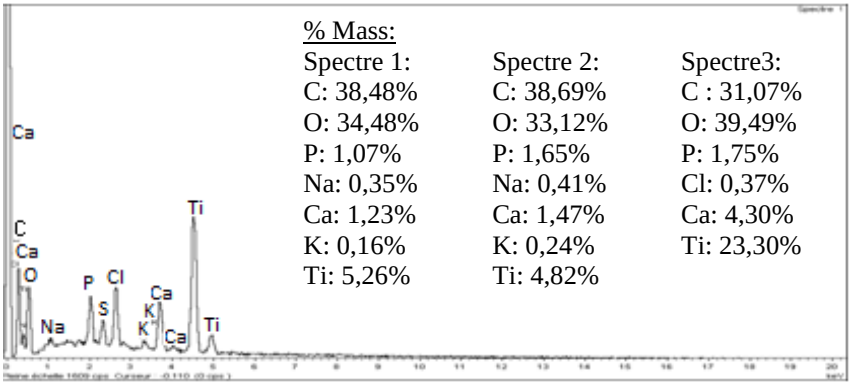

% Mass:

Spectre 1:	Spectre 2:	Spectre3:
C: 38,48%	C: 38,69%	C : 31,07%
O: 34,48%	O: 33,12%	O: 39,49%
P: 1,07%	P: 1,65%	P: 1,75%
Na: 0,35%	Na: 0,41%	Cl: 0,37%
Ca: 1,23%	Ca: 1,47%	Ca: 4,30%
K: 0,16%	K: 0,24%	Ti: 23,30%
Ti: 5,26%	Ti: 4,82%	

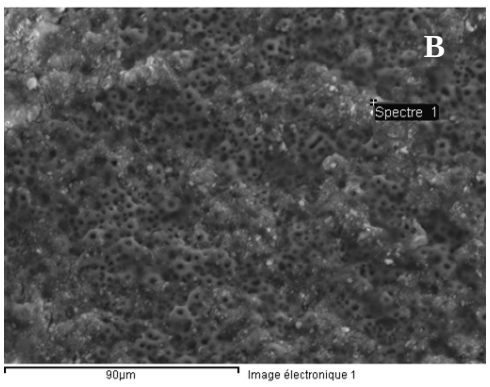

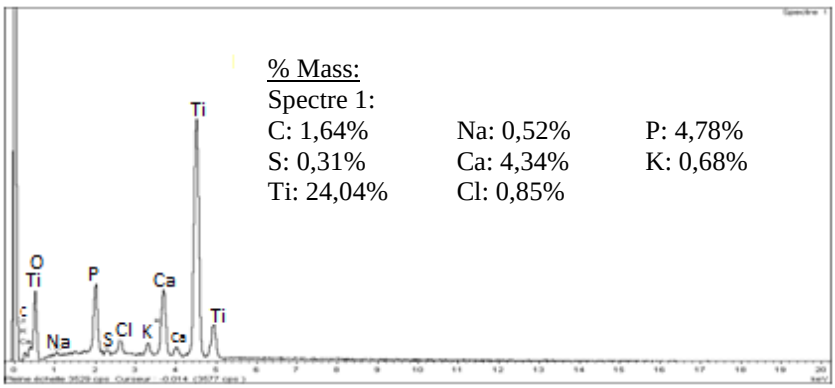

% Mass:

Spectre 1:		
C: 1,64%	Na: 0,52%	P: 4,78%
S: 0,31%	Ca: 4,34%	K: 0,68%
Ti: 24,04%	Cl: 0,85%	

Figure 75 - EDS analysis of biological tissue on the wear track of BioAnodized samples tested at 0,4N and 0,8N.

On the bioAnodized samples, not only the coverage of pores by biological tissue was observed. On the wear track of the bioAnodized samples tested at 0,4N, at certain locations, the structures highlighted (arrows) on Figure 76 A were observed. Since these structures are on the pathway of the counterbody they were in direct contact with it. By the morphology they resemble rolls, which may result from the agglomeration of material due to the movement of the rubbing body. At higher magnification (Figure 76 B and C), the roll shape is clear and the EDS evaluation (Figure 77) reveal a significant amount of carbon, nitrogen, and other components as potassium and calcium, that might be part of cells, proteins and other biological structures that were present on the surface of the Anodized samples due to the cell culture.

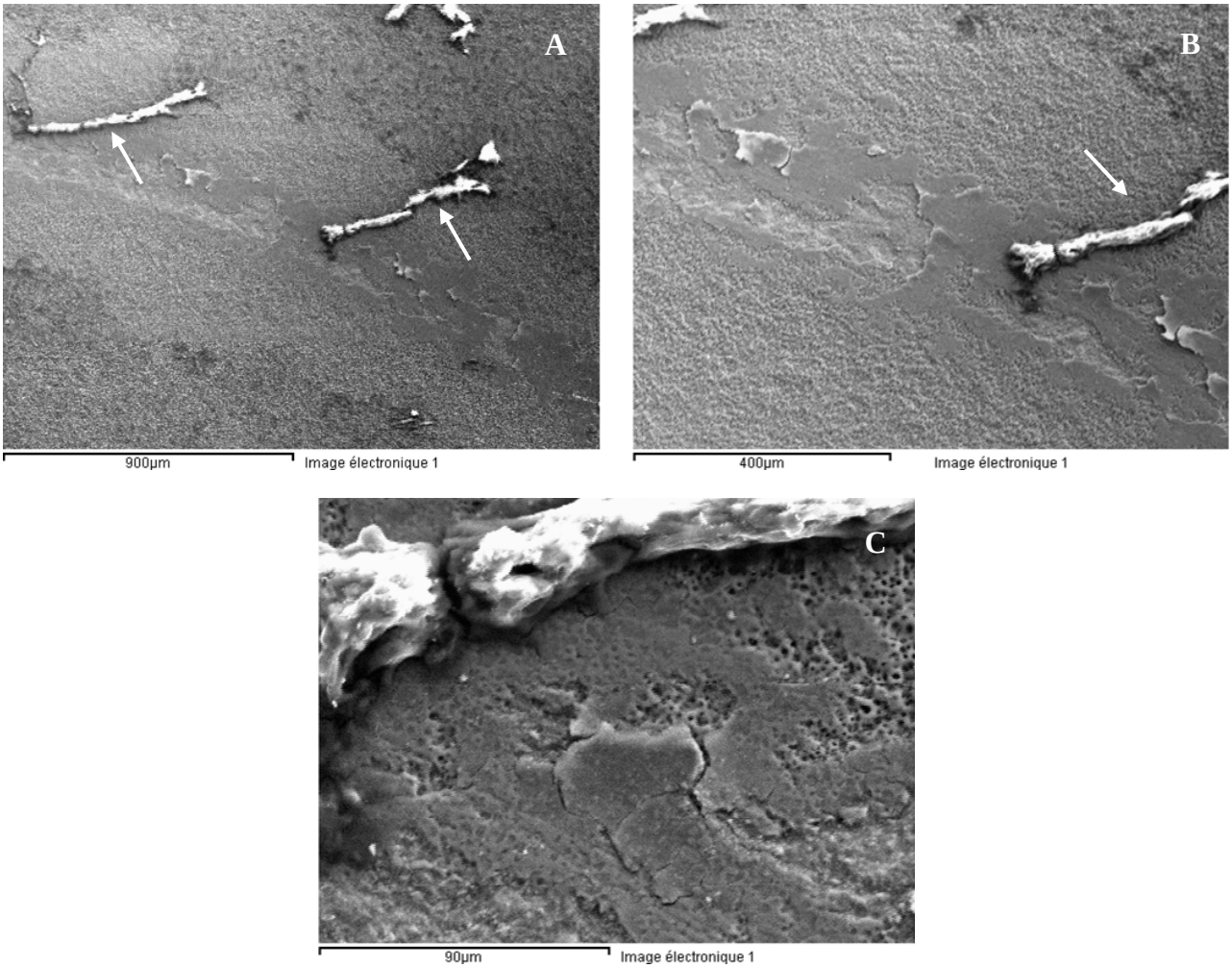

Figure 76 – Rolls of biological material on the wear track of bioAnodized samples tested at 0,4N: A) 75x B) 150x C) 750x. Arrows indicate rolls of biologic material.

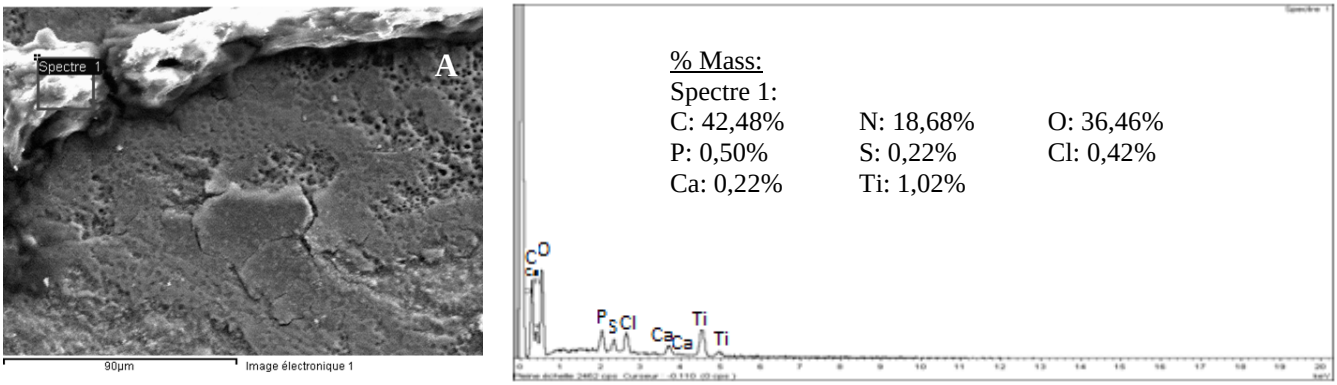

Figure 77 - EDS analysis of biological tissue on the wear track of BioAnodized samples.

Wear Track of Biomodified Samples

The wear track of the biomodified samples revealed interesting aspects. At first, it was possible to confirm the wear mechanisms present on the regular samples. The growth of a cell layer didn't affect the wear mechanisms, abrasion and adhesion were observed on the bioEtched samples as fatigue and abrasion on the bioAnodized samples. Such result was already expected, since mechanically the cells are a soft tissue and will not show any resistance against the counterbody, exposing the base surface of the samples and developing the same mechanisms as with the regular samples. After, on the bioEtched samples it was possible to observe a small group of cells on the wear track, but such finding isn't significant on the overall evaluation of the wear. It was some cells that resisted to the sliding and remained on the wear track. Meanwhile, the bioAnodized samples revealed more differences. The surrounding area of the wear track was different from the rest of the surface even if it wasn't in direct contact with the counterbody. An electrochemical reaction with the electrolyte is excluded as a reason to remove the cells, since only the vicinity of the wear track is affected by the removal of cells instead of all the surface of the sample. So the cause has to be related to the sliding. In this way, the process responsible for that can be the dynamic effect produced by the flow of electrolyte, due to sliding. As the surface of the bioAnodized samples are covered with cells, with sliding, on the contact zone between the counterbody and the sample the surface is damaged but also, a dynamic effect of flow of the electrolyte will be produced after the passage of the counterbody. As cells are sensible structures to environmental changes and as well if they are not completely adhered to the surface of the material, this dynamic effect may easily remove them and expose the pores. For this reason, the pores are not damaged by the direct contact with the counterbody since the contact didn't existed. At the same time, another reason for the removal of the cells from the vicinity of the wear track could be related to the form of the counterbody. The counterbody is a ball of alumina and as the cells are on the top of the surface, they will be in a higher plane in relation to the base material. Due to the spherical form of the counterbody, the alumina ball may remove by contact the material that is on the top of the surface without touching the base material and in this way, not deforming the pores by direct contact. Figure 78 describes the effect of the form of the counterbody.

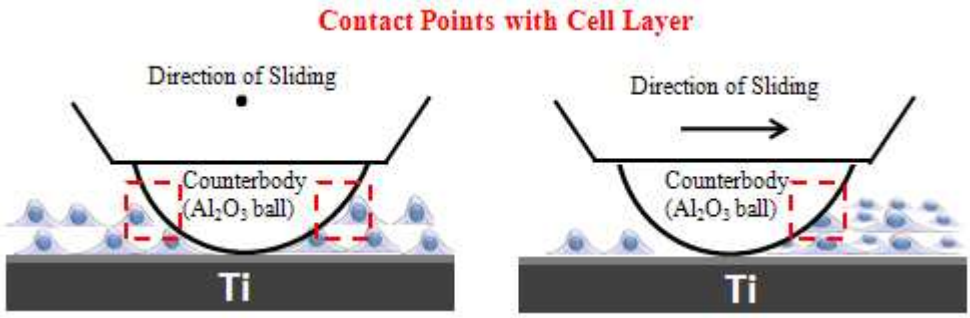

Figure 78 – Removal of the cells by the counterbody without affecting the pores on the surface of the Anodized samples.

Finally, the presence of the rolls of cellular matter was a result of the agglomeration of all the biological material that was removed by the single action of one of the mechanisms described before or even by the conjunction of both of them. Due to the sliding action, the rolls can grow, incorporating more layers of cellular material in displacement by a process similar to a “snow ball” effect. Their final morphology of a compact roll is owned to the contact pressure at the sliding interface. These rolls will play a part on the contact mechanics of the tribological system. It is known that some materials may form rolls on the tribological contact that, in a way, will help the sliding of the counterbody just like a “miniature roller bearings” if they remain in the contact interface for a long period of time.

3.4.6 Quantification of the Synergistic Effect present on Tribocorrosion

The application of the protocol *"A methodology for the assessment of the tribocorrosion of passivating metallic materials"* [55] allowed the quantification of the synergism effect of tribocorrosion on the tested materials. The part of the protocol applied is exposed on Chapter 2.

3.4.6.1 Wear quantification on Etched Samples

Regarding the results of the Etched samples, Table 21 displays the wear values obtained and the values are expressed in volumetric material loss per cycle. The values at 100 rpm are the average values of the tested samples at each condition while at 2 rpm are the values of the tests performed, since it was only one for each condition. Figure 79 and Figure 80 are the plots of the wear results, which allow a better visualization of the outcome of the quantification of the wear.

Table 21 - Tribocorrosion components obtained on the Etched Samples under unidirectional continuous friction against an alumina ball.

Samples	Load (N)	Velocity (rpm)	A_{act} (cm^2)	W_{tr} (cm^3/cyc.)	W^c_{act} (cm^3/cyc.)	W^m_{act} (cm^3/cyc.)
Non-Biomodified	0,4	100	0,185	$1,67 \times 10^{-8}$	$4,45 \times 10^{-10}$	$1,63 \times 10^{-8}$
	0,8	100	0,305	$3,42 \times 10^{-8}$	$4,84 \times 10^{-10}$	$3,37 \times 10^{-8}$
	0,4	2	0,302	$2,60 \times 10^{-8}$	$2,69 \times 10^{-11}$	$2,59 \times 10^{-8}$
	0,8	2	0,312	$3,07 \times 10^{-8}$	$2,35 \times 10^{-11}$	$3,07 \times 10^{-8}$
Biomodified	0,4	100	0,270	$2,10 \times 10^{-8}$	$4,19 \times 10^{-10}$	$2,06 \times 10^{-8}$
	0,8	100	0,328	$3,32 \times 10^{-8}$	$5,07 \times 10^{-10}$	$3,27 \times 10^{-8}$

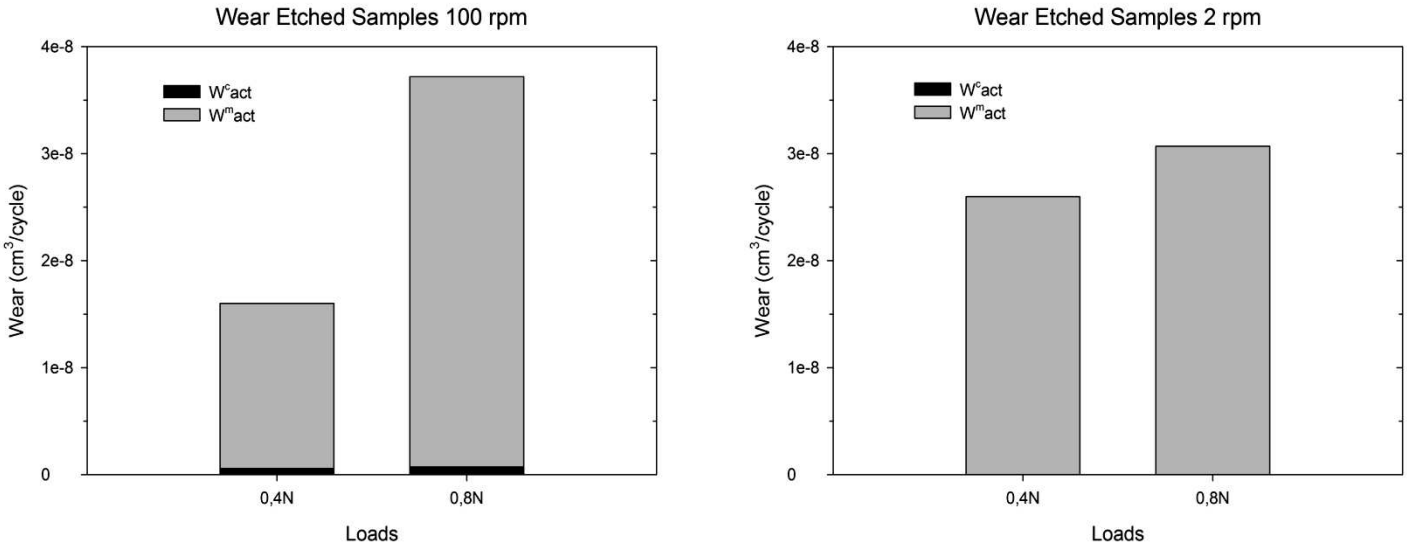

Figure 79 - Contribution of the different tribocorrosion components to the total volumetric material loss in the sliding track on Etched samples for continuous unidirectional sliding tests at 100 rpm and 2 rpm.

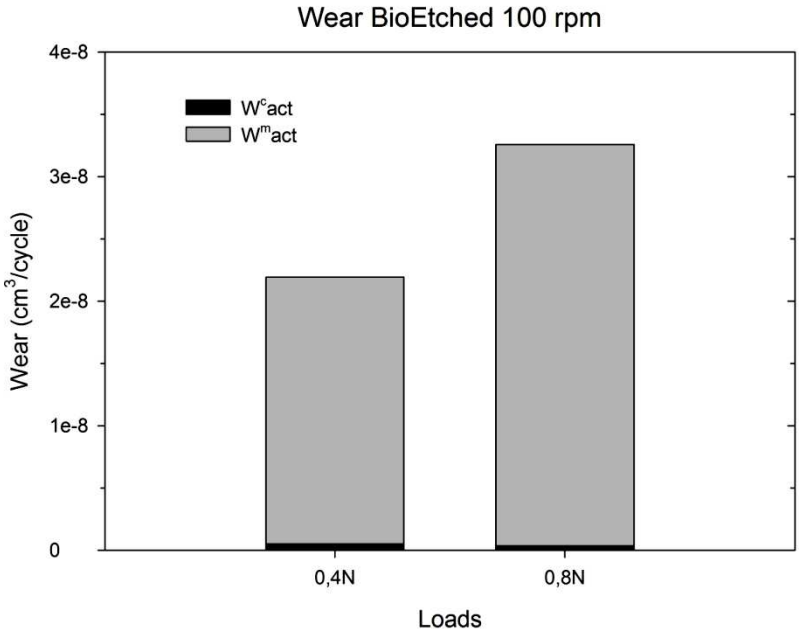

Figure 80 - Contribution of the different tribocorrosion components to the total volumetric material loss in the sliding track on BioEtched samples for continuous unidirectional sliding tests at 100 rpm.

Concerning the presented table and the respective plots, on the non-biomodified samples tested at 100 rpm, an increase on the total wear is seen when the normal force increases. The corrosive wear remained similar on both tested conditions while the mechanical wear evolved to superior values. The samples tested at 2 rpm have the same tendency as at 100 rpm, but a small decrease on the total wear is seen. In this case, the corrosive wear follows the same tendency as at 100 rpm with similar values at both loads (Table 21), but the mechanical wear shows an increase for the 0,4N while for the 0,8N illustrates a decrease. Regarding the bioEtched samples, a similar behaviour with the non-biomodified samples tested at 100 rpm is noticed, with the mechanical wear varying depending on the normal force applied. It increased slightly at 0,4N and a diminutive decrease at 0,8N is observed when compared to the 100 rpm results.

Evaluating the previous results, a shift on the amount of the mechanical removal of the Etched samples was seen with the different velocities. Comparing both velocities, at 2 rpm at 0,4N is seen on the mechanical removal an increase while at 0,8N the opposite was found. In this situation, the different contact dynamics present on the studied conditions may be the justification for such behaviour. At 100 rpm, the wear particles responsible for the abrasive effect may be pushed away from the tribological contact, due to the sliding of the counterbody and to the dynamic effect induced on the electrolyte, decreasing the abrasive effect, while at 2 rpm, as the sliding is slower, the referred phenomena may not have great influence on the dispersion of the particles and in this way, more abrasive particles will be present on the tribological contact and remove more material. While this may be true, if such effect occurred one should also find an increase on the mechanical removal at 0,8N at 2 rpm. Here, when comparing with 100 rpm, a decrease was seen. It means that the nature of the tribological contact was different, even that no major differences were found between the wear tracks.

The combined effect of a higher contact pressure with a lower velocity may, in this case, modify the nature of the wear debris from abrasive bodies to rolling bodies, that are simply on the contact and don't contribute to the removal of material. To prove this effect, one should pay attention to the evolution of the friction coefficient in both cases (0,8N at 100 rpm vs. 0,8N at 2 rpm) and do a thorough evaluation of the wear particles. In the present study, the friction coefficient wasn't measured, so the verification of the presented theory may be assessed on future works.

3.4.6.2 Wear quantification on the Anodized Samples

The quantification of the synergism present on the tribocorrosion tests of the Anodized samples wasn't possible to achieve with the protocol, since the electrochemical state of the active wear track of the Anodized samples wasn't characterized, as already mentioned.

Considering the Anodized samples, these samples were subjected to a anodization treatment that besides the incorporation of inorganic components on its surface, created a multi-layered Anodized film with a thickness of approximately 7,5 µm. In addition, the anodization process changes the mechanical properties of the film since the crystalline structure of the film is also modified, with the presence of both anatase and rutile phase of TiO_2. During the tests, it was possible to state the different electrochemical and surface properties of the Anodized samples when comparing them with the Etched samples, during sliding. For instance, on the Etched samples, when sliding started it was clear the formation of the active wear track on the surface of the sample while on the Anodized samples that situation didn't occur. The wear track on the Anodized samples was only noticed after a certain number of cycles. Also, due to the good mechanical properties of the Anodized film, the degradation imposed by the sliding of the ball wasn't measurable at 0,4N and only at 0,8N it was observed some effect of rubbing on the surface, but it couldn't be distinguished as an active wear track since the Anodized film was still protecting the surface. Also, one should have in mind that, on the Anodized samples, is difficult to distinguish the plastic deformation of the surface with the real wear of the material. Figure 81 shows microtopography measurements of wear tracks of Anodized samples, where it is possible to state the differences on the Anodized samples on both tested conditions.

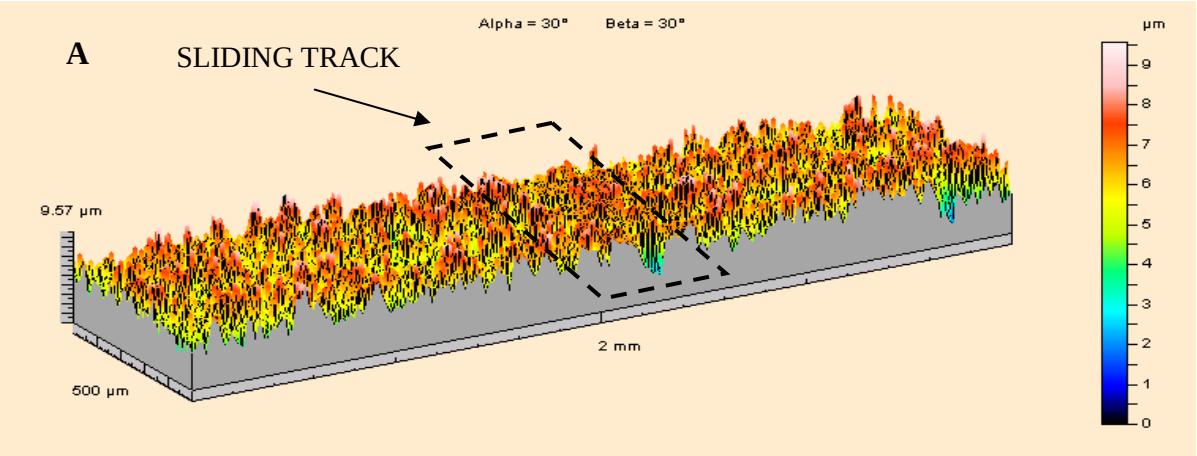

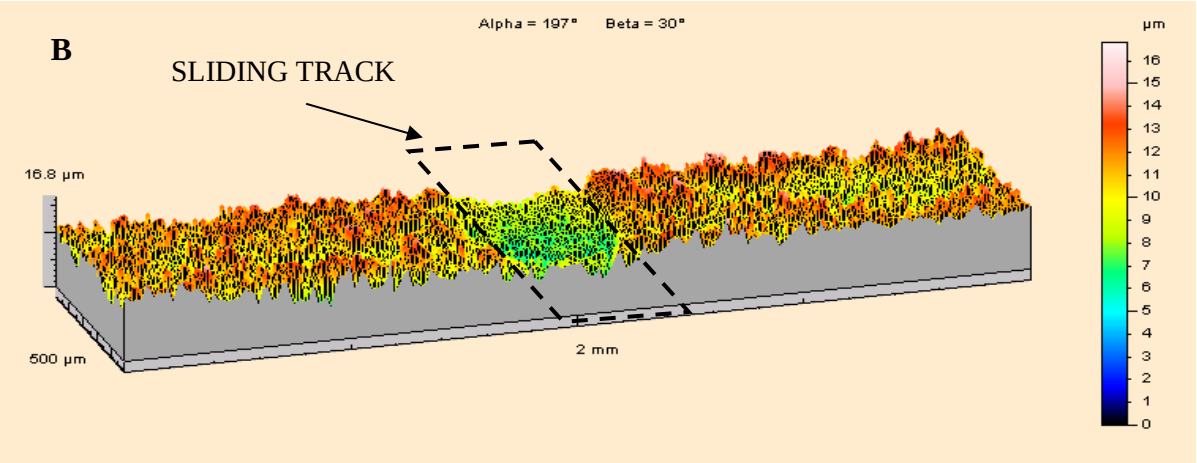

Figure 81 - Microtopography squares of wear track on Anodized samples: A) 0,4N B) 0,8N.

In this way, the major drawbacks for the quantification of the synergistic effect present on tribocorrosion on the Anodized samples are:

- There is no definition of real "active area" on the Anodized samples. Only at certain locations the Anodized film tested at 0,8N reveal the more degradation;
- The impedance is measured at ± 1500 cycles of sliding and the Anodized samples only starts to reveal the cathodic shift at 1660 cycles;
- The impedance measured isn't a mixed impedance of worn and unworn area, due to the fact that the wear track is still composed by the Anodized film, making impossible the use of the equations stated on the protocol to characterize the synergistic effect.

To overcome this situation, the synergism and the wear quantification of the Anodized samples will be performed empirically, based on the information gathered on the tribocorrosion evaluation, the information of the wear track characterization and the values of the total wear per cycle.

Table 22 presents the values of the total wear per cycle of the Anodized samples. On the non-biomodified samples, the values presented for the sample tested at 0,4N at 100 rpm and at 0,8N at 2 rpm are of the only samples that were measurable. All the other values are the average of the three tests. Figure 82 and Figure 83 are the plots of the values of Table 22.

Table 22 - Total wear obtained on tribocorrosion tests on the Anodized Samples under unidirectional continuous friction against an alumina ball.

Samples	Load (N)	Velocity (rpm)	A_{act} (cm^2)	W_{tr} (cm^3/cyc.)
Non-Biomodified	0,4	100	0,05	$1,63 \times 10^{-10}$
	0,8	100	0,06 ($\pm 9,26 \times 10^{-3}$)	$1,79 \times 10^{-9}$ ($\pm 1,14 \times 10^{-9}$)
	0,8	2	0,192	$2,55 \times 10^{-8}$
Biomodified	0,4	100	0,05 ($\pm 1,44 \times 10^{-2}$)	$3,25 \times 10^{-10}$ ($\pm 2,34 \times 10^{-10}$)
	0,8	100	0,10 ($\pm 7,99 \times 10^{-3}$)	$3,38 \times 10^{-9}$ ($\pm 1,18 \times 10^{-9}$)

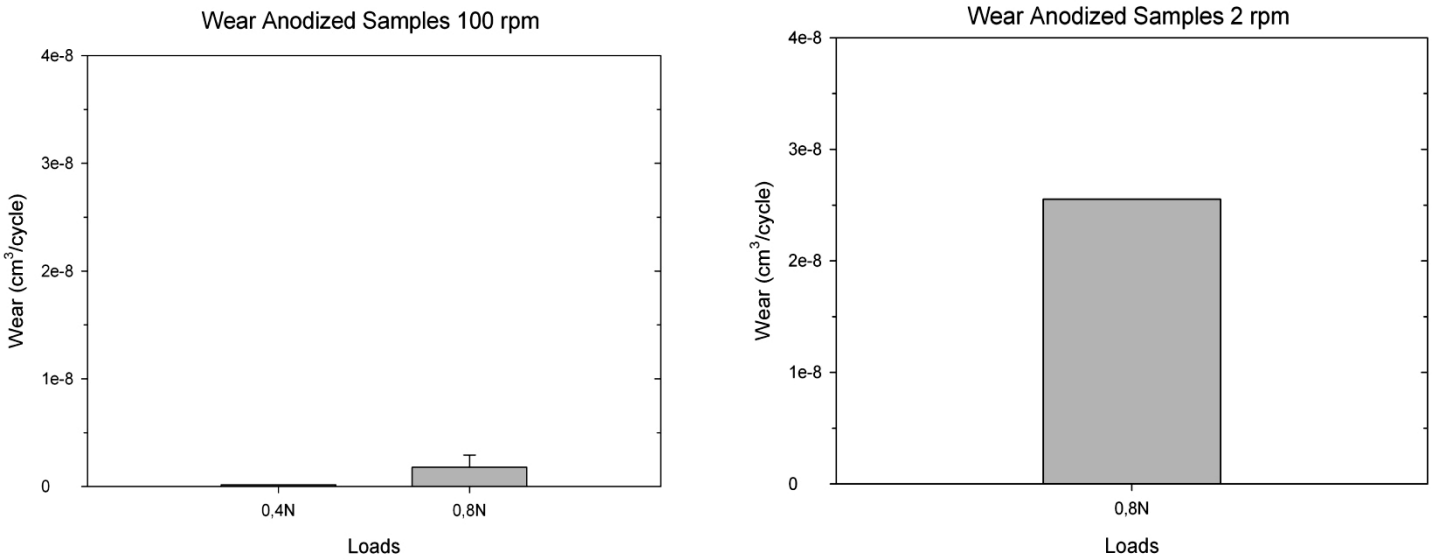

Figure 82 - Total wear of the tribocorrosion test on the sliding track of Anodized samples for continuous unidirectional sliding tests at 100 rpm and 2 rpm.

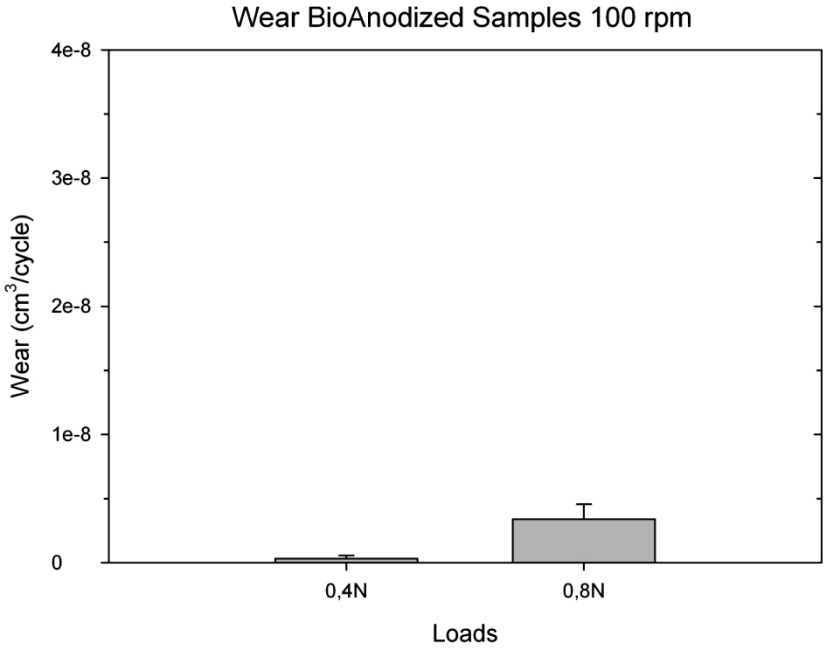

Figure 83 - Total wear of the tribocorrosion test on the sliding track of BioAnodized samples for continuous unidirectional sliding tests at 100 rpm.

The previous results of the non-biomodified samples tested at 100 rpm show that, as the Etched samples, the Anodized samples are sensitive to the increase of the normal load, revealing a higher amount of wear when tested with 0,8N. The BioAnodized samples follow the same trend. When comparing this results with the Etched or BioEtched samples tested on the same conditions, it's notorious the difference on the results. The amount of total wear for the Anodized and BioAnodized samples tested at 100rpm is much smaller, being almost insignificant for the samples tested at 0,4N. This may be very interesting in terms of performance of the material for the final application. The sample tested at 2 rpm with 0,8N have a total wear very similar with the Etched sample tested at 0,4N at 2 rpm, revealing that the Anodized sample resisted better to the increase of the normal load. However, a big difference between the tests performed at 100 rpm and 2 rpm is seen and may be related to the amount of time that the sample was subjected to sliding or to some variability of the anodization process.

Quantification of the Synergistic effect present on Tribocorrosion

At this point, with all the insight on the wear mechanisms, it is possible to discuss and understand the quantification of wear and of the synergism present on tribocorrosion. Starting by evaluating the total wear and considering both types of samples tested at the same velocity, the increase on the total wear for the samples tested at 0,8N is due to the increase of the normal force. A higher pressure will be present on the tribological contact and the surface of the softer material, in this case the samples, will be more damaged. The wear mechanisms were more significant, as it was possible to state with the increase of the width of the wear track and of the grooves produced by the

wear particles for the Etched samples (Figure 57), while on the Anodized samples the film is more damaged, revealing fractures, loss of superficial layers and the presence of wear particles (Figure 64). However, the fact that the distinction between plastic deformation (0,4N) and wear (0,8N) of the Anodized film is complex and difficult to determine, indicates the potentiality of the anodization in terms of resistance to wear. Therefore, the total wear on the different tested conditions, is, in fact, lower on the Anodized samples than on the Etched samples and it's possible to display an idea of the magnitude of the difference between the samples by comparing the graphics of each type of sample.

Nevertheless, as a tribocorrosion system was evaluated, on this total wear there is a contribution of the mechanical degradation and of the electrochemical dissolution. This characterizes the synergism characteristic on tribocorrosion. In this way, on both types of samples, the main mechanism that controls wear is the mechanical removal of material. For the Etched samples, the wear mechanisms of abrasion and adhesion play the major role on wear, since at 100 rpm the corrosion mechanism provides only a minor contribution to the total wear and even at 2 rpm that contribution is so insignificant that is not even represented on the graphic. Thus, the electrochemical dissolution that results from the destruction and repassivation of the passive film is not significant on the total wear of the Etched samples, and the material seems resistant to the corrosive component. Considering now the tribocorrosion and the wear track data obtained for the Anodized samples, under friction, the Anodized samples are electrochemically superior in comparison to the Etched samples due to the anodization, so the corrosion contribution to the total wear is expected to be even lower than on the Etched samples. Also, since the Anodized film provides better mechanical properties to the surface and is less vulnerable to wear phenomena, the mechanical removal of material will also be smaller than the Etched.

In this way the material that reveals the most promising tribocorrosion properties for a dental implant is the anodized titanium.

Chapter 4 – Conclusion

The objective of this work was to better understand the mechanisms of tribocorrosion present on the materials used for dental implants. The effects of the normal load and velocity of rotation were observed and in addition, the effect of the presence of a biological layer on the material on the tribocorrosion process. The main results and observations are summarized as follows:

Material Characterization

- The anodization process clearly changes the surface morphology of the studied material;
- The preparation of the samples before testing revealed to be an important factor to have in mind, since it may be a source of heterogeneity on the surface state of the studied samples;
- At the micro-level, with the selected parameters, there are no significant differences between the surface topography properties of the Etched and Anodized samples;

Electrochemical Evaluation without sliding

- The anodization process changed the electrochemical interface between the material and the studied electrolyte (Artificial Saliva);
- The Electrochemical Impedance diagram of the Etched samples is distinct of the one of the Anodized Samples, being sensible to the structure of the film grown by anodization;
- The Anodized samples are less susceptible to corrosion processes than the Etched samples;

Tribocorrosion Evaluation

Effect of Normal Load:

Etched Samples:

- The increase of the normal force didn't affect the open-circuit potential under sliding;
- The decreases the Polarization Resistance under sliding (R_{ps}) and increase of the Corrosion Current Density under sliding (i_{act}) was seen with the increase of the normal load;

Anodized Samples:

- The increase of the normal force modified the response of the Anodized film, but only after a certain period of sliding. A gradual cathodic shift on the open-circuit potential under sliding is identified on the Anodized samples at 0,8N;
- The effect of the increase of the normal force on the EIS of the Anodized samples wasn't possible to measure due to the dispersion of the electrochemical state before sliding between the samples, which makes a suitable comparison before and after sliding impossible. The sensitivity of the anodization process and the reproducibility of the anodization is an important factor to have in mind;

Effect of Velocity:

Etched Samples:

- With the decrease of the velocity, the open-circuit potential under sliding revealed more anodic potentials for both tested normal forces and the Polarization Resistance under sliding (R_{ps}) is similar for both tested normal forces;

Anodized Samples:

- The decrease of velocity didn't affect the open-circuit potential under sliding at 0,4N;
- With the decrease of the velocity at 0,8N the anodized film was completely removed;
- The polarization resistance of the outer porous layer (R_{pp}) is sensitive to the velocity;

Effect of Cell Layer

BioEtched Samples:

- The cellular layer influences the electrochemical interface between the material and the electrolyte;
- The open-circuit potentials under sliding were slightly more anodic than on the regular Etched samples for the 0,4N and that effect was stronger at 0,8N;
- The cell layer decreases the Polarization Resistance (R_p) before and under sliding and consequently the Corrosion Current Density (i_{corr} and i_{act});

BioAnodized Samples:

- The cellular layer influences the electrochemical interface between the material and the electrolyte;
- Under sliding the open-circuit potentials drifted right after mechanical contact and different behaviours were found under sliding within the same normal force;
- The counterbody has an effect on the periphery of the wear track;
- The cellular layer decreased both polarization resistances of the outer porous layer and of the barrier film;

Wear Mechanisms and Wear Quantification

Wear Mechanisms

Etched Samples

- The main wear mechanisms present were Abrasion and Adhesion;

Anodized Samples

- At 0,4N the Anodized samples didn't reveal a specific wear mechanism;
- The main wear mechanisms present at 0,8N were Fatigue and Abrasion;

Wear Quantification

Etched Samples

- The Etched samples revealed the higher amount of total wear;
- The mechanical wear of active material (W^m_{act}) is the most important component on the tribocorrosion process;

Anodized Samples

- The protocol wasn't possible to be applied to the Anodized samples;
- The mechanical wear of active material (W^m_{act}) is the most important component on the tribocorrosion process;
- The Anodized samples are more resistant to wear than the Etched samples;

Chapter 5 – Suggestions for Future Work

- To perform a similar study and instead of using artificial saliva as electrolyte at room temperature, the electrolyte should be a biological solution that mimics the other fluids than saliva that are in contact with the implant after implantation: blood, plasma, proteins and so on, as well with temperature control to mimic the human body temperature.

- Develop a new method to guarantee the horizontality of the samples without compromising the cellular layer on the surface of the samples. It could be use a piece with a minimal number of contact points with the sample, preferentially will contact on the extremes of the area that is exposed to the electrolyte and away from the zone where the pin will contact the surface to perform the mechanical degradation of the material. Such a piece could be a metallic tripod with a flat surface, made of stainless steel. The material of the piece should not be toxic to the cells.

- To perform a thorough evaluation of the topography of the samples and select the appropriate parameters that characterize an implantable material.

Chapter 6 – Preliminary study on culture of osteoblast cells for tribocorrosion testing

The previous work was performed at room temperature, with artificial saliva as electrolyte and the biomodified samples were cultured during 5 days. In order to mimic closer the biological environment, a preliminary study with different conditions was performed.

The new conditions are:

- Instead of 5 days of culture, the time was increased to 28 days, in order to allow some calcification of the cells;
- The electrolyte chosen to perform the tests was the culture medium, to simulate the biological environment. The composition is given by Table 23.

Table 23 - Culture medium used as electrolyte.

DMEM	FBS	Ps	Fz
88%	10%	1%	1%

- The electrochemical cell remained at room temperature, but in future tests it should be heated to the corporal temperature;

6.1 Electrochemical Evaluation without cells

6.1.1 Open-Circuit Potential Evolution

The evolution of the open-circuit potential of the Etched and Anodized samples without cells on the culture medium is presented on Figure 84. This is the control to compare the results with the cells.

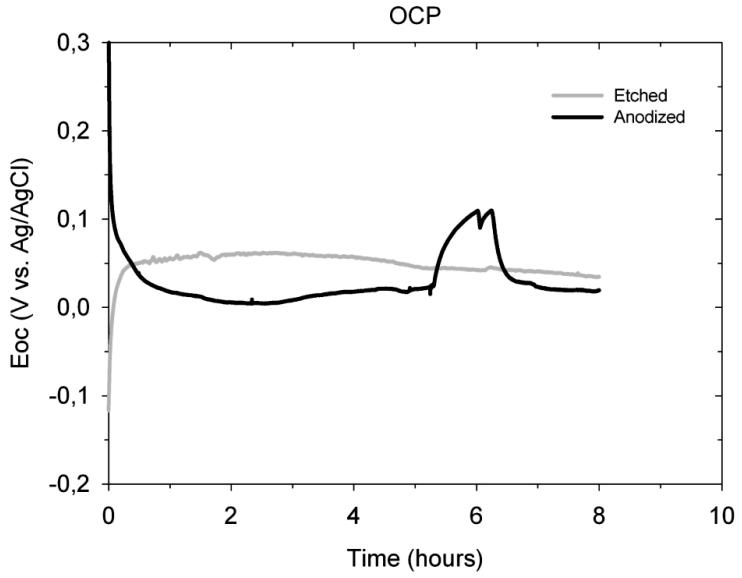

Figure 84 - Evolution of the open-circuit potential with time of an Etched and Anodized sample on culture medium.

The Etched sample show an evolution of the open-circuit potential to positive values, related to the growth of a passive film on the surface of the sample. The potential starts to stabilize and after 1 hour of immersion the potential is at equilibrium with a value of + 0,05 V vs. Ag/AgCl. The potential remains stable during the rest of the test, indicating the stability of the passive film. If one compares this E_{oc} with the one measured with artificial saliva (+ 0,1 V vs. Ag/AgCl), is possible to see that with the culture medium the sample has a more cathodic potential and the passive film developed with the oxidation on the culture medium may not be as protective as the one formed on the artificial saliva. Regarding the Anodized samples, after immersion the potential has a cathodic evolution and starts to stabilize after 1 hour with a potential of 0,0 V vs. Ag/AgCl. At ≈ 5 hours there is a shift on the potential. This shift wasn't a response to any change on the experimental conditions, but even so the electrochemical system changed and after 1 hour was again at the same potential presented before, 0,0 V vs. Ag/AgCl. If this value is compared with the previous tests on artificial saliva, again there is a change on the electrochemical response of the material. The potential drifts to more negative values (cathodic potential), since the equilibrium potential with artificial saliva was of + 0,2 V vs. Ag/AgCl. Again, the material may not have the same protection against corrosion phenomena as in artificial saliva. EIS measurements weren't set on the electrochemical setup and on future tests, impedance diagrams for the control group should be recorded.

These results are interesting, since they clearly show the effect of the change of the electrolyte on the corrosion behaviour of materials. In this case, the Etched and Anodized titanium is more likely subjected to corrosion if the material is in contact with a biological medium with nutrients, proteins and so on, than if is in contact with artificial saliva that mimics the ionic composition found on the oral cavity.

6.2 Tribocorrosion Evaluation

6.2.1 Open-Circuit Potential Evolution

The evolution of the potential was measured before sliding during 1 hour, 2 hours and 3 hours, depending on the time that the samples were delivered to the laboratory. All samples were subjected to the same number of contact events during sliding, N = 7200. EIS measurements under sliding weren't set on the electrochemical setup. Figure 85 shows the evolution of the open-circuit potential of the BioEtched and BioAnodized samples.

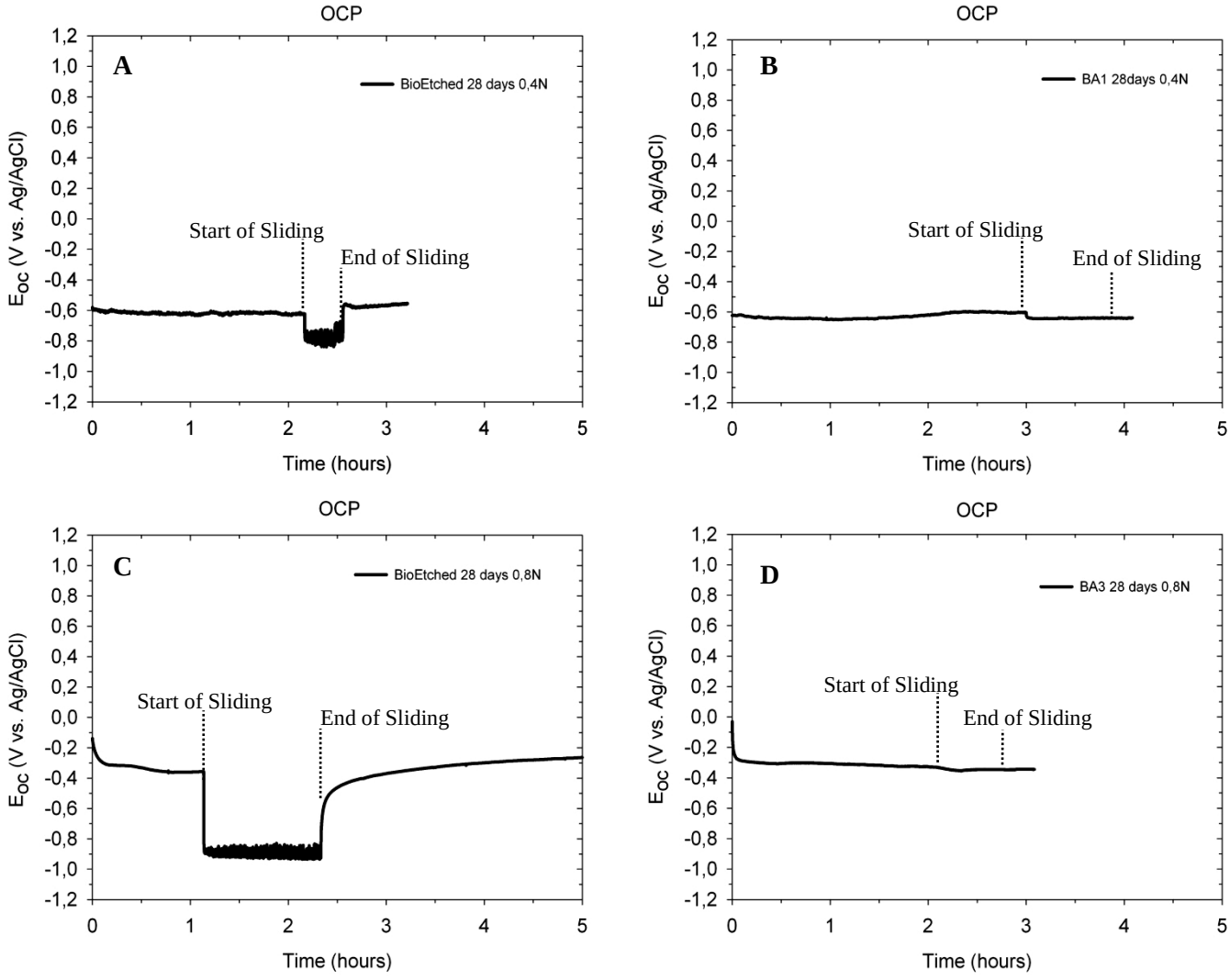

Figure 85- Evolution of the open-circuit potential, before, during, and after continuous unidirectional sliding tests performed at 0,4N and 0,8N at 100 rpm on BioEtched ((A)-(C)) and Anodized samples ((B)-(D)).

Considering the graphics A and C of the previous figure, before sliding, the E_{oc} reveals more negative values of potential than the one recorded on the control. On the control test, the equilibrium potential for the Etched samples was of + 0,05 V vs. Ag/AgCl, but with the cellular layer on the surface of the sample the potential drops to more cathodic values as – 0,6 V vs. Ag/AgCl in the case of graphic A and for -0,3 V vs. Ag/AgCl in the case of graphic C. Both potentials are different, even that the samples were subjected to the same conditions of culture. The fact is that there is always a big

variability when working with cells and the cultures and the responses of the cells towards the materials aren't always the same, creating this variation. When sliding starts, a shift in the potential is recorded. This is due to the destruction of the passive film that is on the surface of the material, exposing the active surface of titanium. The potential on both samples is of about – 0,8 V vs. Ag/AgCl, even with the increase of the normal force from 0,4N to 0,8N from A to C. This follows the findings on the previous tests, but one may not forget that the horizontality of the samples was not verified and an equivalent contact pressure must be obtained all over the surface to discuss properly such effect. After sliding, the increase of the potential is due to the repassivation of the active surface that was exposed to the electrolyte. The potentials stabilize on the same values recorded before sliding.

Regarding the BioAnodized samples (graphic B and D), before sliding, the same effect on the potential as on the BioEtched samples is seen. The potential of the samples are more negative than the value recorded on the control, graphic A with a potential of – 0,6 V vs. Ag/AgCl, graphic B with a potential of - 0,3 V vs. Ag/AgCl, and the control with 0,0 V vs. Ag/AgCl. The cell culture on the samples modifies the electrochemical response of the material, decreasing its protection against corrosion. On the case of the BioAnodized samples, due to the porosity that the samples present, the culture medium has possibility to penetrate deeper on the layers of the Anodized film and interact with the barrier film, as well the presence of the cells and the products of their metabolism may interfere with the corrosion protection provided by the Anodized film. When sliding starts, on both samples the potential isn't affected by the mechanical contact with the ball and during all contact events, the potential remains stable. Even after sliding there is no change on the potential on both graphics B and D. The result of graphic B could be expected, since the sample was tested with a normal force of 0,4N and the previous tests on samples without cells, the potential of the Anodized samples tested with such a normal load was always stable during sliding and even after sliding. However, with the increase of the load (graphic D) to 0,8N, at some point the Anodized film should start to be destroyed and the potential would shift to more negative values. That didn't occurred maybe due to the non-uniform contact of the ball with the surface of the sample. The development of a new system to verify the horizontality of the samples is extremely important for this type of study. The system must have none or minimal contact with the surface of the samples that have a cell layer, otherwise the integrity of the cell layer is compromised and the test isn't performed on the ideal conditions.

In general, one may assume that with the cells the open-circuit potential before sliding of the BioEtched and BioAnodized samples reveals cathodic values, meaning that may be more affected by corrosion phenomena. The cell culture interferes with the electrochemical response of the material and decreases its protection, leading to a higher dissolution of titanium to the system.

6.2.2 Electrochemical Impedance Spectroscopy

Along with OCP, to better understand the passive state of the samples and the mechanisms occurring at the passive film/electrolyte interface, an Electrochemical Impedance Spectroscopy was performed after the stabilization of the potential. However, the only result that is possible to present is related to a BioAnodized sample. The impedance diagrams on the BioEtched samples weren't measurable, maybe due to the fact that the system wasn't in equilibrium or maybe due to some interference from the cell layer on the surface of the material, or even a malfunction of the equipment. The results may not be compared with the control group, since EIS measurements weren't performed on the samples tested on culture medium without cells (control group), but, as this is only a preliminary study, further experiments should be performed in order to confirm the results here presented as well to obtain impedance diagrams on the BioEcthed samples. Figure 86 shows the Nyquist plot of a BioAnodized sample and Table 24 shows the values that characterize the electrochemical state of the BioAnodized sample.

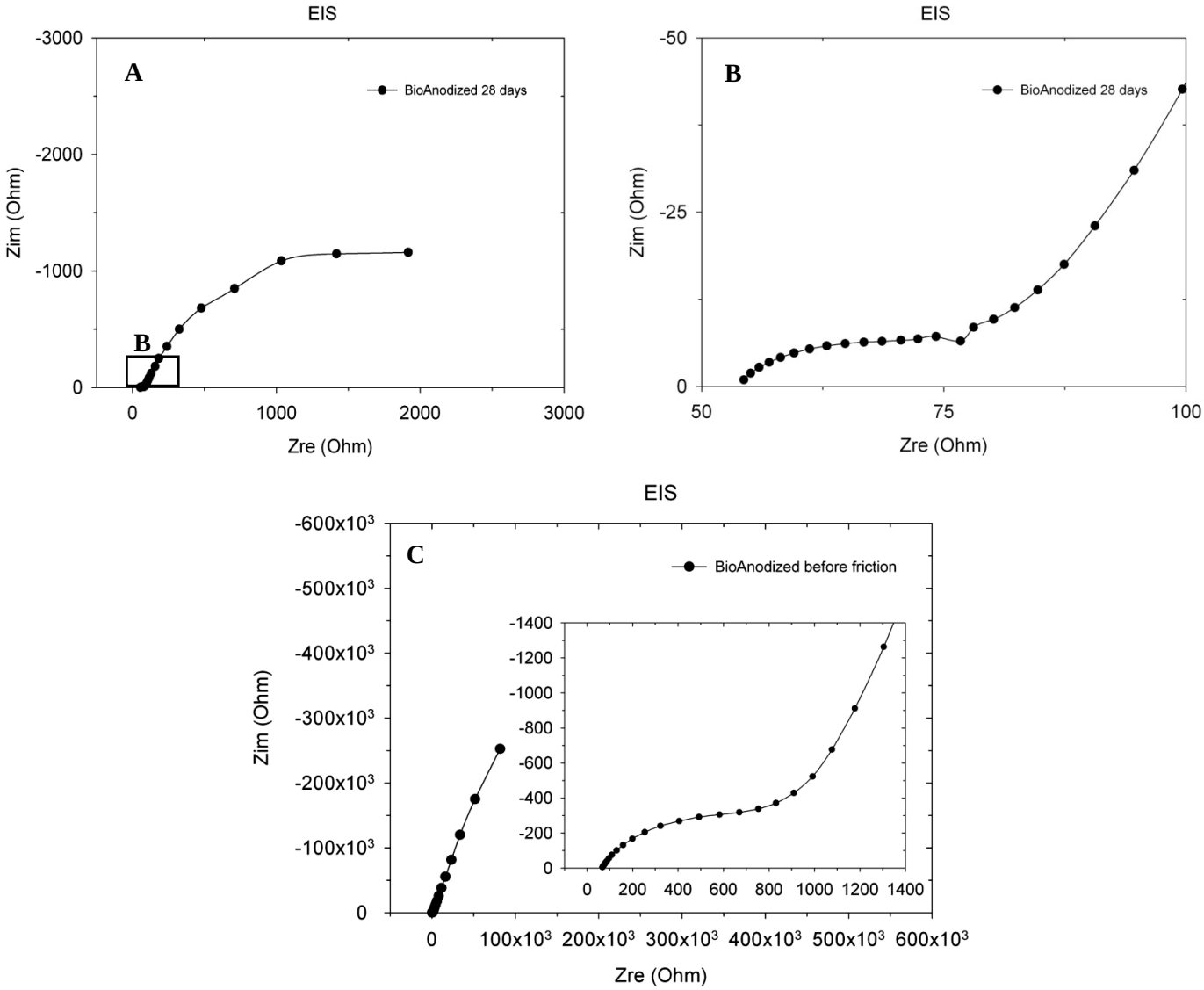

Figure 86 - A) Nyquist plot of BioAnodized sample with 28 days of culture B) High Frequency Range of graphic A) C) Nyquist plot of BioAnodized sample with 5 days of culture.

Table 24 - Polarization resistance (R_{pp}) and specific polarization resistance (r_{pp}) of porous layer and Polarization resistance of barrier film (R_{pb}) and specific polarization resistance of barrier film (r_{pb}) and corrosion current of BioAnodized sample with 28 days of culture, 5 days of culture and no culture.

	A_0 (cm^2)	*Porous Layer*		*Barrier Film*		
		R_{pp} (Ω)	r_{pp} (Ω.cm^2)	R_{pb} (Ω)	r_{pb} (Ω.cm^2)	i_{corr} (A.cm^{-2})
No culture	3,4 (± 0,15)	$4{,}27 \times 10^2$ (± 178)	$1{,}45 \times 10^3$ (± 664)	$7{,}81 \times 10^6$ ($\pm 5{,}02\times10^6$)	$2{,}62 \times 10^7$ ($\pm 1{,}70\times10^7$)	$1{,}29 \times 10^{-9}$ ($\pm 8{,}20\times10^{-10}$)
5 days of culture	3,4 (± 0,01)	$9{,}95 \times 10^2$ ($\pm 4{,}68 \times 10^2$)	$3{,}40 \times 10^3$ ($\pm 1{,}60 \times 10^3$)	$2{,}21 \times 10^6$ ($\pm 4{,}12 \times 10^6$)	$7{,}55 \times 10^6$ ($\pm 1{,}41 \times 10^7$)	$2{,}54 \times 10^{-8}$ ($\pm 3{,}02 \times 10^{-8}$)
28 days of culture	3,23	$3{,}49 \times 10^1$	$1{,}13 \times 10^2$	$3{,}58 \times 10^3$	$1{,}16 \times 10^4$	$2{,}08 \times 10^{-6}$

The impedance diagram of the BioAnodized with 28 days of culture shows the expected impedance diagram. There is a first arc of circle on the high frequency range, due to the porous layer, and after another arc of circle on the low frequency range related to the barrier film. However, is quite different from the one of the BioAnodized samples with 5 days of culture, in terms of magnitude. On the latter, as it can be seen on Figure 86 C, the impedance diagram is almost a straight line and there is no curvature, indicating that the polarization resistance of the Anodized film is quite high. On the other hand, on Figure 86 A, it's possible to see already a curvature of the arc of circle, showing that the polarization resistance decreased, probably due to the effect of the cell culture. Table 24 provides the quantification and comparison of the polarization resistance of the outer porous layer and of the barrier film, without cells, with 5 days of culture and with 28 days of culture. From the samples with no culture to the one with 5 days of culture, the polarization resistance of the outer porous layer increases, but with 28 days of culture, it decreases. On the other hand, the resistance of the barrier film is always decreasing with the increase of the time of culture, resulting on the progressive increase of the corrosion current, or in other words, the progressive increase of the velocity of corrosion. It means that the culture with cells affects the protection provided by the porous layer and the barrier film that results from the anodization. The contact with biological tissue brings lots of electrochemical species and longer the culture period, more is the time provided for the migration of species to the deeper layers of the Anodized film. These species may interact with the barrier film and remove species from the film that will be replaced by the oxidation reaction that compensates the losses of the barrier film. In this way, some species may be adsorbed to the barrier film, changing its properties and its protection against the dissolution of titanium. However, as a control impedance diagram wasn't performed, one should not forget that this can also only be action of the different electrolyte (artificial saliva vs. culture medium).

6.3.3 Wear track of BioEtched and BioAnodized samples with 28 days of culture

After the tribocorrosion test the samples were fixated with formaldehyde and left on the desiccator during 24h. Before SEM evaluation of the wear tracks the samples were covered with gold. Figure 87 presents images of BioEtched (A, B and C) and BioAnodized (D, E and F) samples. Here the objective wasn't to observe carefully the morphology of the wear track, but to see generally the differences between these samples and the ones presented before (with 5 days of culture).

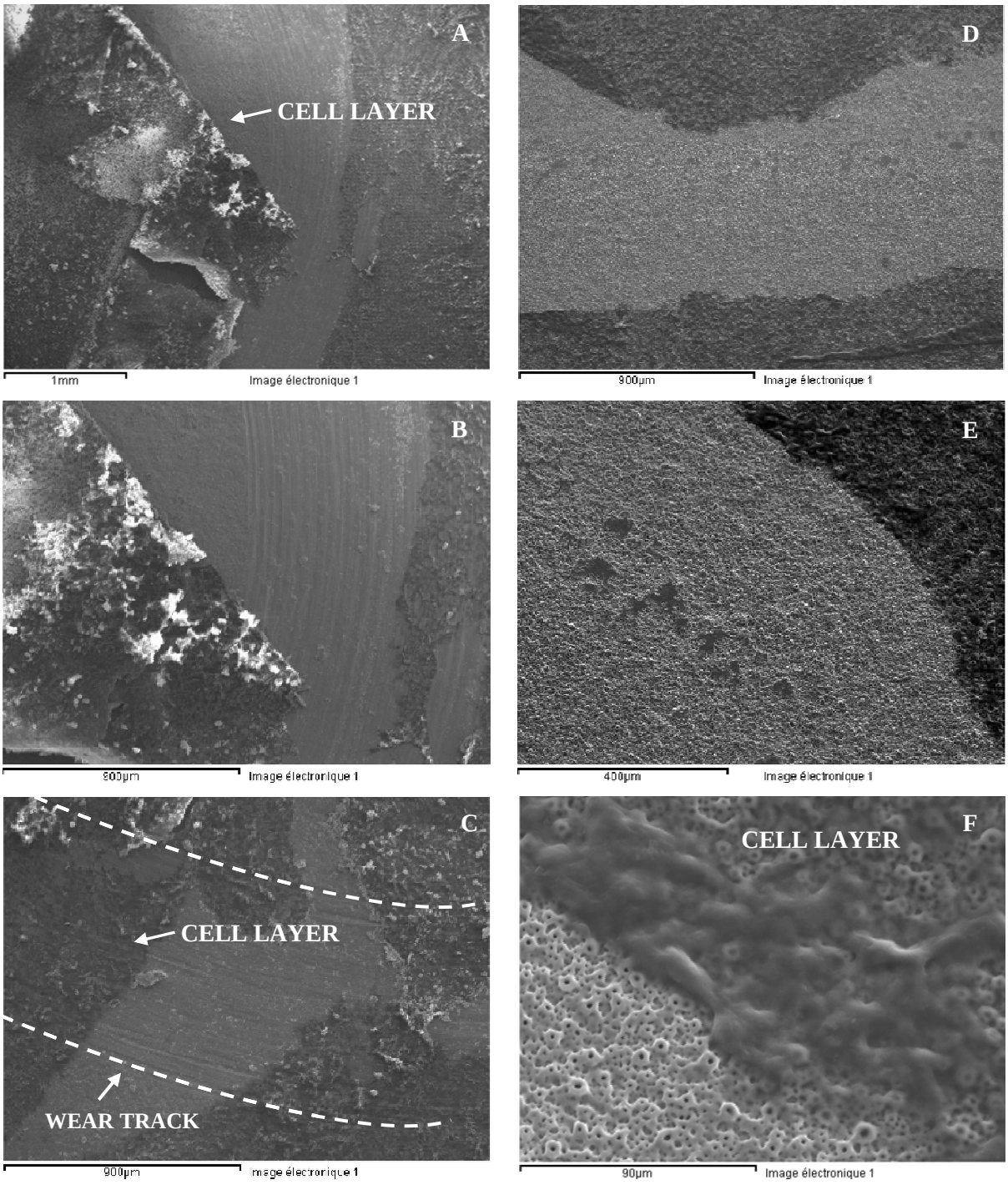

Figure 87 – Wear track of samples cultured during 28 days. BioEtched Samples: A) 35x B) 75x C) 75x BioAnodized Samples: D) 75x E) 150x F) 750x.

The increase of the culture time brought several differences, as well, on the morphology of the wear track of the samples and on the amount of biological material that remained on the sample after the tribocorrosion test. On the samples with 5 days of culture, the BioEtched samples had no biological material left on the surface of the sample, probably due to the environmental conditions that promoted the detachment of the cells. Figure 71 shows the wear track of the BioEtched samples with 5 days of culture. If one compares that figure with Figure 87 A, B and C, identifies clearly difference on the images. On image A of Figure 87 it's visible the presence of the cell layer on the surface of the samples and part of it was removed on the wear track. But in this situation, even some biological material remained on the wear track and wasn't removed with the contact and the motion of the ball. Figure 87 C shows clearly that some biological material is on the wear track of the sample. Also, by the images on the BioEtched samples, it's evident that the amount of biological material is not insignificant, showing that the adhesion of the cells towards the surface after 28 days may be better and also the fact that these samples were tested on culture medium may contributed to provide a better environment for the cells to study their effect on the tribocorrosion process. Respecting the BioAnodized samples, the images that characterize the wear track of the samples with 5 days of culture is Figure 73. The same result was obtained on the samples with 28 days of culture (Figure 87 D, E and F) where it is possible to identify the wear track, then a zone where the cellular layer was removed and after surface still covered with cells. The phenomenon that may induce this result is related to the motion of the ball of the counterbody, the dynamic of the electrolyte and even the volume of the cellular layer. The volume of biological material that is on the border between the zones covered with cells and the exposed zones is clearly higher on the samples cultured with 28 days (Figure 87 F) than with 5 days (Figure 73).

From this preliminary study is evident the advantages on testing the materials with the appropriated conditions for the survival of the cellular layer during the test. Electrochemically was found a difference between the controls tested on culture medium without cells and the ones with cells. The material is less protected against corrosion phenomena when a cellular layer is present on the surface of the samples. Considering the tribocorrosion evaluation, it was interesting to see that the cellular layer was still present after the tribocorrosion test on the BioEtched samples, even on the wear track. On the BioAnodized samples only the amount of material was the significant difference.

References

1. *A review of dental implants and infection.* **Pye, A.D., et al.** s.l. : Elsevier, 2009, Journal of Hospital Infection, pp. 104-110.

2. **Hobkirk, John A., Watson, Roger M. and Searson, Lloyd J.J.** *INTRODUCING Dental Implants.* s.l. : CHURCHILL LIVINGSTONE.

3. **Curtis, R.V. and Watson, T.F.** *Dental Biomaterials - imaging, testing and modelling.* Cambridge : Woodhead Publishing Limited, 2008.

4. Naomi Dental. *Naomi Dental.* [Online] Pham Truong Co.,Ltd. [Cited: 04 26, 2011.] http://www.siteadmincp.com/sites/site135/site_images/IMPLANT_TOOTH.jpg.

5. **Black, Jonathan and Hastings, Garth.** *Handbook of Biomaterial Properties.* s.l. : Springer - Verlag, 1998. ISBN: 978-0-412-60330-3.

6. **Bronzino, J.D., [ed.].** *Biomedical Engineering Handbook.* Second. USA : CRC Press LLC, 2000. ISBN 0-8493-0461-X/00/$0.00+$.50..

7. **Diomidis, N., et al.** A methodology for the assessment of the tribocorrosion passivating metallic materials. *Lubrication Science.* 2009, 21, pp. 53-67.

8. **Enderle, John, Blanchard, S. and Bronzino, J.** *Introduction to Biomedical Engineering.* Second. USA : Elsevier Academic Press, 2005. pp. 257-312. ISBN: 0-12-238662-0.

9. **Wong, Joyce Y. and Bronzino, Joseph D.** *Biomaterials.* USA : CRC Press, 2007. ISBN 0-8493-7888-5.

10. **Ratner, Buddy and Hoffman, Allan, et al.** *Biomaterials Science - An Introduction to Materials in Medicine.* 2ª edição. s.l. : Elsevier Academic Press, 2004. 978-0-12-582463-7.

11. **Williams, D.F.** On the mechanisms of biocompatibility. *Biomaterials.* 2008, 29, pp. 2941-2953.

12. **Marques, A. P.** *in vitro and in vivo testing of biomaterials.* 3 B's Research Group - Biomaterials, Biodegradables and Biomimetics, University of Minho : s.n., 2009.

13. **Recum, A. F. von.** *Handbook of BIOMATERIALS EVALUATION - scientific, technical, and clinical testing of implant materials.* 2ª Edição. s.l. : Taylor&Francis.

14. **Gary E. Wnek, Gary L. Bowlin.** *Encyclopedia of biomaterials and biomedical engineering.* s.l. : Informa Healthcare, 2008. Vol. 3. ISBN: 978-142007956-2.

15. **Le Guéhennec, L., et al.** Surface treatments of titanium dental implants for rapid osseointegration. *Dental Materials.* 2007, pp. 844-854.

16. **Branemark, P.-I.** Osseointegration and its experimental background. *The Journal of Prosthetic Dentistry.* 1983, Vol. 50.

17. **Virtanen, S., Milosev, I. and Gomez-Barrena, E., et al.** Special Modes of corrosion under physiological and simulated physiological conditions. *ActaBIOMATERIALIA.* 2008, Vol. 4, pp. 468-476.

18. **Park, Joon B. and Bronzino, Joseph D.** *Biomaterials - PRINCIPLES and APPLICATIONS.* USA : CRC PRESS, 2003. ISBN 0-8493-1491-7.

19. **Hanawa, Takao.** Metal ion release from metal implants. *Materials Science & engineering C.* 2004, pp. 745-752.

20. **Leyens, Christoph and Peters, Manfred.** *Titanium and Titanium alloys - Fundamentals and Applications.* s.l. : WILEY - VCH, 2003. ISBN 3-527-30534-3.

21. **Donachie, Matthew J.** *TITANIUM A Technical Guide.* USA : ASM International Technical Books Committee, 2000. ISBN 0-87170-686-5.

22. **Roberge, P.R.** *Handbook of Corrosion engineering.* s.l. : McGraw-Hill, 2000. ISBN 978-1-59124-435-6.

23. **Oshida, Yoshiki.** *Bioscience and Bioengineering of Titanium Materials.* USA : Elsevier, 2006. ISBN 10: 0-08-045142-X.

24. **Shreir, L.L., Jarman, R.A. and Burstein, G.T.** *Corrosion.* s.l. : Elsevier, 1994. ISBN: 978-0-7506-1077-3.

25. **Takemoto, S., et al.** Corrosion and surface characterization oftitanium in solution containing fluoride and albumin. *Biomaterials.* 2005, pp. 829-837.

26. **Hanawa, Takao.** In vivo metallic biomaterials and surface modification. *Materials Science & Engineering A.* 1999, pp. 260-266.

27. **Jouanny, I., et al.** Structural and mechanical properties of titanium oxide thin films for biomedical application. *Thin Solid Films.* 2010, pp. 3212-3217.

28. **Shukla, A.K., Balasubraniam, R. and Bhargava, S.** Properties of passive film formed on Cp Titanium, Ti-6Al-4V and Ti-13.4Al-29Nb alloys in simulated body conditions. *Intermetallics.* 2005, pp. 631-637.

29. **Huang, Y.Z. and Blackwood, D.J.** Characterisation of titanium oxide film grown in 0.9% NaCl at different sweep rates. *Electrochimica Acta.* 2005, pp. 1099-1107.

30. **Fonseca, C. and Barbosa, M.A.** Corrosion behavior of titanium in biofluids containing H2O2 studied by electrochemical impedance spectroscopy. *Corrosion Science.* 2001, pp. 547-559.

31. **Eftekhari, Ali.** *Nanostructured Materials in Electrochemistry.* s.l. : Wiley - VCH, 2008. ISBN: 978-3-527-31876-6.

32. **Liu, Xuanyong, Chu, Paul K. and Ding, Chuanxian.** Surface modification of titanium, titanium alloys, and related materials for biomedical applications. *Materials Science and Engineering R.* 2004, Vol. 47, pp. 49-121.

33. **Jackson, Mark J. and Ahmed, Waqar.** *Surface engineered surgical tools and medical devices.* s.l. : Springer Science, 2007. ISBN: 978-0-387-27026-5.

34. **Park, Il Song, et al.** Effects of Anodizing Voltage on the Anodized and Hydrothermally Treated Titanium Surface. *Metals and Materials International.* 2006, Vol. 12, pp. 505-511.

35. **Krupa, D., et al.** Modifying the properties of titanium surface with the aim of improving its bioactivity and corrosion resistance. *Journal of Materials Processing Technology.* 2003, Vols. 143-144, pp. 158-163.

36. **Oh, Han-Jun, et al.** Microstructural characterization of biomedical titanium oxide film fabricated by electrochemical method. *Surface & Coatings Technology.* 2005, Vol. 198, pp. 247-252.

37. **Souza, M.E.P., Ballester, M. and Freire, C.M.A.** EIS characterization of Ti anodic oxide porous films formed using modulated potential. *Surface & Coatings Technology.* 2007, Vol. 201, pp. 7775-7780.

38. **Zhu, Xiaolong, Kim, Kyo-Han and Jeong, Yongsoo.** Anodic oxide films containing Ca and P of titanium biomaterial. *Biomaterials.* 2001, Vol. 22, pp. 2199-2206.

39. **Mathew, M.T., et al.** Significance of Tribocorrosion in Biomedical Applications: Overview and Current Status. [ed.] Braham Prakash. *Advances in Tribology.* 2009, Vol. 2009, p. 12.

40. **Landolt, D.** Electrochemical and materials aspects of tribocorrosion systems. *Journal of Physics D: Applied Physics.* 2006, 39, pp. 3121-3127.

41. **Landolt, D., Mischler, S. and Stemp, M.** Electrochemical methods in tribocorrosion: a critical appraisal. *Electrochimica Acta.* 2001, 46, pp. 3913-3929.

42. **Landolt, D., et al.** Third body effects and material fluxes in tribocorrosion systems involving a sliding contact. *WEAR.* 2004, 256.

43. **Watson, S.W., et al.** Methods of measuring wear-corrosion synergism. *WEAR.* 1995, 181-183, pp. 476-484.

44. **Aussi, F. and Suter, T., Bohni, H.** A new electrochemical technique to study tribocorrosion at the micrometric scale. *Tribotest.* 1999, Vol. 6, pp. 17-28.

45. **Diomidis, N., et al.** Tribocorrosion of stainless steel in sulfuric acid: Identification of corrosion-wear components and effect of contact area. *WEAR.* 2010, 269, pp. 93-103.

46. **Diomidis, N., et al.** Assessment of the surface state behaviour of Al71Cu10Fe9Cr10 and Al3Mg2 complex metallic alloys in sliding contacts. *Intermetallics.* 2009, 17, pp. 930-937.

47. **Lemaire, E. and Le Calvar, M.** Evidence of tribocorrosion wear in pressurized water reactors. *WEAR.* 2001, 249.

48. **Vieira, A.C., et al.** Influence of pH and corrosion inhibitors on the tribocorrosion of titanium in artificial saliva. *WEAR.* 2006, 261, pp. 994-1001.

49. **Souza, J.C.M., et al.** Do oral biofilms influence the wear and corrosion behavior of titanium? *Biofouling.* 2010.

50. **Pan, J., Thierry, D. and Leygraf, C.** Electrochemical Impedance Spectroscopy Study of the Passive Oxide Film on Titanium for Implant Application. *Electrochimica Acta.* 1996, pp. 1143-1153.

51. **Yan, Y., Neville, A. and Dowson, D.** Biotribocorrosion of CoCrMo orthopedic implant materials - Assessing the formation and effect of the film. *Tribology Internacional.* 2007, pp. 1492-1499.

52. **Ide, K., et al.** The effect of fluoride and albumin on corrosion of titanium. *Dental Materials Journal.* 2001.

53. **Cheng, X. and Roscoe, S.G.** Corrosion behavior of titanium in the presence of calcium phosphate and serum proteins. *Biomaterials.* 2005, pp. 7350-7356.

54. **O'Mahony, Conor, et al.** Characterization of micromechanical structures using white-light interferometry. *Measurements Science and Technology.* 2003, pp. 1807-1814.

55. **Diomidis, N., Celis, J.-P., Ponthiaux, P. and Wenger, F.** A methodology for the assessment of the tribocorrosion of passivating metallic materials. *Lubrication Science.* 2009, pp. 53-67.

56. **Trethewey, K.R. and Chamberlain, J.** *CORROSION for Science and Engineering.* UK : Lonbgman Group Limited, 1995. ISBN 0-582-238692.

57. **Normand, Bernard, et al.** *Prévention et lutte contre la corrosion.* s.l. : Presses Polytechniques et Universitaires Romandes, 2004. ISBN 2-88074-543-8.

58. **Ponthiaux, P., et al.** Electrochemical techniques for studying tribocorrosion processes. *WEAR.* 2004, Vol. 256, pp. 459-468.

59. **Wu, P.-Q. and Celis, J.P.** Electrochemical noise measurements on stainless steel during corrosion-wear in sliding contacts. *WEAR.* 256, pp. 480-490.

60. **Orazem, Mark E. and Tribollet, Bernard.** *Electrochemical impedance Spectroscopy.* s.l. : John Wiley & Sons, 2008. ISBN 978-0-470-04140-6.

61. **Research, Princeton Applied.** Basics of Electrochemical Impedance Spectroscopy Application note AC-1. *Princeton Applied Research.* [Online] Princeton Applied Research. [Cited: 10 15, 2010.] http://www.princetonappliedresearch.com/Literature/index.aspx.

62. **Goldstein, Joseph, et al.** *Scanning Electron Microscopy and X-Ray Microanalysis.* s.l. : Springer, 2003. ISBN 978-0-306-47292-3.

63. **Reimer, Ludwig.** *Scanning Electron Microscopy - Physics of Image Formation and Microanalysis.* s.l. : Springer, 1998. ISBN 3-540-63976-4.

64. **Kuo, John.** *Electron Microscopy Methods and Protocols.* s.l. : Humana Press, 2007. ISBN 13: 978-1-58829-573-6.

65. **Garratt-Reed, A.J. and Bell, D.C.** *Energy-Dispersive X-Ray Analysis in the Electron Microscope.* s.l. : BIOS Scientific Publishers Limited, 2003. ISBN 0-203-48342-1.

66. **Neale, M.J.** *The Tribology Handbook.* s.l. : Butterworth Heinemann, 1995. ISBN 7506-1198-7.

67. **Stachowiak, Gwidon W. and Batchelor, Andrew W.** *Engineering Tribology.* s.l. : Buttherworth Heinemann, 2001. ISBN 0-7506-7304-4.

68. **Smith, Graham T.** *Industrial Metrology Surfaces and Roughness.* s.l. : Springer, 2002. ISBN 1-85233-507-6.

69. **STIL.** *Non Contact Measurements Solutions.* s.l. : STIL, 2010. E1010.

70. **Bhushan, Bharat.** *Nanotribology and Nanomechanics An Introduction.* s.l. : Springer, 2008. ISBN 978-3-540-77607-9.

71. **Oh, Han-jun, et al.** Microstructural characterization of biomedical titanium oxide film fabricated by electrochemical method. *Surface & Coatings Technology*. 2005, pp. 247-252.

72. **Zhu, Xiaolong, et al.** Effects of topography and compostition of titanium surface oxides on osteoblast responses. *Biomaterials.* 2004, pp. 4087-4103.

73. **Park, Il Song, et al.** Surface characteristics of titanium Anodized in the four different types of electrolyte. *Electrochimica Acta.* Elsevier, pp. 863-870.

74. **Ehrenfest, D.M.D., et al.** Classification of osseointegrated implant surfaces: materials, chemistry and topography. *Trends in Biotechnology.* 2009, pp. 1-9.

75. **Elias, Carlos Nelson, et al.** Relationship between surface properties (roughness, wettability and morphology) of titanium and dental implant removal torque. *Journal of the Mechanical Behavior of Biomedical Materials.* 2008, pp. 234-242.

76. **Rosales-Leal, J.I. and Rodriguez-Valverde, M.A. et al.** Effect of roughness, wettability and morphology of engineered titanium surfaces on osteoblast-like cell adhesion. *Colloids and Surfaces A: Physicochemical and Engineering Aspects.* 2010, pp. 222-229.

77. **Lee, J.M., Lee, J.I. and Lim, Y.J.** In vitro investigation of anodization and CaP deposited titanium surface using MG63 osteoblast-like cells. *Applied Surface Science.* 2010, pp. 3086-3092.

78. **Rupp, F., et al.** Roughness induced dynamic changes of wettability of acid Etched titanium implant modifications. *Biomaterials.* 2004, pp. 1429-1438.

79. **Celis, J.-P., Ponthiaux, P. and Wenger, F.** Tribo-corrosion of materials: Interplay between chemical, electrochemical, and mechanical reactivity of surfaces. *WEAR.* 2006, pp. 939-946.

80. **Yu, Wei-qiang, Qiu, Jing and Zhang, Fu-qiang.** In vitro corrosion study of different TiO2 nanotube layers on titanium in solution with serum proteins. *Colloids and Surfaces B: Biointerfaces.* 2011, pp. 400-405.

81. Direct-Healthcare. *Direct-Healthcare.* [Online] [Cited: 03 02, 2011.] http://www.direct-healthcare.com/images/metal_on_metal.jpg.

82. Sciencephoto. [Online] [Cited: 03 02, 2011.] http://www.sciencephoto.com/images/download_wm_image.html/M580161-Tissue_scaffold_used_to_make_artificial_organs-SPL.jpg?id=775800161.

83. Universitas Bergensis. [Online] [Cited: 03 02, 2011.] http://www.uib.no/imagearchive/ingressbilde_biomat_oral_restorations.jpg.

84. **Souza, J.C.M., et al.** Do oral biofilms influence the wear and corrosion behaviour of titanium? 2010.